

10-1-2006

2006 Summer Research Experience for Undergraduate Program

Chad S. Kusko

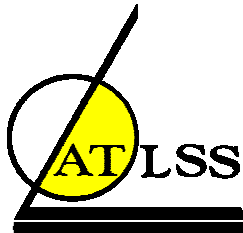
Follow this and additional works at: <http://preserve.lehigh.edu/engr-civil-environmental-atlss-reports>

Recommended Citation

Kusko, Chad S., "2006 Summer Research Experience for Undergraduate Program" (2006). ATLSS Reports. ATLSS report number 06-21:.

<http://preserve.lehigh.edu/engr-civil-environmental-atlss-reports/85>

This Technical Report is brought to you for free and open access by the Civil and Environmental Engineering at Lehigh Preserve. It has been accepted for inclusion in ATLSS Reports by an authorized administrator of Lehigh Preserve. For more information, please contact preserve@lehigh.edu.



2006 Summer Research Experience For Undergraduate Program

by

Chad S. Kusko, Ph.D.

ATLSS Report No. 06-21

October 2006

**ATLSS is a National Center for Engineering Research
on Advanced Technology for Large Structural Systems**

117 ATLSS Drive
Bethlehem, PA 18015-4729

Phone: (610)758-3525
Fax: (610)758-5902

www.atlss.lehigh.edu
Email: inatl@lehigh.edu

PITA PROJECT PIT-657-06

FINAL REPORT

**2006 Summer Research Experience For
Undergraduate Program**

by

Chad Kusko, Ph.D.

REU Participants

Andrew Adams

Michael Angis

Chintan Desai

Christopher Hsiao

Geoffrey Madrazo

Mia Simmons

Gabriel Valencia

ATLSS Report No. 06-21

October 2006

Acknowledgements

The Summer 2006 program was financed in part by a grant from the Commonwealth of Pennsylvania, Department of Community and Economic Development, through the Pennsylvania Infrastructure Technology Alliance, Project Number PIT-657-06, and in part by the George E. Brown, Jr. Network for Earthquake Engineering Simulation (NEES) Consortium (NEESinc) through funding provided by the National Science Foundation.

The author would like to thank the Advanced Technology for Large Structural Systems (ATLSS) Research Center for support of the program and associated research projects. In addition, the following individuals are individually acknowledged for their contribution to the program:

- Richard Sause, Bob Alpago, Betty MacAdam, and Phyllis Pagel for administrative support;
- Peter Bryan, Tommy Marullo, Frank Stokes, Ian Hodgson, Carl Bowman, John Hoffner and the ATLSS technician staff, and Ed Tomlinson and the ATLSS Instrumentation Group for their technical guidance in support of student projects;
- Professors Jim Ricles, Richard Sause, Clay Naito, Yungfeng Zhang, and Sibel Pamukcu, along with ATLSS staff member Sougata Roy, for taking the time to advise students on research projects;
- Graduate students Oya Mercan, David Roke, Lynne Starek, Songye Zhu, Joe Creek, Charles Labarbera, and Mark McElroy for their daily mentorship of the students;
- Lehigh University staff members Randy Shebby, Sharon Siegler, Amy Holtzman Vazquies, and Eli Schoomer for their presentations as part of professional skills workshops, and Will Hlay and Mary Kay Baker for their assistance in working through administrative details;
- Brad Nesland from Dorney Park, Bob Cisneros from High Steel Structures, Inc., Glenn Peterson from Parsons and the Susquehanna River Bridge Project, and Travis Matthews from Carpenter Technology for their participation in providing the students with industrial tours.
- Ryan Manning, Operations Manager for Valley Association for Specialized Transportation Incorporated (VAST), for assistance with student transportation.

Finally, the author would like to thank the students that participated in the Summer 2006 program, Andrew Adams, Michael Angis, Chintan Desai, Christopher Hsiao, Geoffrey Madrazo, Mia Simmons, and Gabriel Valencia, for their time, effort, and diligence.

Table of Contents

Cover Page.....	1
Acknowledgements.....	2
Table of Contents.....	3
Abstract.....	4
1.0 Introduction.....	4
2.0 Summer 2006 Program.....	5
2.1 Recruitment of Students.....	5
2.2 Selection of Students.....	6
2.3 Participating Students.....	6
2.4 Overview of Program.....	6
2.4.1 Professional Development Workshops.....	6
2.4.1.1 Laboratory and Construction Safety.....	7
2.4.1.2 Library Search Techniques.....	7
2.4.1.3 Resume Building.....	7
2.4.1.4 Developing Effective Presentations.....	7
2.4.1.5 Writing Technical Reports.....	7
2.4.2 Industrial Tours.....	8
2.4.2.1 Susquehanna River Bridge.....	8
2.4.2.2 Dorney Park.....	8
2.4.2.3 High Steel Structures, Incorporated.....	8
2.4.2.4 Carpenter Technology Corporation.....	8
2.4.3 Miscellaneous Project Activities.....	9
2.4.3.1 NEES@Lehigh: Real-Time Multi-Directional Seismic Testing Workshop.....	9
2.4.3.2 4 th Annual NEES Conference in Washington, D.C.....	9
2.4.3.3 ATLSS Laboratory Scheduling Meetings.....	9
2.4.3.4 NEESreu Conference Calls.....	9
2.4.3.5 Student Luncheons.....	10
2.4.3.6 End of Program Picnic.....	10
2.5 Student Deliverables.....	10
2.6 Student Feedback.....	10
2.6.1 Overall Assessment of Program.....	10
2.6.2 Program Impact on Future Plans.....	10
2.6.3 Recommendations.....	11
2.7 Summary.....	11
2.8 References.....	11
Tables and Figures.....	13
Appendix A: Summer 2006 REU Program Application Package.....	21
Appendix B: Summer 2006 REU Program Schedule of Activities.....	23
Appendix C: Student Final Reports.....	25

Abstract

Lehigh University's Advanced Technology for Large Structural Systems (ATLSS) Research Center conducted a ten week Research Experience for Undergraduates (REU) program during Summer 2006. The program was comprised of two parallel programs, ATLSSreu, funded by the Commonwealth of Pennsylvania, Department of Community and Economic Development, and NEESreu, funded by the National Science Foundation through the Network for Earthquake Engineering Simulation (NEES) Consortium. The REU program provided undergraduate students with the opportunity to conduct research on a Civil-Engineering based research project under the direction of the project's Principal Investigator and graduate student mentor. Additionally, the students participated in an array of professional development workshops, industrial tours, and miscellaneous cohort activities to provide the students with a well-balanced educational experience. At the completion of the course, students were required to present the findings of their research in a formal presentation and document their findings in a technical report.

1.0 Introduction

Lehigh University's Advanced Technology for Large Structural Systems (ATLSS) Research Center, under financial support from the Commonwealth of Pennsylvania, Department of Community and Economic Development through the Pennsylvania Infrastructure Technology Alliance (PITA), has an established history of organizing and operating highly successful Research Experience for Undergraduates (REU) programs designed around ongoing Civil, Environmental, Structural, and Earthquake Engineering research topics. Such courses were completed during the summers of 2002 and 2003 [Ref. 1]. As part of these programs, students conducted research covering a wide range of Civil Engineering-related research topics, including earthquake hazard mitigation, building systems, fatigue and fracture, bridge systems, and bridge field monitoring, under the direction of project Principal Investigators and graduate students. The programs included workshops highlighting proper library search techniques, presentation organization and delivery, and report writing, along with tours of active construction sites and material fabrication plants. Feedback from students following participation in the 2003 program indicated that 5 out of 6 students had definitive plans to attend graduate school, with 3 of these students indicating that Pennsylvania-based universities would be included in the application process. One of the students applied for a position at an engineering company that was visited as part of the program. Of the 5 students that participated in the 2002 program, 4 of the students were either completing their undergraduate curriculum in engineering or were pursuing graduate degrees in engineering at a Pennsylvania-based university [Ref. 1].

In 2004, Lehigh University's ATLSS Research Center was enhanced by the construction of the George E. Brown Network for Earthquake Engineering Simulation (NEES) Real-Time Multi-Directional (RTMD) equipment site, under financial support from the National Science Foundation (NSF), PITA, and Lehigh University. This equipment site represents one of only fifteen national equipment sites constructed during this period, with goals that include the advancement of earthquake engineering research

and education. A parallel REU program focusing on earthquake engineering, under sponsorship by the NSF and direction by the NEES Consortium (NEESinc), has been developed to utilize the technical capabilities of the national equipment sites. Lehigh's RTMD site was one of only three national sites selected to participate in the inaugural program during the Summer 2006.

2.0 Summer 2006 Program

Lehigh University's ATLSS Research Center, under financial support from the Commonwealth of Pennsylvania, Department of Community and Economic Development, through the PITA program, and the NSF through NEESinc, conducted a joint REU program during Summer 2006. The parallel programs, termed ATLSSreu for the students supported under funding from PITA, and NEESreu for the students funded by NEESinc, were run in parallel under the direction of program administrator and PITA Project Principal Investigator Dr. Chad Kusko. The joint program was developed to provide students from both programs with similar opportunities in the areas of professional development, industrial experience, and cohort activities. Requirements of the NEESreu program excluded ATLSSreu students from certain activities, including attendance at the 4th NEES Annual Meeting and weekly teleconferences.

2.1 Recruitment of Students

In order to attract applicants for the ATLSSreu program, Lehigh University developed a program announcement poster highlighting participant requirements and program expectations. The poster was electronically distributed to Civil Engineering professors and/or administrative contacts at 71 universities, in addition to 22 contacts affiliated with different geographic regions of the Lewis Stokes Alliance of Minority Participation (LSAMP). Figure 1 illustrates the ATLSSreu program announcement poster. In addition to the poster, an application package including an application checklist, an application form, a statement of purpose, and a letter of recommendation form, were distributed. Appendix A exhibits the application package utilized for the Summer 2006 ATLSSreu program.

NEESinc was responsible for recruitment of students for the NEESreu program. The NEESreu program announcement poster is provided in Figure 2. NEESinc also required an application package to be completed for the program. A copy of the NEESinc application form is not available for this report.

2.2 Selection of Students

Four completed applications were received for the ATLSSreu program. Each completed application was reviewed and assessed as to whether the student's qualifications were sufficient for the program. All four students qualified for the program and were subsequently offered the opportunity to participate. Each student accepted the offer for participation.

The NEESreu program students were selected and assigned to Lehigh University by NEESinc. Five students selected Lehigh University as their primary choice for

program participation. However, due to the timing of Lehigh's NEESreu program in relation to the conclusion of the academic semesters at these students' home institutions, only three students were able to participate in Lehigh's program. These students were assigned to Lehigh's NEESreu program by NEESinc.

2.3 Participating Students

Table 1 summarizes the students that were selected for participation in both the ATLSreu and NEESreu programs, in addition to their respective home institutions and academic majors. Students selected to participate in the ATLSreu program included Andrew Adams (Pennsylvania State University), Michael Angis (Lehigh University), Chintan Desai (Manhattan College), and Christopher Hsiao (Lehigh University). Students selected to participate in the NEESreu program included Geoffrey Madrazo (The Georgia Institute of Technology), Mia Simmons (North Carolina Agricultural and Technical State University), and Gabriel Valencia (San Jose State University). Summer 2006 program participants are shown in Figure 3.

2.4 Overview of Program

The Summer 2006 program was a ten week program that ran from May 30 through August 4. A total of seven students participated in the program. Four students were selected by Lehigh University to participate in the ATLSreu program, which included research projects in the following research thrust areas: advanced materials, earthquake hazard mitigation, bridge field monitoring, and fatigue and fracture. Three students were assigned to Lehigh University by NEESinc to participate in the NEESreu program at Lehigh's RTMD Equipment Site within the ATLS Research Center. All research projects conducted under the NEESreu program can be classified under the earthquake hazard mitigation thrust area.

Each REU student was assigned a specific research project within the one of the aforementioned thrust areas. Figure 4 illustrates a NEESreu student conducting research within the ATLS Research Center as part of the program. The research projects were conducted under the direction of project Principal Investigators, represented by either a Lehigh University faculty or staff member, and graduate student mentors. For each respective student, Table 1 also provides the title of the research project, along with each project's Principal Investigator and graduate student mentor. In addition to the research, a series of professional development workshops and industrial tours were integrated into the program to provide the students with a well-rounded educational experience. Each student was provided with a desk and personal computer, which were located within one office at ATLS, in order to provide the students with daily opportunity for communication and teamwork development with other program participants. At the conclusion of the program, students were required to submit a technical report detailing the research project and provide an accompanying twenty minute presentation. The schedule of activities for the Summer 2006 ATLSreu and NEESreu programs is provided in Appendix B.

2.4.1 Professional Development Workshops

A series of professional development workshops were developed in order to enhance the students' skills and knowledge-base in specific areas that would benefit the student not only during the program but also during future professional opportunities. A brief summary of each workshop is provided in the subsequent sections.

2.4.1.1 Laboratory and Construction Safety

Randolph Shebby, Assistant Director of Environmental Health and Safety at Lehigh University, gave the students a presentation focusing on safety practices both within a structural laboratory and at a construction site. Figure 5 illustrates the safety presentation offered during the program. The goal of the activity was to instruct the students as to how to incorporate best safety practices into their laboratory activities and industrial tours that will occur throughout the program. At the conclusion of this presentation, Dr. Chad Kusko, Lehigh's RTMD Equipment Site Research Operations Manager and Principal Investigator of the PITA REU program, discussed safety practices specific to the ATLSS Research Center and NEES RTMD Equipment Site. Subsequent to the presentation and discussion, students were required to complete online tests offered by Lehigh University's Department of Environmental Health and Safety on fall protection, confined space, and hearing protection.

2.4.1.2 Library Search Techniques

Sharon Siegler, Senior Engineering Librarian within Lehigh University's Library and Technology Services, provided the students with a presentation focusing on library search techniques, including conducting literature searches, as illustrated in Figure 6. The goal of the activity was to introduce the students to efficient methods of searching through library resources to support research activities. Specific examples utilizing Lehigh University's library system were included.

2.4.1.3 Resume Building

Amy Holtzman Vazquies, Career Counselor within Lehigh University's Career Services, gave the students a presentation on developing an effective resume, including topics such as content, formatting, and order. The goal of the activity was to provide the students with proper techniques for creating effective personal resumes. Figure 7 shows the students and instructor during the activity.

2.4.1.4 Developing Effective Presentations

Elia Schoomer, Team Leader of Media Services within Lehigh University's Library and Technology Services, gave the students a presentation on creating and delivering effective presentations, as exhibited by Figure 8. The goal of the activity was to provide the students with best practices of creating and delivering effective formal

presentations in order to prepare the students for developing a presentation due at the conclusion of the program.

2.4.1.5 Writing Technical Reports

Dr. Chad Kusko, Research Operations Manager for Lehigh's NEES RTMD Equipment Site and REU program Principal Investigator, gave the students a presentation on writing technical reports. The goal of the activity was to introduce the students to proper techniques for writing technical reports in order to prepare the students for drafting of the reports due at the conclusion of the program.

2.4.2 Industrial Tours

A series of industrial tours were conducted in order to provide the students with exposure to an industrial setting. The activities included are detailed in the subsequent sections.

2.4.2.1 Susquehanna River Bridge

Glenn Peterson, P.E., Principal Segmental Engineer for Parsons, provided the students with a tour of the Susquehanna River Bridge Project (www.kci.com/projects/srb/). The Susquehanna River Bridge utilizes an innovative bridge design, known as the precast concrete segmental bridge, for a six-lane signature bridge across the Susquehanna River. Upon completion, the bridge will be the first major vehicular bridge in Pennsylvania to employ segmental design and construction. Students reviewed the concrete girder casting operation, traveled along segments of the bridge, and discussed the precast box girders and trusses utilized in the design and fabrication in order to better understand the structural engineering aspects associated with the project. Images from this activity are provided in Figure 9.

2.4.2.2 Dorney Park

Brad Nesland, Vice President of Maintenance and Construction at Dorney Park, provided the students with a tour of the amusement park. Dorney Park is an amusement park in Allentown, PA that is comprised of various amusement rides and games (www.dorneypark.com). Students were provided with a review of various roller coaster designs and technologies, and for each, discussed scientific, safety, maintenance, and construction aspects. Images from this activity are provided in Figure 10.

2.4.2.3 High Steel Structures, Inc.

Robert Cisneros, P.E., Chief Engineer at High Steel Structures, Inc, provided the students with a tour of High Steel's Lancaster fabrication facility. High Steel Structures, Inc. (www.highsteel.com) is the industry leader in the fabrication of steel bridge superstructures. The activity included a presentation on High Steel's history and current

operations, along with a tour of its fabrication plants and operations. Images from this activity are provided in Figure 11.

2.4.2.4 Carpenter Technology Corporation

Travis Matthews, Engineer at Carpenter Technology Corporation, provided the students with a tour of Carpenter's operations. Carpenter Technology Corporation (www.carttech.com), located in Reading, PA, is a leading international manufacturer of specialty alloys and engineered products. The activity included tours of various metal manufacturing processes, including melting, pressing, annealing, rolling, drawing, forging, cutting, grinding, and coating.

2.4.3 Miscellaneous Project Activities

In addition to the aforementioned professional development workshops and industrial tours, the students were exposed to additional activities. These activities are detailed in the subsequent sections.

2.4.3.1 NEES@Lehigh: Real-Time Multi-Directional Seismic Testing Workshop

Both ATLSSreu and NEESreu students attended a full day training session entitled NEES@Lehigh: Real-Time Multi-Directional Seismic Testing Workshop at Lehigh University's RTMD NEES Equipment Site. The students were part of a group of attendees that included undergraduate, graduate, and post-doctoral students and faculty from several institutions. The students attended the workshop in order to gain experience with regard to participating in a professional workshop, to interact with students and faculty from other institutions, and to better understand the technical capabilities available at the RTMD site.

2.4.3.2 4th Annual NEES Conference in Washington, D.C.

NEESreu students, under funding from NEESinc, attended the 4th Annual NEES Conference in Washington, D.C. The students attended a full day workshop on technical report writing, in addition to attending the technical sessions and workshops included with the conference. The experience provided the students exposure to a professional conference environment and an opportunity to interact with researchers from industry and other institutions. Figure 12 shows the NEESreu students at the meeting.

2.4.3.3 ATLSS Laboratory Scheduling Meetings

Both ATLSSreu and NEESreu students attended two ATLSS laboratory scheduling meetings. The meetings, facilitated by the ATLSS Laboratory Manager, are attended by ATLSS Research Center faculty, staff, and students in order to schedule upcoming laboratory and personnel requirements. Attendance at the meetings provided

the students with exposure to issues related to planning, set-up, and execution of structural testing experiments within the ATLSS laboratory.

2.4.3.4 NEESreu Conference Calls

NEESreu students participated in weekly conference calls with representatives from NEESinc and students participating in the NEESreu program at other institutions. The conference calls provided the students with the opportunity to collaborate with students from other institutions and discuss the results of their research findings.

2.4.3.5 Student Luncheons

Both ATLSSreu and NEESreu students attended student luncheons in order to get the students together to discuss the program, activities, and the progress of their research projects. Luncheon was held within the ATLSS Research Center and as part of industrial tours.

2.4.3.6 End of Program Picnic

Both ATLSSreu and NEESreu students attended an end of program picnic at the ATLSS Research Center. The purpose of the luncheon was to recognize the REU students for their contributions to the ATLSS Research Center during the program. The picnic was attended by ATLSS Research Center faculty, staff, and students.

2.5 Student Deliverables

Requirements for successful completion of the program included each student formally presenting the findings of his/her research at the conclusion of the program. Presentations, targeted at 20 minutes in duration, took place at the ATLSS Research Center. Illustrations of students during presentation are provided in Figure 13. Cover slides from select presentations are provided in Figure 14.

In addition to the presentations, each student was required to submit a final technical report detailing his/her research findings. A copy of each student's final technical report is provided in Appendix C.

2.6 Student Feedback

Initial and final surveys were conducted in order to gather student expectations prior to and student evaluations following the program. Feedback from these surveys are detailed in the subsequent sections.

2.6.1 Overall Assessment of Program

In general, overall student assessments of the program were extremely positive. The program was termed "a very worthwhile experience" and "a good learning

experience” that would be “highly recommended to anyone that is interested”. A separate student was “very pleased with ATLSS/NEES program this summer”. Additionally, the students noted that the preparation and administrative aspects of the program were sufficient. Students felt that the number of workshops and activities were favorable for balancing the research requirements of the program, but also offered some recommendations for future programs. These recommendations are noted in Section 2.6.3.

2.6.2 Program Impact on Future Plans

Prior to the program, of the seven participating students, four of the seven students were considering graduate school, with none of the students considering Lehigh University. At the conclusion of the program, five out of seven students were considering graduate school, with four of the students considering Lehigh University. Additionally, four out of the seven students acknowledged that they would attend a similar program, if available, next summer, with three of the students declaring the question as not applicable due to their academic standing (graduation).

2.6.3 Recommendations

Recommendations regarding potential improvements to the program included providing the students with project-specific information prior to the onset of the course and incorporating an interviewing workshop into the program. Additional recommendations included incorporating an industrial tour focused on concrete and adding additional student luncheons to the schedule.

One recommendation introduced by the program’s Principal Investigator is to create and distribute the project poster early in the calendar year in order to attract more students to submit applications to the program. The current poster was solicited in April, which is somewhat late considering the start of the program at the end of May.

2.7 Summary

A ten week summer REU program was conducted at the ATLSS Research Center at Lehigh University under the direction of Dr. Chad Kusko. The program consisted of two parallel programs, ATLSSreu and NEESreu. The ATLSSreu program was funded by the Commonwealth of Pennsylvania, Department of Community and Economic Development. The NEESreu program was funded by the National Science Foundation, through NEESinc. The REU program provided undergraduate students with the opportunity to conduct research on a Civil-Engineering based research project under the direction of the project’s Principal Investigator and graduate student mentor. Additionally, the students participated in a diverse matrix of professional development workshops, industrial tours, and miscellaneous activities to provide the students with a well-balanced educational experience. At the completion of the course, students were required to present the findings of their research in a formal presentation and document these findings in a technical report.

2.8 References

1. Naito, C. and R. Connor, "Final Report 2003 Research Experience for Undergraduates", ATLSS Report No. 03-23, December 2003.

<p>Dr. Chad Kusko Principal Investigator Research Operations Manager, NEES RTMD Equipment Site</p> 						
						
ATLSSreu	ATLSSreu	ATLSSreu	ATLSSreu	NEESreu	NEESreu	NEESreu
Andrew Adams	Michael Angis	Chintan Desai	Christopher Hsiao	Geoffrey Madrazo	Mia Simmons	Gabriel Valencia
Pennsylvania State University	Lehigh University	Manhattan College	Lehigh University	The Georgia Institute of Technology	North Carolina Agricultural and Technical State University	San Jose State University
Research Advisor: Dr. Sougata Roy	Research Advisor: Dr. Sibel Pamukcu	Research Advisor: Dr. Clay Naito	Research Advisor: Dr. Yungfeng Zhang	Research Advisor: Dr. Richard Sause	Research Advisor: Dr. Clay Naito	Research Advisor: Dr. James Ricles
Graduate Student Mentor: Charles Labarbera	Graduate Student Mentor: Mark McElroy	Graduate Student Mentor: Lynne Starek	Graduate Student Mentor: Songye Zhu	Graduate Student Mentor: David Roke	Graduate Student Mentor: Joe Creek	Graduate Student Mentor: Oya Mercan
Research Project: Cost-Effective Connection Details for Highway Sign, Luminaire, and Traffic Signal Structures	Research Project: Thermoelastic Damping of Granular Media	Research Project: Destructive Evaluation of Failed Prestressed Adjacent-box Girders over I-70 near Washington, PA	Research Project: Shape Memory Wire Damper for Earthquake Resistant Steel Structures	Research Project: Behaviors of Post-Tensioning and Anchor Systems	Research Project: Development of Seismic Design Methodology for Precast Diaphragms	Research Project: Visualization Tool for Real-Time Hybrid Testing

Table 1. Outline of REU program administration and students, along with students' home institutions, project advisors and graduate student mentors, and project title.

LEHIGH UNIVERSITY **PITA** **ATLSS**

ATLSS/PITA Summer 2006 REU Program

Program Description and Outline
 Lehigh University's Center for Advanced Technology of Large Structural Systems (ATLSS) is offering undergraduate research fellowships for summer 2006. Funding for the fellowships is provided by the Pennsylvania Infrastructure Technology Alliance (PITA). The program is a 10-week research experience (May 30 – August 4) with a total stipend of \$4,400. Student will work under the direction of faculty and mentoring of graduate students on active research project in structures or materials. Workshops on report and presentation writing, along with Civil Engineering related site tours, will be included in the program. Students will be responsible for developing report and presentation on their research findings at conclusion of program.

ATLSS Research Areas
 Field Testing; Laboratory Testing; Structural Design; Structural Analysis; Finite Element Modeling; Innovative Materials; Blast Resistant Engineering; Earthquake Engineering; Sensor Technology; Bridge Systems; Building Systems; Foundation Engineering

Requirements
 Cumulative GPA 3.30 Preferred
 Junior or Senior status
 U.S. Citizen or permanent resident
 Minorities and women strongly encouraged
 Applications Available
<http://www.atlss.lehigh.edu/atlssreu>
 Application Deadline: April 28, 2006
 Notification Date: May 5, 2006

Contact Information
 Dr. Chad Kusko
cmk205@lehigh.edu
 ATLSS Research Center
 Lehigh University
 117 ATLSS Drive
 Bethlehem, PA 18015
 Phone: 610-758-6488
 Fax: 610-758-5302

Figure 1. ATLSSreu program 2006 announcement poster.

Research Experience for Undergraduates
NEESreu Program
Summer 2006

NEES

This is not your typical REU...
 Are you interested in changing the world around you? Do earthquakes and tsunamis excite you? Spend the summer studying these things and more while joining cohorts around the country.

Overview
 The George E. Brown, Jr. Network for Earthquake Engineering Simulation (NEES) is a shared network of experimental sites and tools, a centralized data repository, and an archive of earthquake engineering simulation software, all linked together by ultra-high-speed Internet connections. Together, these resources provide the means for collaboration and discovery in the form of more advanced research based on experimentation and computational simulations of earthquakes.

About the Program
 The NEESreu is a dynamic 10 week summer research program for upper division undergraduate students interested in Civil Engineering, Computer Science/Engineering and/or seismic risk mitigation. The program period is June through August, exact dates to be determined. Students receive a stipend plus additional funds for housing, meals and travel expenses. They will work with NEES researchers and participate in enrichment activities. Mentors will include university faculty, researchers and graduate students. Students may choose one of the following research sites: NEES in San Diego, CA at the Supercomputing Center or NEES at Auburn, NEES at Davis, or NEES at Lehigh. See www.nees.org for more information on these equipment sites.

Complete Application Includes

- Application form, including statement of purpose
- Academic Transcript form from all Universities attended
- One Academic Reference

All application materials should be received no later than: April 30, 2006

Application Requirements

- Minimum GPA for acceptance into the program is 3.0
- NEES limits participation in the program to U.S. citizens and permanent residents of the United States.
- The online application form is available at www.nees.org/NEESreu

www.nees.org/NEESreu

Figure 2. NEESreu program 2006 announcement poster.

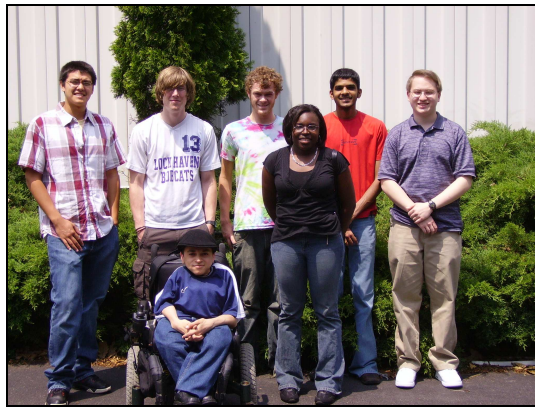


Figure 3. Summer 2006 REU program participants.



Figure 4. NEESreu student conducting research within the ATLSS laboratory.



Figure 5. Safety workshop incorporated into Summer 2006 REU program.



Figure 6. Library search workshop incorporated into Summer 2006 REU program.

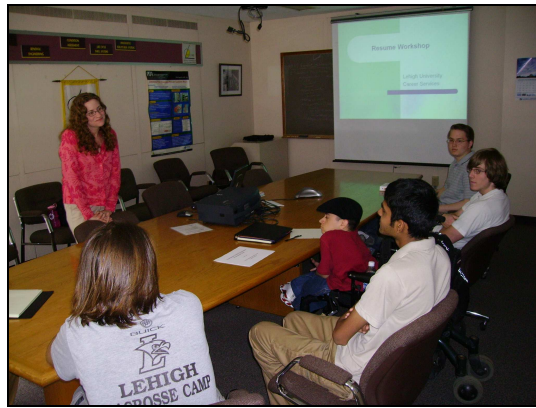


Figure 7. Resume building workshop incorporated into Summer 2006 REU program.



Figure 8. Effective presentation workshop incorporated into Summer 2006 REU program.



Figure 9. Images from visit to Susquehanna River Bridge Project.



Figure 10. Images from visit to Dorney Park.



Figure 11. Images from visit to High Steel Structures, Incorporated.



Figure 12. NEESreu students at 4th NEES Annual Meeting in Washington, D.C.



Figure 13. REU students presenting findings of research projects during program end presentations.

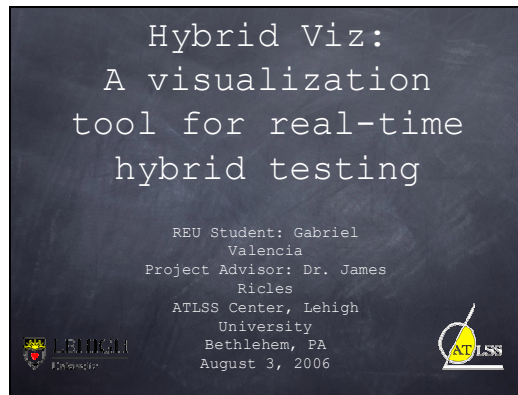
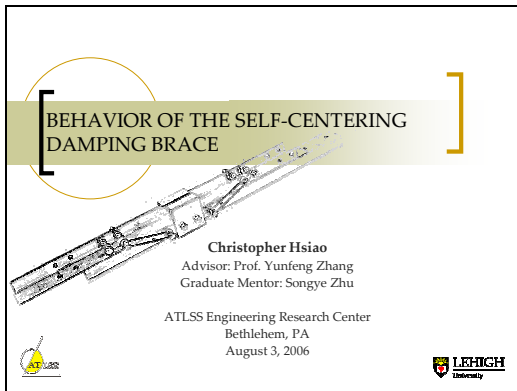


Figure 14. Title page from select student presentations.

Appendix A

Summer 2006 REU Program Application Package



ATLSS REU 2006 Application
(May 30, 2006 - August 4, 2006)

The application package (which is also available on the ATLSS REU homepage: <http://www.lehigh.edu/atlsreu>), consists of:

1. Personal information sheet
2. One page essay
3. Resume
4. Transcript
5. One letter of recommendation

Send the complete package to:

Dr. Chad Kusko
ATLSS REU Program
Lehigh University
ATLSS Research Center
117 ATLSS Drive
Bethlehem, PA 18015

The application package can also be e-mailed to chk205@lehigh.edu as an attachment and type in the Subject header: ATLSS REU 06, followed by the applicant's first and last name.

For additional information contact:

Dr. Chad Kusko, chk205@lehigh.edu, or 610-758-5488
Or visit the ATLSS REU homepage: <http://www.lehigh.edu/atlsreu>

Application Deadline: Friday, April 28, 2006

1

ATLSS REU 2006



ATLSS REU

Application Form Summer 2006

Personal Information	
Last name:	First name:
Name of institution:	Email:
Department:	Cumulative GPA (1-4.0):
Degree:	Current status (junior, senior...):
Major:	Name of recommender:
Campus address where you can be reached during the academic year:	Permanent home address:
Campus Phone:	Home Phone:
Post graduate plans:	Interests: Structural design <input type="checkbox"/> Structural analysis <input type="checkbox"/> Earthquake Engineering <input type="checkbox"/> Sensor Technology <input type="checkbox"/> Innovative Materials <input type="checkbox"/> Building Systems <input type="checkbox"/> Soil Behavior <input type="checkbox"/> Foundation Engineering <input type="checkbox"/>
MS: <input type="checkbox"/> Ph.D.: <input type="checkbox"/> M.D.: <input type="checkbox"/> work: <input type="checkbox"/> Not sure yet: <input type="checkbox"/>	Social Security Number:
<input type="checkbox"/> U.S. Citizen: <input type="checkbox"/> Permanent Resident	List any honors, prizes or awards:
Opposite information: <input type="checkbox"/> Male <input type="checkbox"/> Female Ethnic background (specify one or more): <input type="checkbox"/> African American <input type="checkbox"/> Asian <input type="checkbox"/> Hispanic, Native American, <input type="checkbox"/> Other	
Package includes: <input type="checkbox"/> Statement of purpose: <input type="checkbox"/> Resume: <input type="checkbox"/> Transcript: <input type="checkbox"/> One letter of recommendation	

Mail complete application package to: Dr. Chad Kusko, ATLSS REU Program, Lehigh University, ATLSS Research Center, 117 ATLSS Drive, Bethlehem, PA 18015-4729

2

ATLSS REU 2006

Statement of Purpose	
(Shows your reasons for applying to the ATLSS REU program; note any prior research experience and career goals.)	
Enter your name:	

3

ATLSS REU 2006

ATLSS REU Program Lehigh University	
Recommendation Letter Due: April 28, 2006	
Name of Applicant:	
This student has applied for the ATLSS REU 2006 program whose goal is to provide motivated and bright undergraduate students with hands-on research experience in the general area of civil and environmental engineering. Please comment on the student's intellectual qualifications, attitude towards research, and maturity. A letter can substitute this form.	
Admission to RITA REU Program is: <input type="checkbox"/> Strongly recommended <input type="checkbox"/> Recommended <input type="checkbox"/> Recommended with reservations <input type="checkbox"/> Not	
Recommender's name:	Signature
Position or title:	Date:
Delivery options: Please either give this form to the student in a sealed envelope or mail it directly to: Dr. Chad Kusko, ATLSS REU, Lehigh University, ATLSS Research Center, 117 ATLSS Drive, Bethlehem, PA 18015-4729.	
If e-mail or fax is preferred, please e-mail to: chk205@lehigh.edu or fax to Dr. Chad Kusko at 610-758-5502 with the subject: ATLSS REU 2006, followed by the applicant's first and last name.	

4

ATLSS REU 2006

Appendix B

Summer 2006 REU Program Schedule of Activities

Lehigh University NEES and ATLS 2006 Summer REU Program

Lehigh University NEES and ATLS 2006 Summer REU Program

Legend	
	Group on-campus activity
	Group off-campus activity
	NEES conference
	Holiday

May 29 Holiday	May 30 Housing Check-in 9:00 am – 12:00 pm @ Campus Square D lounge Program Orientation @ 12:30 pm in ATLS B101	May 31 Lab Safety and Tour – Chad Kuko @ 9:00 am in ATLS B101 Lab and Construction Safety – Randy Shelby @ 10:15 am in ATLS B101	June 1 Sharon Siegler – Library Search Training @ 9:00 am in ATLS B101 (both groups)	June 2
June 5	June 6	June 7	June 8 Amy Holzman Vasquez – Resume Building Workshop @ 8:45 am in ATLS A202 ATLS Lab Scheduling Meeting @ 12:10 pm (both groups)	June 9
June 12	June 13 Susquehanna River Bridge Tour @ 10:00 am (both groups)	June 14	June 15 Presentation Training – Elia Schoemer @ 9:00 am in ATLS B101 (both groups)	June 16
June 19 NEES@Lehigh: RTMD Seismic Training Workshop (8:00 am – 5:00 pm) in ATLS B101 (both groups)	June 20 NEES Annual Meeting in Washington, D.C. (NEES only)	June 21 NEES Annual Meeting in Washington, D.C. (NEES only)	June 22 NEES Annual Meeting in Washington, D.C. (NEES only)	June 23 NEES Annual Meeting in Washington, D.C. (NEES only)
June 26	June 27	June 28 Dorney Park Tour @ 8:30 am (both groups) ATLS Lab Scheduling Meeting @ 12:10 pm (both groups)	June 29 Technical Report Discussion – Chad Kuko @ 9:00 am in ATLS B101 (both groups) NEES REU Conference Call @ 1:00 pm (NEES only)	June 30
July 3	July 4 Holiday	July 5	July 6 NEES REU Conference Call @ 1:00 pm (NEES only)	July 7
July 10	July 11	July 12	July 13 NEES REU Conference Call @ 1:00 pm (NEES only)	July 14 Preliminary Presentations @ 10:00 am in ATLS B101 (both groups)
July 17	July 18	July 19 High Steel Tour @ 10:00 am (both groups)	July 20 NEES REU Conference Call @ 1:00 pm (NEES only)	July 21 Preliminary Reports Due to Project PI
July 24	July 25	July 26 Carpenter Technology Tour @ 9:30 am (both groups)	July 27	July 28 REU lunch @ 1:00 pm in ATLS B101
July 31	August 1	August 2	August 3 Final Presentations and Reports @ 9:00 am in ATLS B101 (both groups) NEES REU Conference Call @ 1:00 pm (NEES only)	August 4 End of Program Picnic at ATLS @ 12:00 pm

Appendix C
Student Final Reports

Thermoelastic Damping of Granular Geomedia

Michael Angis

Abstract:

This study looks at using recycled rubber as a geomedia in soil to lessen the harmful effects of earthquakes. It is a continuation of a study that proved that the inclusion of similarly sized rubber particles in soil can actually improve both the damping ability and the strength of a soil. In this experiment two smaller sizes of rubber are tested to determine how their inclusion affects the damping ability and the soils stiffness. Also tests were done to determine the effect of pressure on both of the aforementioned soil characteristics. It was found that the particles were too small and light to yield improvements in either stiffness or damping; however the sequence of increasing confining pressure increased both the strength of the soil and the soil's ability to attenuate vibrations.

Introduction

The notion that man-made products and waste products have valuable uses as geomedia mixed into soil has existed for close to 30 years (McGown et al. 1978). Since then many new innovative studies have produced evidence that waste products can have specific uses such as slope stabilization using pins made of recycled plastic (Loehr et al. 1999). Also studies have looked at mixing recycled fibers with sand for road construction and other purposes (Murray et al. 2000; Santoni et al. 2001). In addition the effectiveness of shredded recycled tire rubber was investigated for a number of different purposes including; as a lightweight construction material or backfill and as an attenuator of seismic waves around buried pipes or earthen systems in general; all yielding favorable results (Ishibashi and Sethabouppha 2000; Selgado et al. 1999; Farrag and Morvant 2000; Pamukcu and Akbulut 2006).

Contrary to intuition, it has been shown that the inclusion of rubber particles similar in size to the sand particles they are mixed with, not only increases the damping potential (due to rubbers elastic and ductile nature as well as its energy dissipating properties), but it simultaneously can increase the shear modulus (G) up to an optimal percentage of rubber in the mixture (Pamukcu and Akbulut 2006). Essentially the addition of 'stretchy' rubber into a mixture of fairly rigid soil actually can increase the soils overall stiffness if the optimum amount of these rubber particles are added. This observed behavior was believed to be a result of Herzian particle contact effects and mechanical damping, resulting from thermoelastic effects between the dissimilar particles (sand and rubber.)

This study, which parallels the above findings, seeks to determine the influence of the inclusion of dissimilarly sized rubber particles on the damping and shear modulus of the soil rubber mixture. The tests for both the previous findings and for this study were conducted on a resonant column device. The soil samples comprised of uniform size Ottawa sand, .6 - .85 mm particles, compacted with 10% kaolinite clay by weight at the mixture's optimum moisture content. In the aforementioned study the rubber inclusions

were uniformly sized particles in the range from .6 to .92 mm, while this study had powdered inclusions of two uniform sizes; sieve 20 (850 μm and sieve 30 (60 μm). The damping and shear modulus data were examined in an attempt to reveal whether or not both the damping and stiffness improved at an optimum mixture as occurred in the above mentioned study.

Background

Seismic attenuation is when vibrations are dampened by energy losses and become gradually weaker. Vibrations from highways or earthquakes can deteriorate infrastructures such as underground pipes or even buildings and bridges if the soil supporting these structures cannot adequately attenuate the waves through energy losses. The energy lost is dissipated as heat or absorbed in phase transformations (Pamukcu and Akbulut 2006). In soil the energy loss per cycle of free vibration is small, making it a low-loss media.

The two main components of energy losses in soil are hysteretic damping and viscous damping. Hysteresis refers to a system that slowly reacts to the forces applied to it and/or it does not return to its original state. Hysteretic damping is simply the frictional energy losses caused by global slippage at particle contacts. In other words the sliding at particle contacts plus the overall rearrangement of particles causes constant creation and destruction of contacts throughout the soil (Pamukcu and Akbulut 2006). It is typically independent of strain amplitude and frequency of vibration

Viscous damping is caused by dispersive effects of wave-fluid interaction (Biot 1956a,b). Viscous losses are the relative displacement of pore fluid with respect to the solid phase. Biot stated that on the large scale viscous damping is related to the permeability, grain size, and pore structure of the mixture. Also it is rate dependent meaning that the attenuation of shear waves depends on the wavelength, and the value of viscous damping will initially increase with frequency until a critical frequency is reached (Ellis et al. 2000). Locally viscous damping is related to liquid motion between the particles.

Although the energy losses are not as large as viscous or hysteretic damping, there are two other types of damping relevant to this study. First is apparent damping, which simply refers to wave attenuation caused by reflection and scattering in non-homogenous media (Pamukcu and Akbulut 2006). A mechanical energy dissipating process called thermoelastic damping is quite relevant as well. Thermoelastic damping is due to two complementary processes; the piezocaloric effect and thermal diffusion.

The piezocaloric effect is complimentary to thermal expansion (Zener 1938). It is associated with a change in temperature in response to strain. Thermal expansion occurs when materials are loaded at a constant temperature and then unloaded too quickly for heat flow. The result is an overall decrease in temperature. Thermal diffusion is a result of heat transfer between dissimilar materials in a mixture (Lakes 1997). Heat is created by strain and then flows through the non-homogenous mixture with different thermal expansion properties. The heat causes elastic deformations of the particles in the mixture, which in turn creates more strain. Finally, the phase difference between the created and applied strain fields dissipates mechanical energy.

Damping can occur many ways in non-homogenous mixtures of soil. Thus, since damping is the attenuation of energy waves or vibrations it is logical to try to utilize damping types (such as thermoelastic damping) as a means to reduce the harmful effects of earthquakes, highway traffic, and other vibrations by introducing man-made geomedia into naturally occurring soil in an attempt to alter the elastic, thermal, mechanical, or other properties of the soil.

Experimental Program

Planning

A control was needed as a basis of comparison for the rubber tests to help quantify its effects on the soil properties. The control contained 90% sand by dry weight and 10% kaolinite. The kaolinite clay was added to keep like particles from clumping together and to generally bind the material together. The optimum water content was found to be 4% of the total dry weight by means of a compaction test and was held constant for all samples. The majority of the water is soaked up by the clay to form the 'paste' that holds everything together. Since clay is such a small percentage of mass (and even smaller percentage of volume) it is reasonable to assume that the clay in the mixture had negligible effect on particle-to-particle interaction.

The sieve 20 and sieve 30 sized rubber testing samples contained their respective size of rubber in three different percentages by dry mass 7.5, 15, and 22.5%. The clay stayed constant at 10% and the water content at 4%. Thus, when either size rubber was added, the component that was lessened in mass percent was the sand.

Materials and Sample Preparation

The tests for the control and the three different percentages of each rubber were performed on laboratory-compacted 71 mm diameter and 135-145mm high cylindrical specimens of each respective mixture. As stated previously the percent clay was 10% and percent water was 4% of the total dry weight for each specimen. The synthetic particles added were round powdered rubber size sieve 20 and sieve 30. The minerals in the soil were rounded and sub-rounded.

Each sample was prepared by first adding all the necessary sand and clay, then mixing the proper amount of water to achieve the predetermined optimum moisture content of 4%. The synthetic particles were then mixed into the wet soil mixture. The specimens were prepared by compacting a moist mixture of the soil into a column. This was done by loading four layers of the mixture into a latex membrane lined split mold using a ceramic damper (all of which may be seen below in Figure 1.)

Fig. 1. Sample Preparation Equipment



Also its important to note that as the percentage of rubber in the sample increased the mass density decreased because the rubber is much less dense then any of the components of the wet soil mixture. Also since the water is added before the rubber it is logical that the actual water content of the samples decrease as higher percentages of rubber are added.

Testing

Fig. 2. Drenvich Longitudinal-Torsional Resonant Column



A Drnevich longitudinal-torsional resonant column was used in torsional excitation mode to test the dynamic properties of all samples (Drnevich et al. 1978). Compression and shear wave velocities of soils tested in a resonant column can be determined from their resonant frequency (Pamukcu and Akbulut 2006). The shear modulus, G , can be determined from equation 1 below:

$$(1) \quad G = \rho(2\pi L)^2 \left(\frac{f_L}{F_T} \right)^2$$

where ρ is the mass density, L is the length of the sample, F_T is the natural resonance fundamental frequency of the resonant column, and f_i is the soil's resonance frequency for a given torsional strain amplitude.

The strain is controlled by the input voltage to the coils driving excitation platen resting on top of the sample. It is calculated by the following equation:

$$(2) \quad \gamma_d = \frac{.4 \times RCF \times RTO \times d}{L}$$

where the RCF is the resonance calibration factor of the column divided by the square of the resonant frequency for a particular amplitude, the RTO is the soil torque response to a given solicitation amplitude, d is the diameter of the sample, and finally L is the length of the sample.

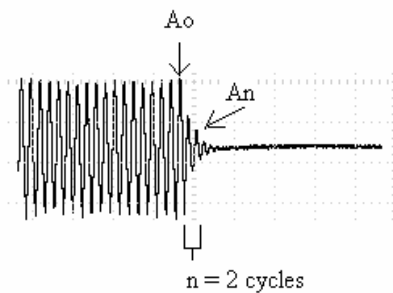
The compacted samples were loaded at a sequence of 5, 10, 15, 20, and 25 psi of confining pressure. The resonant frequency of each test sample was measured by analyzing the input and output signal on an oscilloscope at increasing strain amplitudes by increasing the applied voltage. The resonant frequencies in testing ranged from 4 to 11 Hz. For each mixture vibration amplitude decay was performed at resonant frequency to determine the corresponding damping ratio.

The damping ratio, a measure of the sample's ability to attenuate vibrations, can be calculated by conducting the run-down tests (which consists of cutting off the vibration signal to the sample and evaluating the attenuation) and then using the following equation:

$$(3) \quad D = \frac{1}{2\pi \cdot n} \times \ln\left(\frac{A_0}{A_n}\right) \times 100\%$$

where A_0 is the amplitude directly after shutting off the vibrations and A_n is the amplitude n cycles away from A_0 (as shown below).

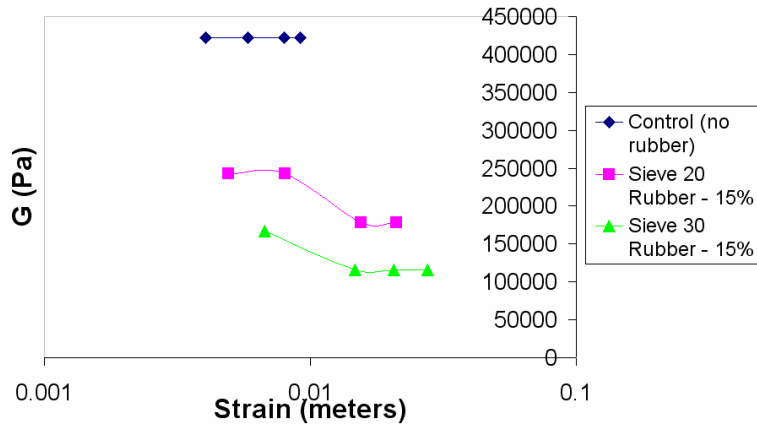
Fig. 3.



Results

Shear Modulus

Fig. 4. G vs. Strain at 15 psi



In Fig. 4 the shear modulus, G , is plotted against the strain for the control and for 15% by mass mixtures of the two different sized rubbers. The graph is a representation of how the soil's shear strength is affected by the magnitude of vibration. The G gets smaller because the soil's particles are moving more and the whole sample is less solid and stiff. This graph also shows that the control is much stiffer than the two samples with rubber mixed in and that the control was unaffected by increased strain, unlike the rubber mixtures.

Confining Pressure and Shear Modulus

Each sample was confined under a series of 5 varying pressures; 5, 10, 15, 20, and 25 psi to test pressure effect on the soil's stiffness. In addition at each pressure strain was gradually increased so that the effect of pressure could be seen on a G vs. Strain plot. Fig.'s 5, 6, and 7 show the effect of the sequence of confining pressure on the control, the 20 sieve rubber, and the 30 sieve rubber respectively.

Fig. 5.

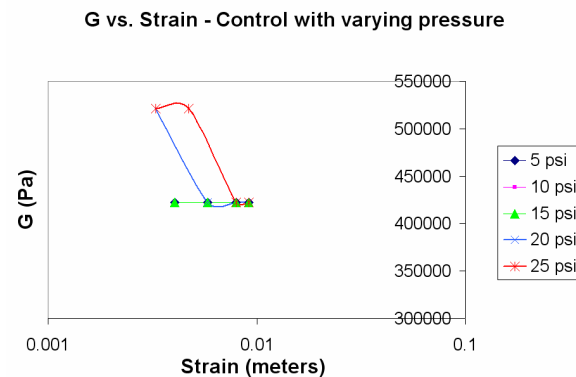


Fig. 6.

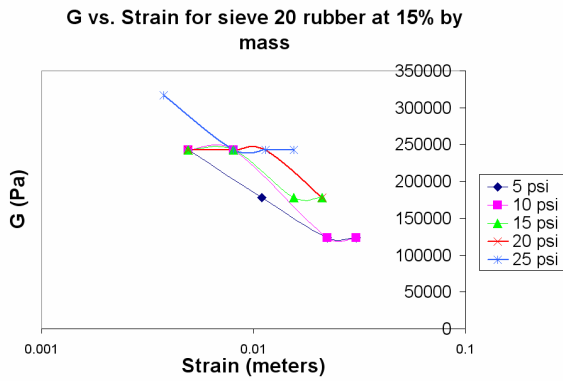
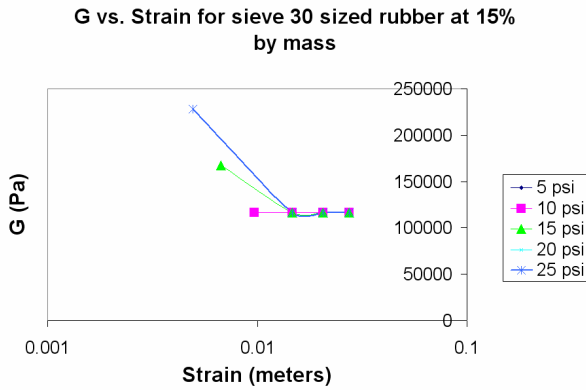


Fig. 7.



Essentially all three of these graphs show that for their respective mixture composition, as pressure increases so does the stiffness at equal strains. Also it shows consistency with Fig. 3 because as strain increases the stiffness decreases and because of the scale of the y axis on each graph indicates that overall the control is the stiffest, followed by the sieve 20 rubber mixture, and finally the sieve 30 rubber mixture.

Damping

Fig. 8.

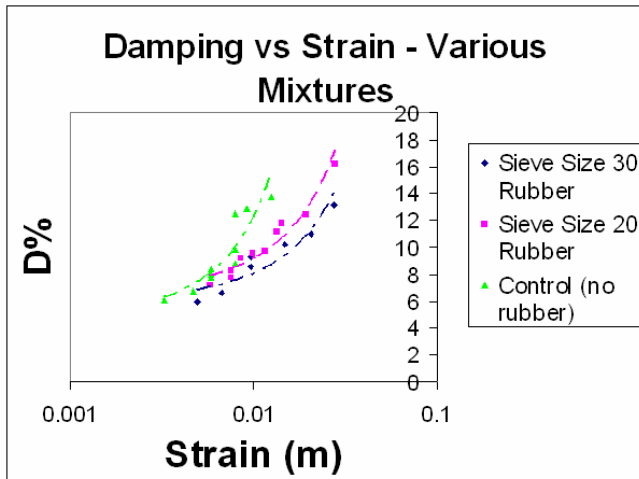
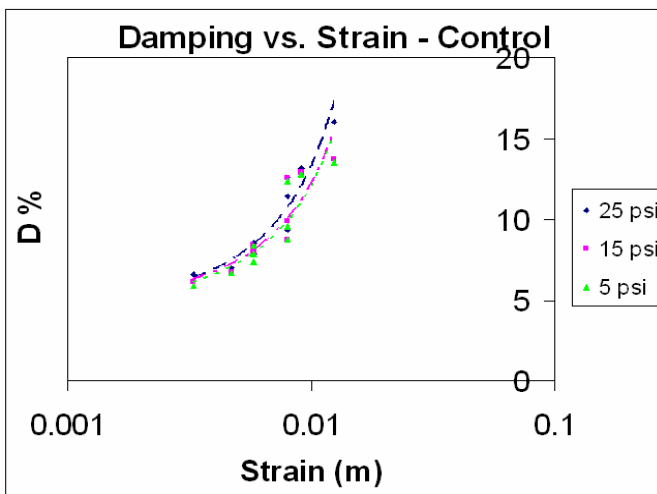


Fig. 8. above, represents each different mixture's ability to dampen the signals of vibration. It shows that at equal values of strain the control was the best at damping the energy from the column. The larger sized (sieve 20) rubber mixture was the next most effective in attenuating waves of vibration, finally followed by the smallest size rubber mixture (sieve 30).

Confining Pressure and Damping Ratio

Figures 9, 10, and 11 to the right and below show how a sequence of confining pressures affected the damping ratio on each mixture.

Fig. 9.



Basically this shows that for the control the increasing pressure also made the ability of the soil to attenuate vibrations increase. Below are figures that depict a consistent result with the other two mixtures.

Fig. 10.

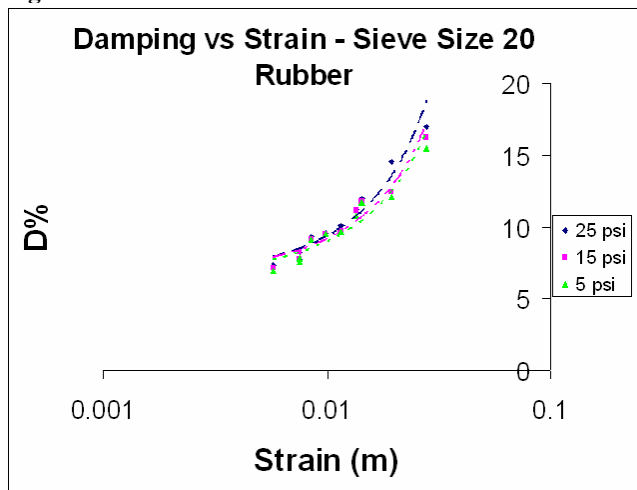
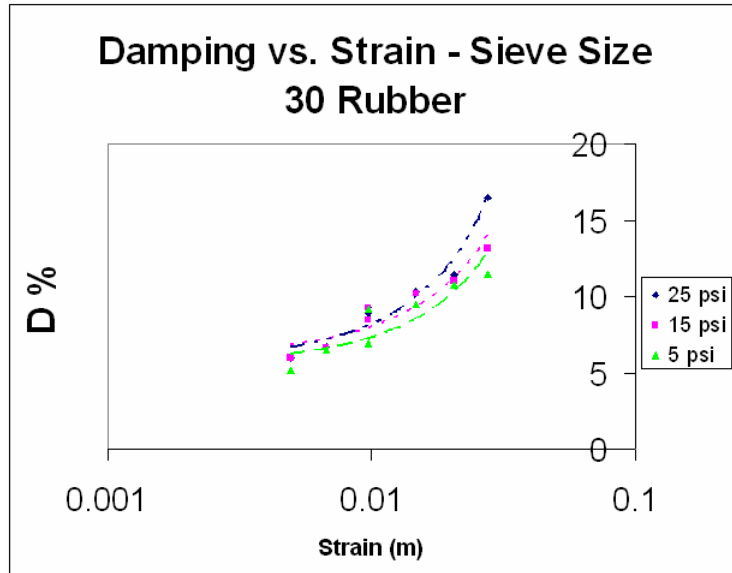


Fig. 11.



Conclusions

Previous evidence indicated that synthetic rubber particles similar in size to the minerals in the soil would actually increase both the stiffness and the damping potential of a soil if mixed in at the optimum percentage. In this case the stiffness (measured by shear modulus, G) was lower than the control for all mixtures that included the rubber. This is most likely due to the fact the rubber particles used in this study were not of similar size or density to the sand. Part of what makes the soil stiffer is that dissimilar particles (rubber and sand) are contacting each other and when vibrations go through the contacts the sand pushes on the rubber causing it to stretch, thus dissipating energy. This allows soil with rubber to be more elastic than regular soil, but if too many rubber particles are touching each other the overall stiffness may be sacrificed. This is most likely what occurred during this study. The rubber used was so small that to make up the desired mass percentages in the mixture a very large number of tiny particles had to be added. The addition of such a large number of small rubber particles most likely created very non-uniform particle contacts (i.e. places where rubber touched rubber or where sand touched a different number or a different sized cluster of rubber particles) and thus, the overall stiffness did not increase because the size differential of the sand and rubber particles created an unstable mixture.

As far as the confining pressure sequence applied to each sample is concerned, the basic conclusion to make is that confining a sample under a higher pressure causes its strength (measured by shear modulus) to increase as well as its damping potential. This makes sense intuitively because basically the confining pressure is like the sample's atmosphere and its atmosphere is pushing in on the sample in all directions. Inward pressure at all directions makes it harder to agitate because the air is doing some of the

work of holding it together. Thus, when the pressure increases, G will increase as well at a particular strain value because it is harder for the column of soil to be agitated with forces acting inward on it.

The main conclusion that can be made from the damping results is that the control is the best at attenuating waves and that the inclusion of rubber was not helpful in improving either the strength or the damping ability. Most likely this is due to the same reasons discussed in the shear modulus conclusion. Dissimilar particle contacts, which are what makes rubber inclusion helpful for damping, were not prevalent in the mixture because there were too many very small, light, rubber particles in relation to the amount of sand particles.

Rubber *can* effectively be used to dampen energy from earthquakes when mixed into the soil as previously proven (Pamukcu and Akbulut 2006). However, if the size and density of the particles of rubber and sand are not similar; the soil may be stronger and superior at attenuating vibration waves as it exists naturally without the addition of rubber or any other geomedia of unmatched size.

Notation

The following symbols are used in the paper:

A_0, A_t, A_n = amplitudes of vibration at various times and cycle numbers;

D = damping ratio;

d = diameter of sample;

F_T = natural resonance fundamental freq.

of the resonant column;

f_t = soil resonance freq. for given torsional amplitude

G = shear modulus;

L = length of sample;

n = number of cycles of vibration;

RCF = resonance calibration factor;

RTO = soil torque response to given amp.

w = water content;

α = coefficient of thermal expansion;

γ = shear strain;

ρ = mass density.

Acknowledgements

Professor Sibel Pamukcu, Department of Civil and Environmental Engineering
Lehigh University

Mark McElroy, Graduate Student, Department of Civil and Environmental
Engineering, Lehigh University

Dr. Chad Kusko, ATLSS Research Center, Lehigh University

References

- Biot, M. A. (1956a). "Theory of propagation of elastic waves in a fluid saturated porous solid: I. Low frequency range." *J. Acoust. Soc. Am.*, 28, 168-178
- Biot, M. A. (1956b). "Theory of propagation of elastic waves in a fluid saturated porous solid: I. High frequency range." *J. Acoust. Soc. Am.*, 28, 179-191
- Drnevich, V.P., Hardin, B. O., and Shippy, D. J. (1978). "Modulus and damping of soils by the resonant-column method." *Dynamic geotechnical testing*, ASTM STP 654, Reston, Va., pp. 91-152
- Ellis, E. A., Soga, K., Bransby, M. F., and Sato, M. (2000). "Resonant column testing of sands with different viscosity pore fluids." *J. Geotech. Geoenviron. Eng.*, 126(1), 10-17
- Farrag, K., Morvant, M., (2000). "Evaluation of the use of shredded tires around buried pipes." *Louisiana Transportation Research Center*, 1, 11-13
- Ishibashi, I., Sethabouppha, S., (2000). "Use of EPA-filled recycled tires as lightweight construction material." *79th Annual Transportation Research Board Meeting, Washington, D.C., January 2000*, 1
- Lakes, R. (1997). "Thermoelastic damping in materials with a complex coefficient of thermal expansion." *J. Mech. Behav. Mater.*, 8, 201-216
- Lee, J.H., Salgado, R., Bernal, A., and Lowell, C. W. (1999). "Shredded tires and rubber-sand as lightweight backfill." *J. Geotech. Geoenviron. Eng.*, 125(2), 132-141
- Loehr, J. E., Bowders, J. J., Owen, J. W., Sommers, L., Liew, W., (1999). "Stabilization of slopes using recycled plastic pins." *TRB 01 August 1999*, 1, 13-14
- McGown, A. K. Z., and Al-Hasani, M. M. (1978). "Effect of inclusion properties on the behavior of a sand." *Geotechnique*, 28(3), 327-346
- Murray, J. J., Frost, J. D., and Wang, Y. (2000). "Behavior of a sandy silt reinforced with discontinuous recycled fiber inclusions." *Transportation Research Record*, Transportation Research Board, Washington, D.C., 9-17
- Pamukcu, S., Akbulut, S.,(2006). "Thermoelastic enhancement of damping of sand using synthetic ground rubber." *J. Geotech. Geoenviron. Eng.* 132(4), 501-510
- Santoni, R. L., Tingle, J.S., and Webster, S.L. (2001). "Engineering properties of sand-fiber mixtures for road construction." *J. Geotech. Geoenviron. Eng.*, 127(3), 258-268
- Zener, C. (1938). "Internal friction in solids. II: General theory of thermoelastic internal friction." *Phys. Rev.*, 53, 90-99

PRELIMINARY TESTING AND ANALYSIS OF THE REUSABLE SELF-CENTERING DAMPING BRACE

Christopher Hsiao
Lehigh University
REU Institution: Lehigh University
Project Instructor: Professor Yunfeng Zhang

1. Abstract

A new type of bracing element termed self-centering damping brace (SDB) is examined. This brace exploits the superelastic property of NiTi SMA wires to self-center the structure after an earthquake and absorb some energy, but uses the concept of the friction damper as the main source of seismic energy dissipation. NiTi possesses outstanding fatigue properties that allow it to be subjected to hundreds of cycles under cyclic loading without any residual deformation. The results from tests performed on a prototype suggest that this brace can possess excellent energy absorption and still retain the self-centering capability of superelastic SMA, reducing permanent structural damage following an earthquake.

2. Background

2.1. SMA materials

Shape Memory Alloys (SMA) have been greatly researched and examined for use as passive energy dissipaters in dampers and braces for structures, but have not been widely implemented in current structures. This is mainly due to a lower hysteretic behavior than other common dampers, although their self-centering ability is very useful. NiTi is the most common, commercially-produced SMA because of the ability of the material to retain its original form. It can also endure 100,000 cycles under cyclic strain while $\epsilon_{\max} = 0.02$ (Funakubo 1987), and over 2000 of cycles under 6-8% strain (Zhang and Zhu, 2006). NiTi has good hysteretic behavior and is capable of attaining a maximum of 8% strain, and yet recover its original position and length with no residual deformation.

SMA materials possess two key characteristics: the shape memory effect, and the superelastic effect. These two effects are temperature dependent. However, by varying the composition of NiTi, the effect can be changed so that either the shape memory effect or the superelastic effect can be present at any temperature. The shape memory effect occurs when the SMA is “deformed” under some load. When heat is applied to the material, it self-centers itself so that no residual strain remains, as long as the maximum strain the SMA is exposed to does not exceed 8%. This entire process is displayed in the graph of Figure 1 (shown on top of next page). Under the superelastic effect (Figure 2), the SMA wire reacts almost like a rubber band, snapping back into its original position and length between loading cycles. Here it must be noted that superelastic SMA is most often used with potential brace design and seismic research.

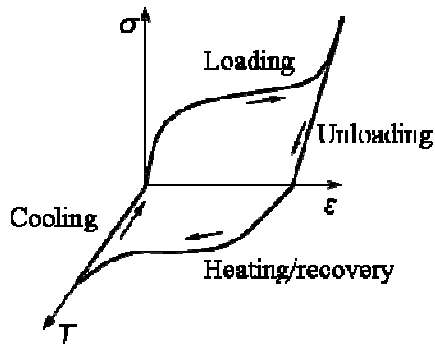


Figure 1. The shape memory effect. Stress vs strain (or deformation) vs temperature

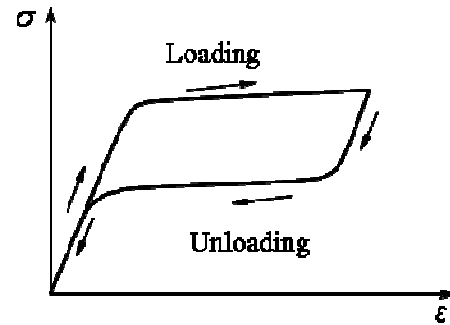


Figure 2. The superelastic effect. Stress vs strain (or deformation)

2.2. Conventional damping devices

Different types of passive energy dissipation systems are in use around the world, and many of them utilize deformation or yielding during earthquakes as a primary source of energy dissipation. However, in the event of a strong earthquake, this often results in structural deformation and requires the replacement of such devices, which very quickly turns into a costly investment.

Moment-resisting frames use joints that have high plasticity, making the building less rigid, and allowing the building to sway rather than attempting to eliminate lateral movement. This design has been proven very effective in energy absorption, but at the same time makes the frame vulnerable to high lateral displacements during a strong earthquake (Zhang and Zhu 2006). This creates concern for the integrity of the structure, and steps must be taken to avoid problems with ductile and brittle fracture at the connections of these structures following an earthquake (FEMA 2000).

Buckling restrained braces (BRB) are moment-resisting braces that are rigid, and achieve a high hysteretic behavior by yielding of the brace's core under compression and tension (Uang et al. 2004). The BRB brace possesses a large amount of stiffness, but also achieves the same ductility as moment-resisting frames. This brace is currently being used as a viable solution to conventional braces in moment-resisting frames because of the ability of BRB to withstand buckling (Sabelli et al. 2003). However, under medium to strong earthquakes, this brace usually needs to be replaced, because the material does yield, and performance will decrease following an earthquake. Permanent story drift of the structure might require costly repairs to satisfy the Immediate Occupancy requirement, and also convince the occupants that the building is safe. At the same time, some residual stress will always remain in the brace.

Friction dampers have recently been implemented in centrally loaded moment-resisting frames. These dampers usually consist of two parts with a friction surface in contact. The basic design of most of the dampers consists of hard, specially treated metal as the friction surface to improve the damper's usage life (Morgen and Kurama 2004). This has

greatly increased the energy dissipation of the structure, and also decreased the amount of residual drift experienced. However, friction dampers will deform from frequent earthquakes and need to be replaced.

2.3 SDB concept

The self-centering damping brace is a novel concept of using friction in a brace as the main source of energy dissipation, and then using Nitinol SMA wires to self-center the beam and absorb additional energy. As seen in Fig. 3, the hysteretic behavior of the SMA brace should be greater than either the friction damper or the SMA brace, and still exhibit the self-centering effect, key to reducing residual story drift following an earthquake.

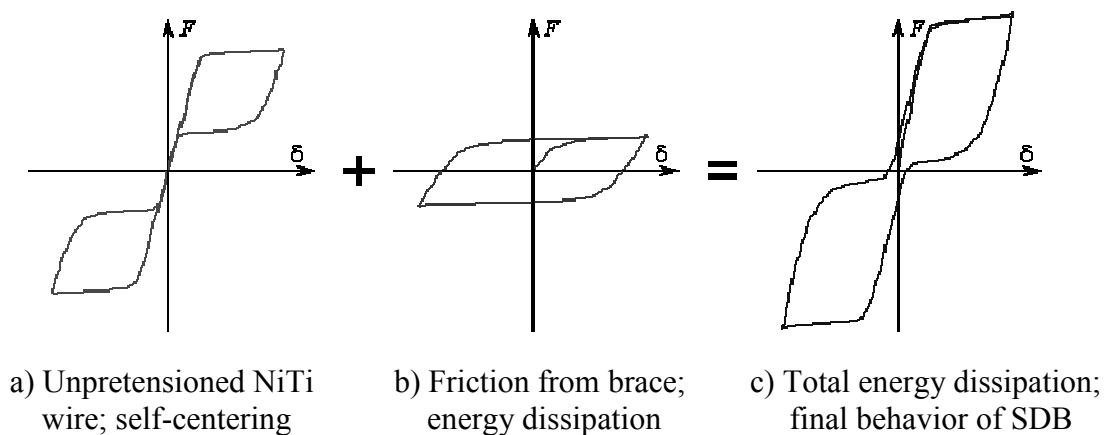


Figure 3. Force vs Deformation graphs

Studies by Zhang and Zhu (2006) indicate that the NiTi wires used in this project can recover “deformation” up to 8% of its initial length without residual deformation. If exceeded, permanent deformation will begin to occur. The 8% maximum recovery corresponds to a story drift ratio of 2%; therefore if the strain of the structure utilizing SDB braces remains below 2%, the structure should be capable of recovering its original position without deformation. The potential reusability of this device is perhaps the most intriguing aspect of the self-centering damping brace. Unlike the BRB brace, which will yield under frequent earthquakes, the NiTi wires in the SDB have the potential to absorb energy without any residual strain whatsoever. This would only hold true for earthquakes within the designed parameters.

3. Testing Conditions

3.1. Model of SDB

The SDB prototype was constructed at 1/6 of the theoretical size of an actual SDB brace (estimated length would be ~20 feet). The model was composed of two separate parts made from aluminum with steel plates attached to one side. The two pieces were then

allowed to slide past each other (with the steel surfaces in contact), to emulate the friction part of the brace. Bolts were then used to increase the normal force between the steel plates, thus increasing the friction. Superelastic Nitinol SMA wires were then anchored on the two pieces, allowing for two pairs of strands to always be in tension regardless of whether the brace itself is in tension or compression.

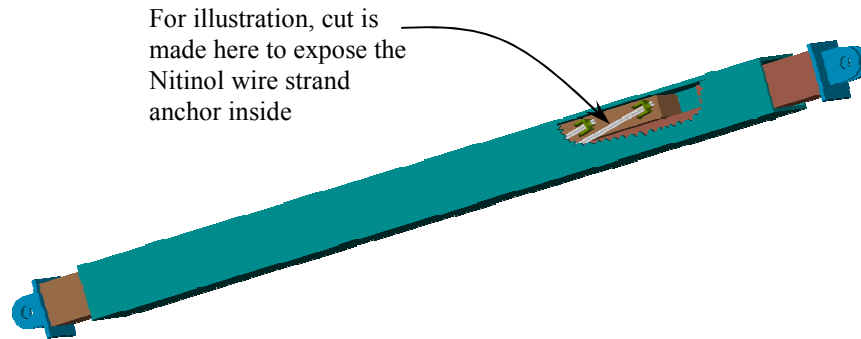


Figure 4: Schematics of the mechanical configuration of SDB

3.2. Test machine

The tests of the prototype were conducted on a 5500lb MTS machine using an Instrum controller (Figure 5; top next page).

3.3. Materials used in prototype

- Aluminum channel (Fig 5 displays the model loaded on machine; top of next page)
- Stainless steel plates attached to frame simulate the friction surfaces
- Steel hex bolts increase normal force between friction surfaces (1/2 x 13 x 2)
- Unpretensioned, Superelastic Nitinol (NiTi) wires of ten inch length (shown in Fig. 6); composition: 49% Ni, 51% Ti; diameter .023 inches
-10 loops for fourteen tests
- Temperature: 23 degrees centigrade

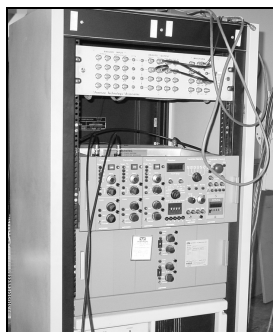


Figure 5. Instrum Controller



Figure 6. Prototype loaded onto MTS



Figure 7. Superelastic SMA wires attached

3.4. Test results

The SDB model was tested without any friction, in order to obtain the hysteretic behavior of the NiTi wires utilized in this experiment, and the resulting data was calculated and analyzed to obtain the hysteretic behavior of the brace and the minimum friction force (see Figure 8: a and d, respectively). To obtain this data, a lubricant was applied between the two steel plates then the SDB was subjected to cyclical loading. The SDB was also tested with only the steel friction plates in contact as shown in Fig. 8: b and e. The normal force applied by the steel bolts was then tested, and displayed the average hysteretic behavior of the brace graphed in the last column of Fig 8. Please note that this data is from the test performed on the prototype, and is merely to illustrate how the energy dissipation is enhanced and distributed between the friction and SMA parts of the SDB brace.

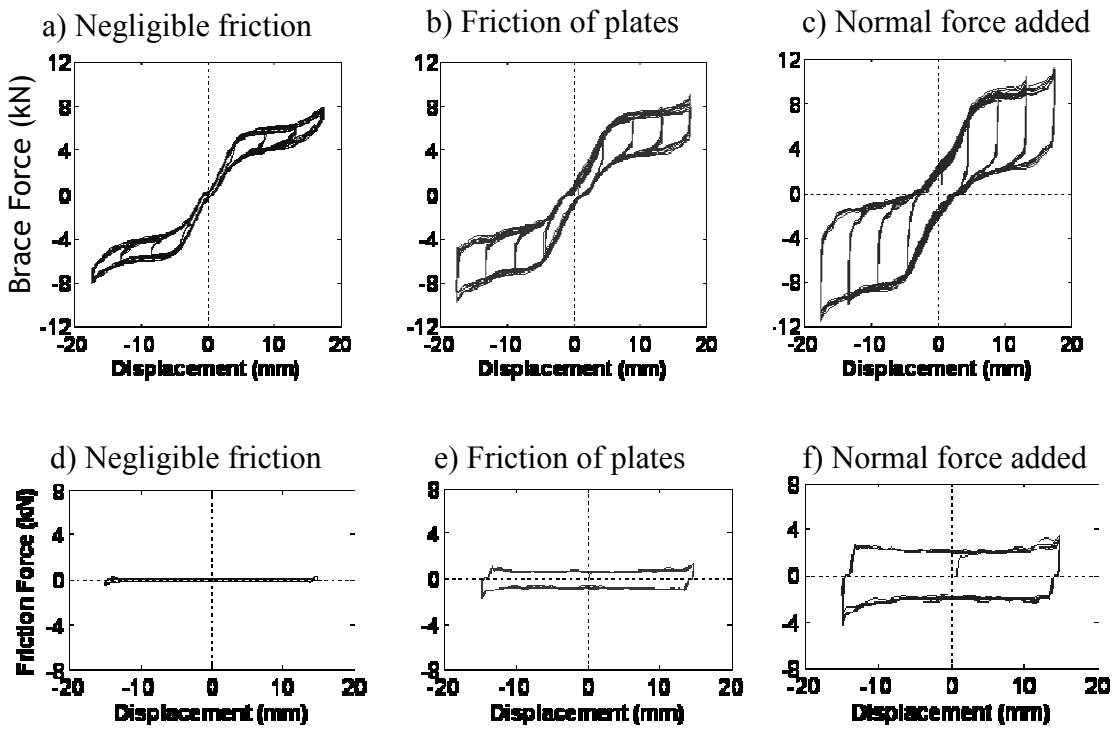


Figure 8. Hysteresis of SDB brace (a-c) and friction force in SDB (d-f)

The loading was applied to the prototype in the form of a sinusoidal wave, as the plot of displacement vs time (shown in Figure 9) displays. Also worth noting is how the wires start and end with zero displacement, displaying the self-centering effect of the SMA wires.

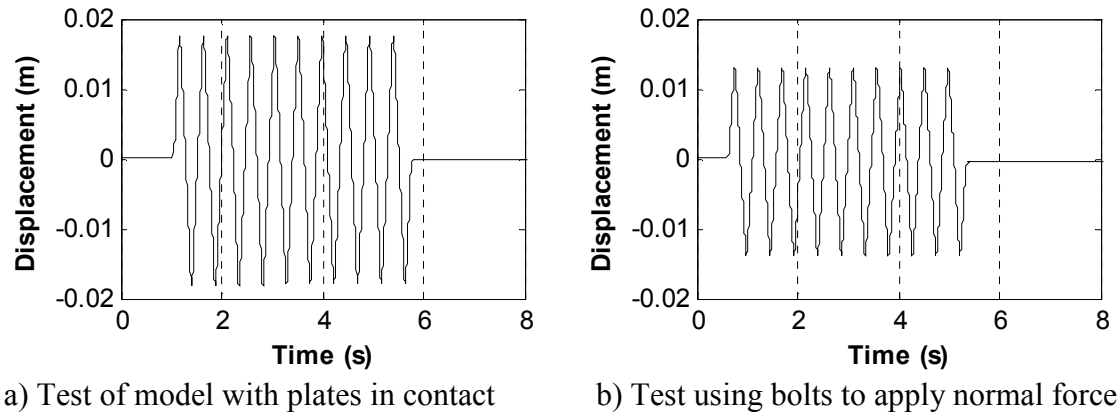


Figure 9. Sinusoidal wave used in testing

5. Results

5.1. Analysis of test results

When comparing the hysteretic behavior of the SDB brace displayed in the first row of Figure 8, it is easily seen that the energy dissipation by this brace enhances both the energy dissipated by friction and the SMA NiTi wires. The friction force, displayed in the bottom row of Figure 8, demonstrates that the friction force is playing the key role in energy dissipation. The Nitinol wires are enabling the brace to absorb some additional energy, as shown in Figure 8 (a, d), and will self-center the brace itself.

5.2. Pushover analysis of SDB

Pushover analysis uses a predefined load pattern applied in increments laterally against the structure to perform static analysis of the frame. This is useful because it emulates how the structure would react, and determines what nodes or columns are weaknesses in the structure (Habibullah and Pyle, 1998). This procedure was applied to a model of the SDB following testing of the prototype.

Pushover analysis was carried out in DRAIN-2DX using a new element model designed by Zhang and Zhu (2006) and presented at the 4th World Conference on Structural Control and Monitoring. This element simulates the hysteretic behavior of the SMA damping brace under seismic loads. The frame, shown in Fig. 11, was subjected to twenty loading patterns provided by data from the Los Angeles 1994 Northridge earthquake, and proved comparable to the BRB in almost every respect.

Test data from the analysis showed that the SDB brace was capable, in this example, to self-center itself with no residual deformation following the loading of the earthquake data. However, the BRB braced structure withstood the earthquake, but with a permanent deformation of approximately .01 per story (as demonstrated in figure 10 at top of next page, where the BRB data is displayed in red).

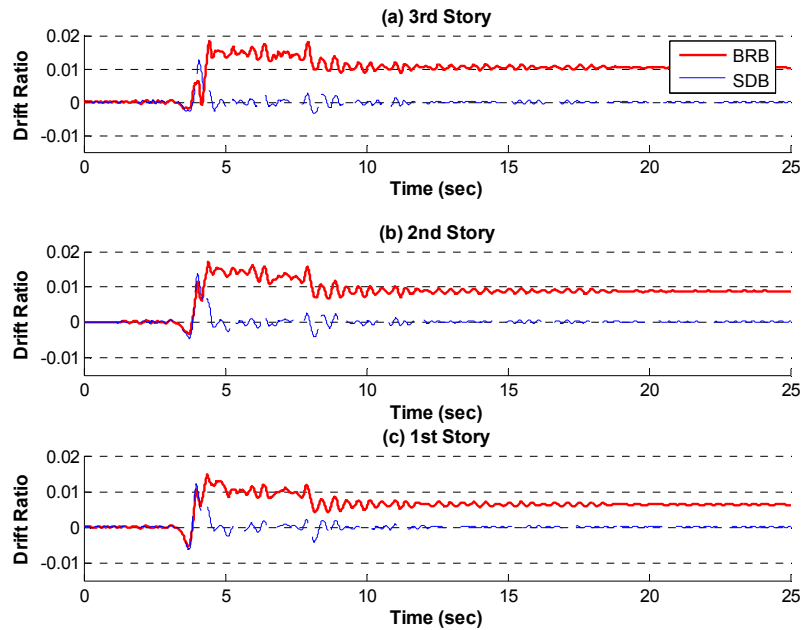


Figure 10. SDB and BRB Drift Comparison

In the pushover analysis performed for this project, the frame was subjected to a lateral load, increasing at a constant increment until failure occurred. The BRB brace and SDB brace were both modeled and analyzed in DRAIN-2DX.

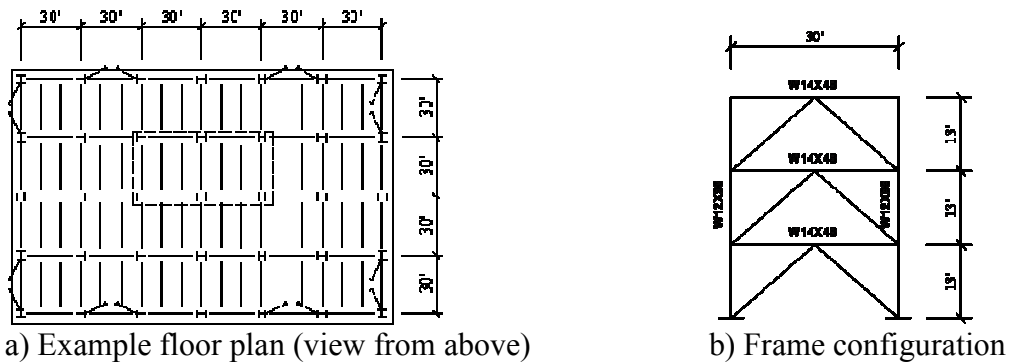


Figure 11. Prototype structure

The loading pattern for this analysis of the SDB brace was determined according to the procedure presented in the FEMA 369 provisions on provisions for seismic regulations for new buildings (FEMA 2001). Equations 1 and 2, shown below, define how the load pattern was determined (F_{xm} = modal force, V_m = base shear in m^{th} mode, C_{vxm} = vertical distribution factor in m^{th} mode, W_i and W_x = portion of total gravity load on level i or x , Φ_{xm} and Φ_{im} = displacement amplitude at the x^{th} or i^{th} level).

$$C_{vxm} = \frac{W_x \Phi_{xm}}{\sum_{i=1}^n W_i \Phi_{im}} \quad (\text{Eq. 1})$$

$$F_{xm} = C_{vxm} V_m \quad (\text{Eq. 2})$$

The base shear and roof displacement (as a percentage of building height) of the SDB brace was subsequently calculated from the load pattern determined, and plotted in Figure 12. This analysis was also carried out on the BRB brace, and plotted in Figure 13 for comparison with the results from the SDB brace.

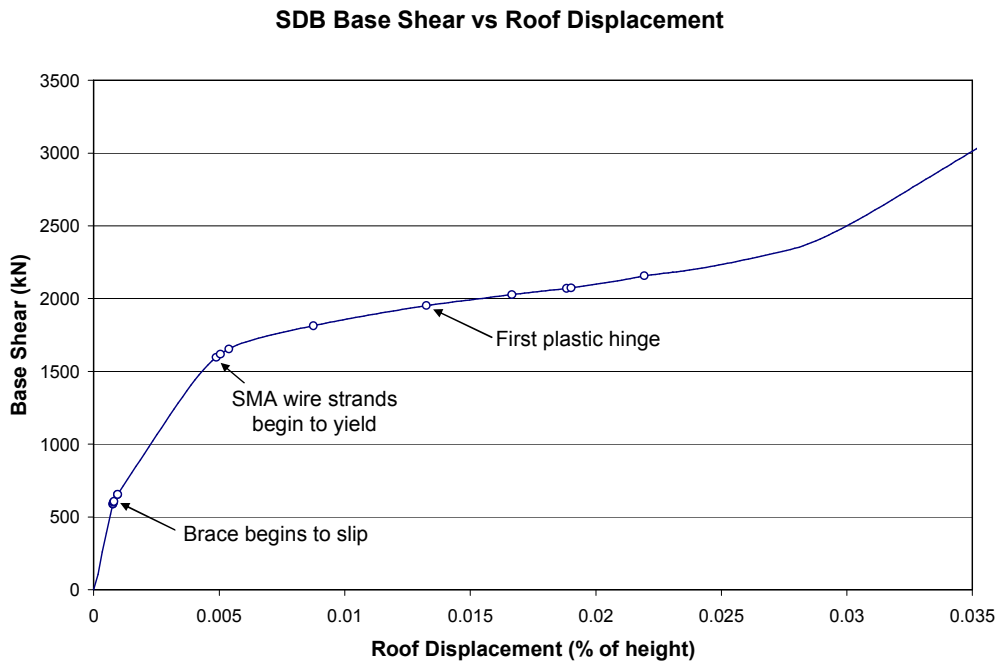


Figure 12. Behavior of SDB brace

As seen above, the SDB brace originally has much stiffness, but then once the friction portion of the brace begins to slip, the stiffness decreases to a certain extent. Next, the SMA wires begin to yield (as labeled), and soon after the first plastic hinge begins to occur in the frame itself (in this case, the left-hand side of the third floor of a frame like that in Fig. 11.b). After the components of the structure begin to yield, the SDB brace then begins to stiffen once again. This is due to strain hardening in the SMA wires. Of course, the maximum amount of energy this brace can dissipate is also limited to the force the components of the building's frame is able to withstand as well.

The BRB brace, displayed on the top of the next page, behaves with more stiffness over the initial loading of the earthquake. The brace begins to yield at about the same point as the SMA wires in the SDB. However, after the first plastic hinge occurs in the structure and the other parts of the structure begin to yield, the brace loses almost all stiffness,

accounting for the horizontal line after a roof displacement (as a percentage of building height) of 0.3.

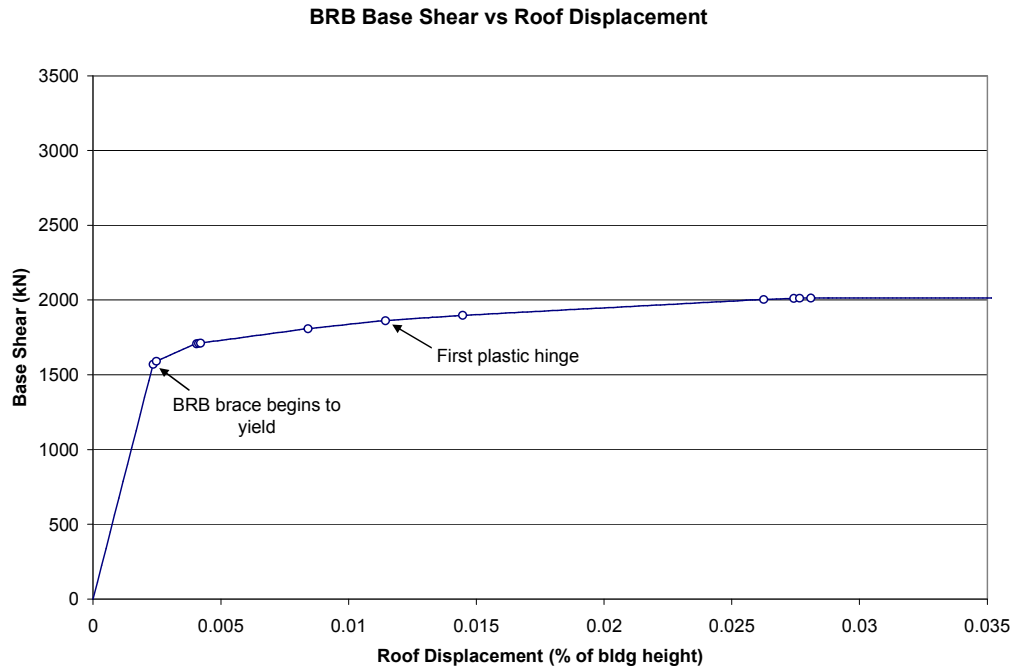


Figure 13. Behavior of BRB brace

6. Final conclusions

This paper presents the concept of the self-centering damping brace. The data obtained from the prototype tested verifies the theoretical predictions and basic concept of the SDB. As demonstrated in Figure 8 (a-c), the Nitinol SMA wires enables the SDB to self-center itself following all tests and promises to enable the brace to withstand frequent earthquakes with minimal damage. Residual structure damage would potentially be reduced or eliminated following a small to medium-range earthquake, as well as the added cost of replacing or repairing the damper itself. The sliding friction surfaces absorbed the majority of the energy, and the coupling of the SMA wires with the friction concept enhanced the capability of the brace to dissipate seismic energy.

The SDB has been shown in studies by Zhang and Zhu (2006) to also have better performance and less deformation in earthquakes than other conventional braces currently in use. The BRB and SDB were modeled in DRAIN-2DX and subjected to dynamic testing under seismic loads provided by data obtained from the Northridge earthquake. In every test, the SDB was comparable to the BRB brace in performance, and also provided little or no residual strain on the structure, even when the BRB braced structures had slight permanent deformation.

Overall, the SDB potentially provides an alternative to conventional braces and dampers, and will possibly offer reusable damping under frequent earthquakes with little or no residual structure damage.

7. Acknowledgements

The author would like to thank Professor Yunfeng Zhang and Songye Zhu for all of their assistance, Dr. Chad Kusko (REU Program Coordinator), Pennsylvania Infrastructure Technology Alliance (PITA), Center for Advanced Technology for Large Structural Systems (ATLSS), and Lehigh University

8. References

- Azom. "Nickel-Titanium Shape Memory Alloys," July 17, 2006.
<<http://www.azom.com/details.asp?articleID=1365>>
- FEMA (2000), "NEHRP Recommended Provisions for Seismic Regulations for New Buildings and Other Structures," *Federal Emergency Management Agency, Washington DC, USA*
- FEMA (2000), "Recommended Seismic Design Provision for New Moment Frame Buildings Report FEMA 350," *Federal Emergency Management Agency, Washington DC, USA*
- Grigorian, C., Yang, T. and Popov, E., "Slotted Bolted Connection energy Dissipators," Report No. UCB/EERC-94/02, University of California, Berkley, Ca, February 1994
- Morgen, B., Kurama, Y. (July 2004) "A Friction Damper for Post-Tensioned Precast Concrete Moment Frames," *PCI Journal*, Precast/Prestressed Concrete Institute, Vol. 49
- Sabelli, R., Mahin, S.A., and Chang, C., (2003) "Seismic demands on steel-braced buildings with buckling-restrained braces," *Engineering Structures*, 25
- Texas A&M SmartLab. July 18, 2006. <<http://smart.tamu.edu/index.html>>
- Uang, C.M., Nakashima, M., and Tsai, K.C., (2004) "Research and application of buckling-restrained braced frames," *International Journal of Steel Structures*, 4
- Way, D., (August 1993) "Friction-Damped Moment Resisting Frames," *Earthquake Spectra*, Earthquake Engineering Research Institute, V. 12, No. 3
- Zhang, Y. and Zhu, S. (2006) "Seismic behavior of framed structure with self-centering damping braces," *4th World Conference on Structural Control and Monitoring* San Diego, California
- Zhang, Y. and Zhu, S. (2006) "Seismic response control of building structures with superelastic shape memory alloy wire damper," *ASCE Journal of Engineering Mechanics*

Post-Tensioning and Anchorage Systems

**By Geoff Madrazo
Georgia Institute of Technology
REU at Lehigh University**

**Graduate Mentor: David Roke
Faculty Advisors: Dr. Richard Sause and Dr. James Ricles**

Table of Contents

- 1.0** Abstract
- 2.0** Introduction
 - 2.1** What is Prestressing?
 - 2.1.1 Science of Post-Tensioning
 - 2.1.2 History
 - 2.1.3 Applications
 - 2.2** Purpose
 - 2.3** Objectives
 - 2.3.1 Stress Testing
 - 2.3.2 Behaviors of Anchorage
 - 2.3.3 Range of Use
- 3.0** Methods and Materials
 - 3.1** PT Strand
 - 3.2** Anchors and Wedges
 - 3.3** Testing
 - 3.3.1 Static Tests
 - 3.3.2 Tensile Tests
- 4.0** Results
 - 4.1** Static Tests
 - 4.1.1 Stress Testing
 - 4.1.2 Two-part vs. Three-part Wedge
 - 4.2** Tensile Tests
 - 4.2.1 Stress vs. Strain
 - 4.2.2 Rate of Elongation
- 5.0** Conclusions
 - 5.1** Anchorage System
 - 5.2** Strands
- 6.0** Acknowledgements
- 7.0** References

1.0 Abstract

This project was designed to acquire data regarding the behaviors of a post-tension strand and anchorage system. Failure in the strand is caused by the wedges making a notch in one or more of the wires, therefore inducing the strand the break at high loads. The use of post-tensioning in real-world applications is limited by this failure, so knowing the specific behaviors of the system is valuable for testing and research that involve post-tensioning.

Numerous stress tests demonstrated the strength of the three-part wedge under heavy loading, as well as the strand and anchor system's ability to exceed yielding. Referencing this information for future testing will help researchers understand the properties of the PT strand and anchors, and will hopefully promote exploiting the advantages of post-tensioning.

2.0 Introduction

2.1 What is Prestressing?

Prestressing is a method of reinforcing different kinds of structural elements. It was based off of the use of rebar in concrete as reinforcement, with the main distinction being that an induced stress changes the properties of the concrete (PTI). In most applications, prestressing is used to overcome a materials' weak tensile strength. A highly tensile steel strand or rod passes through the material, is pulled into tension and anchored on both ends to couple their properties. This prestressing applies a compressive stress on the material, which offsets the tensile stress the material might face under loading (Figure 2.1). A technique of prestressing is called post-tensioning, commonly used in concrete structures, in which the tension is applied after the material is in its final state, such as a concrete slab or a complete structure.

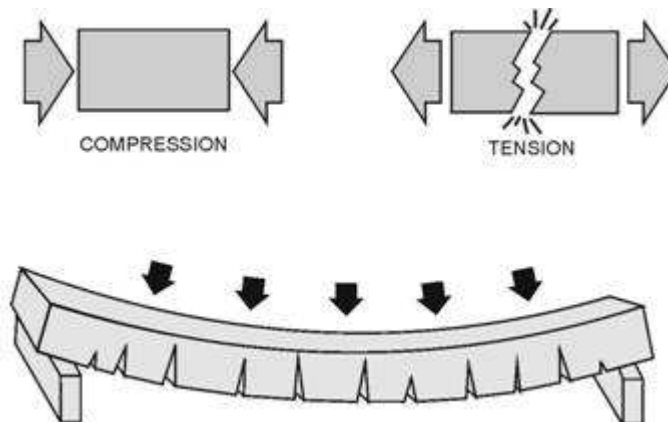


Figure 2.1 Concrete under loading
Source: PTI

Post-tensioning has been in practice since the early 20th century, but only recently have companies really taken advantage of its structural and financial benefits. For example, to a stronger concrete slab means you can build with less concrete but still retain the same structural properties as a much larger slab without post-tensioning. Less concrete means it will be less costly to manufacture, lighter to ship, and easier

to install. It also allows for new designs to take advantage of a lighter concrete slab without compromising its strength.

The method of prestressing has been implemented for several decades in all types of bridges, many kinds of elevated slabs (i.e. residential and high-rise structures, parking garages, etc.), as well as foundations, walls and columns (Figure 2.2). Post-tensioning has driven the potential for longer bridge spans, larger structures, unique constructions, and more structurally sound buildings (PTI). And because of its “rubber band-like” properties, which are very tolerant to lateral loads, prestressed members have long been used in seismic resistant structures (DSI).

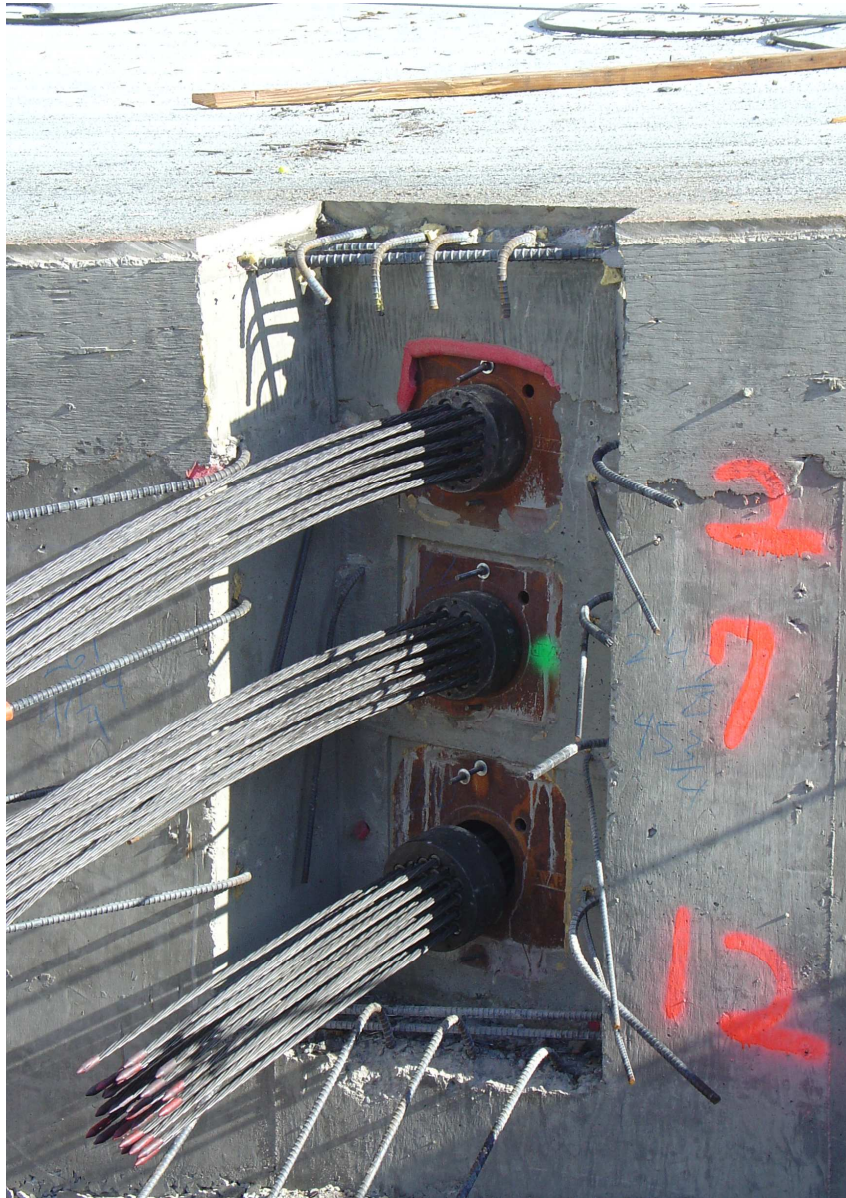


Figure 2.2 Post-tensioning on a highway overpass
Source: Charlie La Barbera

2.2 Purpose

The purpose of this project is to obtain useful data on the strength and behaviors of the post-tension strand and anchor system. A reliable data set will be a valuable reference for future projects which implement post-tensioning.

2.3 Objectives

The first objective of my project is to perform multiple stress tests on the post-tension strand and anchor system. I will collect different forms of data, such as the breaking strength (T_{exp}), elongation ($\epsilon_{max,est}$), and time (t) and analyze the sets of information. By plotting different manipulations of the data, I will observe and exploit certain trends and findings.

Dr. Maria Garlock researched Seismic Resistant Post-Tensioned Steel Moment-Resisting Frames as her Ph.D. study, which included post-tensioning running along the steel beams of a structure. Under certain loads, she observed the strand breaking near the anchors, but documented “the fracture was a ductile fracture and not caused by a notch or “bite” produced by the wedge” (Garlock). Part of the data collection from the stress tests will be to observe and understand the behaviors of the anchorage system. By carefully watching and photographing the seating and post-break states of the wedges, we should be able to see how the anchorage reacts to breaking loads.

Testing and analyzing the post-tension strand and anchor system will give me an understanding of the kind of loads and conditions it can withstand. From there I will be able to determine the right conditions and usage for the system and find a practical scope for using it.

3.0 Methods and Materials

3.1 Post-Tension Strand

Post-tension (PT) strands are manufactured in accordance to the standard American Society for Testing and Materials (ASTM) A416. It is composed of seven treated carbon steel wires, six of which are arranged in a helical pattern around a slightly larger center wire (Figure 3.1). PT strand is available in several diameters ranging from .250 in. to .600 in. For most post-tensioning applications, the standard size strand is either the .500 in. or .600 in. diameter (ASTM). Breaking strength requirements and yield strength requirements are shown in Table 3.1.

Strand Diameter (in.)	.500	.600
Min. Breaking Strength, T_U (kips)	41.3	58.6
Steel Area (in²)	.153	.217
Strand Weight (lb/ft)	.520	.740
Min. Yield Strength, 1% Elongation, T_Y (kips)	37.17	52.74

Table 3.1 ASTM A416 requirements
Source: ASTM

3.2 Anchors and Wedges

Anchorage and wedges are manufactured in different ways for different applications. They follow the American Concrete Institute (ACI) code 318, which fundamentally states that the anchorage system is guaranteed up to 95% of the breaking strength of the strand (T_U) (ACI). For projects that require higher tensile strengths, there are various kinds of multi-strand anchors which can accommodate from two to 156 strands (Figure 3.2) (DSI). The largest anchors are mainly used in cable stayed bridges to hold up the roadway, while the smaller anchors are used in more common applications such as a highway overpass or a parking garage. For our testing we used monostrand anchorages so we wouldn't be dealing with immense amounts of released energy while breaking the strand (Figure 3.3). Wedges sit in the anchor and grip onto the strand to hold it in place (Figure 3.4). They are manufactured in two- and three- parts, both of which we tested.



Figure 3.2 Multi-strand anchor
Source: DSI



Figure 3.3 Monostrand anchor
Source: DSI

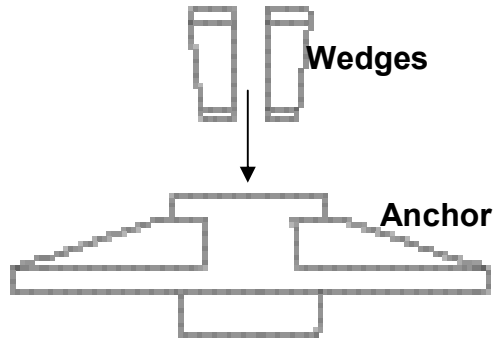


Figure 3.4 Wedges insert into anchor
Source: DSI

3.3 Testing

The first set of testing we performed were static (monotonic) stress tests on an analog universal testing machine at Fritz lab. These initial tests were performed with strand and anchors leftover from previous testing at the Advanced Technology for Large Structural Systems (ATLSS) lab. The materials were not outdated, yet their condition was somewhat in question which is why we tried to make a clear distinction for these tests in our data. Before we could begin any kind of testing, we made sure that the proper safety precautions were taken. When taking the strand to its breaking strength, there is the risk of the wedges popping out of the anchor. To account for that we put a cover over the ends to control any pieces that came loose (Figure 3.6).

The basic setup for the testing was a five foot segment of PT strand that was anchored on both of the crossheads of the universal testing machine at Fritz lab (Figure 3.5). The wedges were hand-set to be as level as possible before adding tension to the strand. After covering up the anchors to contain any flying debris, we added some tension to seat the wedges into the anchors. We tried to achieve a four to six minute elongation period (between 10 and 15 kips/min load rate), but for these tests we could only rely on knobs to fine tune the crosshead displacement and a stopwatch to monitor the time. The strands were loaded until at least one of the wires ruptured, and at that point the breaking strength and time were recorded. That process was repeated for several trials.



Figure 3.5 Universal Testing Machine setup at Fritz

The next phase of testing was completed with new strand, anchors and wedges provided by Dywidag-Systems International (DSI). Testing began at Fritz lab with the same procedure as before, but we ended up moving our testing to the SATEC universal testing machine in the ATLSS lab. The SATEC machine can be more controlled by a computer, and it also records data straight from the machine. Stress, head displacement, and time were the parameters that we monitored during our testing. To ensure the wedges set properly a “soft zone” was implemented, in which the crossheads displaced at a rate of .1 in/min until there was 100 lbs. tension in the strand. After the “soft zone,” we programmed the machine to load the strand at a rate of 12.00 kips/min for the first three tests, and 9.00 kips/min for the next three tests. As an added safety precaution, there was also a break detection mechanism which would stop the machine if there was a drop of at least 10% of the load past the 5000 lb. stress level. The tests were physically set up the same way as in Fritz lab (Figure 3.6).

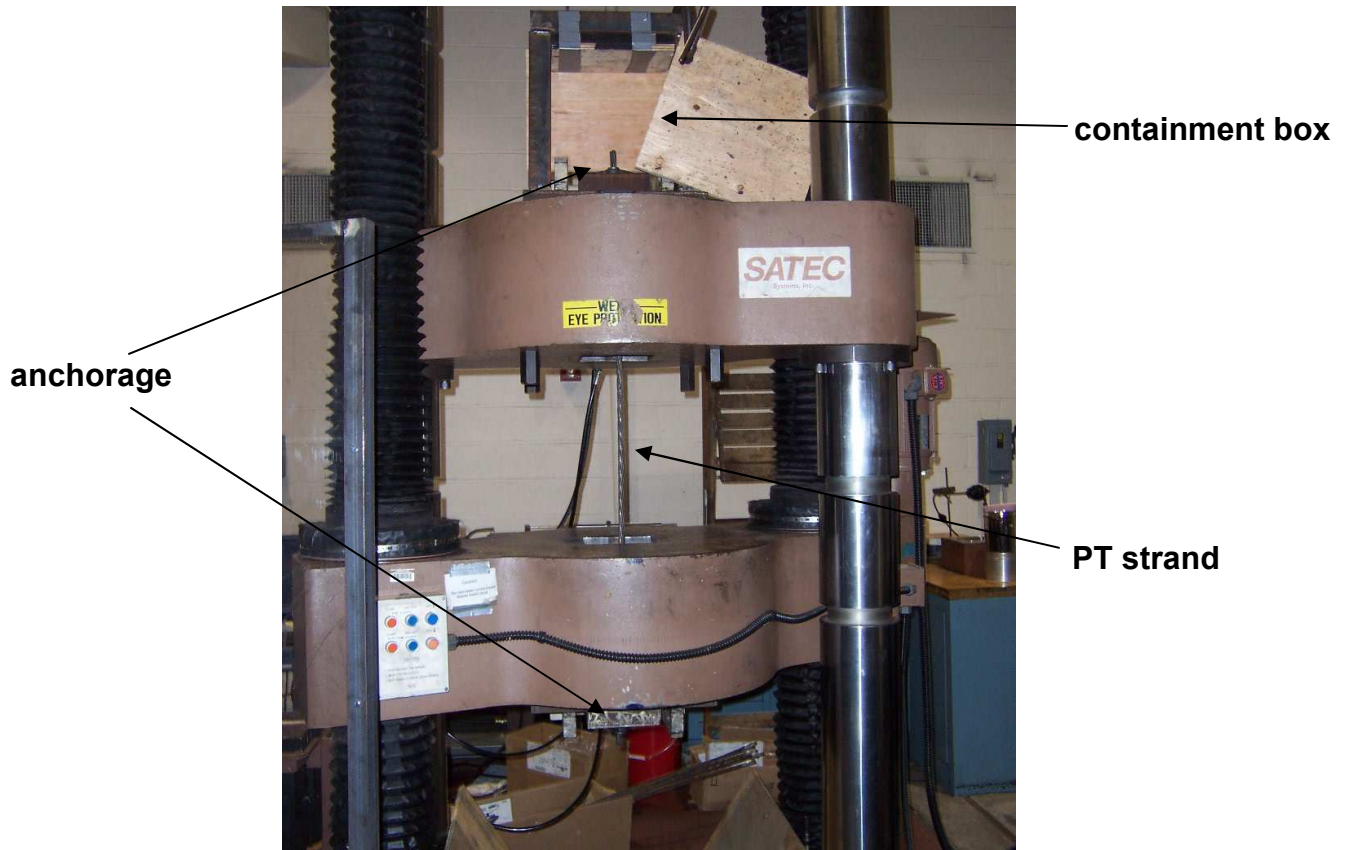


Figure 3.6 SATEC machine setup

To perform proper tensile tests to obtain a stress-strain curve of the strand, we had to find a new way of anchoring the ends. The conventional anchor-wedge system is only guaranteed to 95% T_U , so we would be missing a very important part of the



Figure 3.7 Wirelock being pouring into a socket
Source: Millfield Group

curve using that system. As an attempt to solve this problem, we turned to a cold-socketing compound called Wirelock. This material is composed of a liquid resin and a granular compound (Millfield). When mixed and poured into the socket around a wire, the two components quickly form a solid resin that is greatly resistant to compressive forces (Figure 3.7). The key to getting correct results from the Wirelock is the preparation of the strand or wire that you are bonding to. The resin is primarily used on wire ropes, which are made up of many finer wires spun around each other. Splaying the wires out and unraveling them so they appear like a broom maximizes the surface area of wire for the resin to bond to and allows for a strong connection between the wire rope and the Wirelock.

As an alternative to Wirelock, we also tried using old grips that were found at Fritz lab. A grip is composed of two copper plates about six inches long that get compressed around the wire. The compressive force comes from inserts in the crossheads of the universal testing machine that create a wedge-like effect on the plates.

4.0 Results

4.1 Static Testing

test	# of wedges	T_{exp} (kips)	$T_{exp}/T_{u,n}$	$T_{exp}/T_{u,m}$	$\epsilon_{max,est}$ (%)	elong. rate (in/s)	load rate (kips/min)
1	3	57.50	0.98				
2	2	53.85	0.92				
3	3	53.85	0.92				
4	3	56.55	0.97	0.9371	1.341	0.1833	
5	3	55.70	0.95	0.9230	1.040	0.2880	
6	3	57.80	0.99	0.9578	2.443	0.4581	
7	3	57.30	0.98	0.9495	2.002	0.3889	
8	3	57.87	0.99	0.9589	2.504		11.459
9	3	57.68	0.98	0.9558	2.339		11.772
10	3	56.65	0.97	0.9387	1.428		11.720
11	3	56.81	0.97	0.9414	1.569		8.077
12	3	56.52	0.96	0.9366	1.315		8.901
13	3	57.08	0.97	0.9459	1.810		8.850

Table 4.1 Test data

The data collected from the static tests are documented in Table 4.1. The tests 1-3 were performed at Fritz lab with old materials, tests 4-7 at Fritz lab with new materials, and tests 8-13 using new strand on the SATEC machine. The value $T_{exp}/T_{u,m}$ is the recorded breaking strength, T_{exp} , normalized with the breaking strength ($T_{u,m} = 60.347$ kips) provided by DSI, the manufacturer of the strand. These values show us that one-third of our tests actually reached the 95% T_U mark that the anchors are guaranteed to by ACI codes.

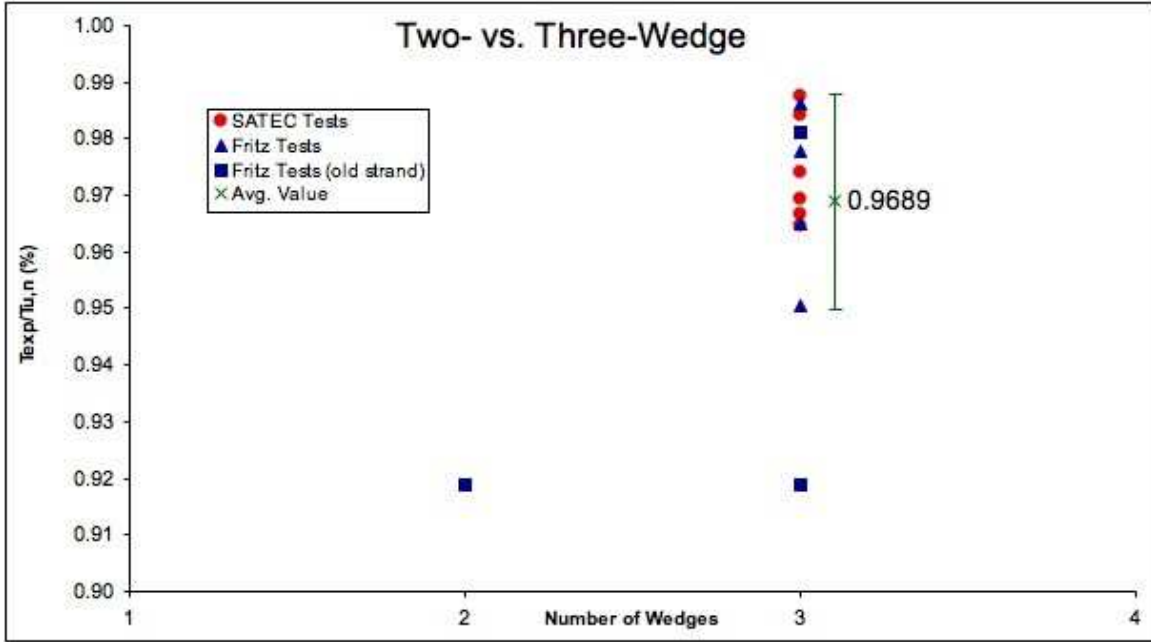


Figure 4.1 Two-part versus three-part wedges

The data in Figure 4.1 shows the difference between the breaking strength of two-part and three-part wedges. The value shown is a normalized T_{exp} with the ASTM standard minimum breaking strength 58.6 kips. This value gives a standard of comparison for the tests, and is not representative of the actual breaking strength of the strand. This figure shows a strong set of data within one standard deviation of the average and higher breaking strength for three-part wedges, but the fact that we only performed a single two-part wedge test cannot be overlooked.

The tensile tests didn't turn out as we had hoped, both ending up in the wire slipping out. The Wirelock tests slipped because there wasn't enough surface area of strand for the resin to bond to, so when taking a heavy load it started to slip (Figure 4.2). This method could still be implemented and prove successful, but we would need to expose more strand to the Wirelock for more friction. The PT strand also slipped out of the grips of the copper plates when a load was applied. We tried it several times, even pre-compressing the plates on the wire in a smaller universal testing machine. That process helped, but we still came nowhere close to the breaking strength of the wire.

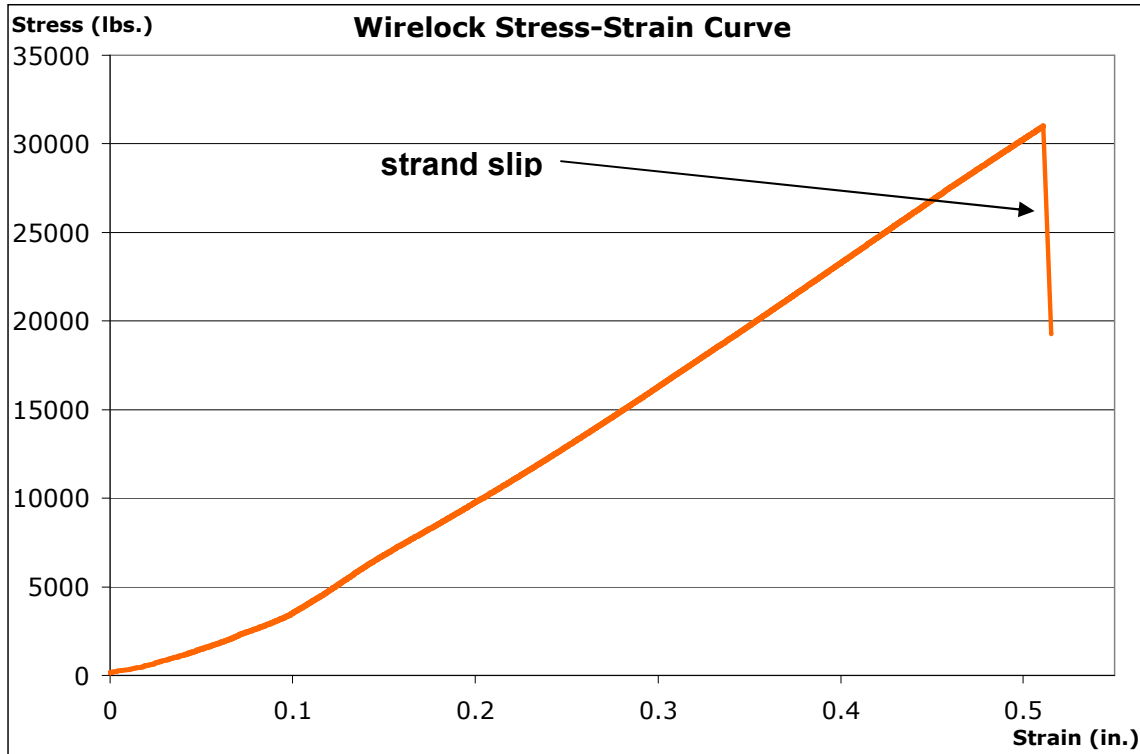


Figure 4.2 Stress-strain curve showing slipping in Wirelock

Even though we didn't get what we wanted out of the tensile tests, we were lucky enough to be able to construct a stress-strain curve of the strand with data given to us by the manufacturer. One thing about the fabricated curve is that they data given to us only goes up to around 55 kips because the strain gauges were taken off at that point. The data given to us had the ultimate breaking strength and the elongation at the break, so we were able to fill in the rest of the curve, but we have to be very aware that we didn't capture the precise behavior of the strand past the point where they took the strain gauges off. On the stress-strain curve, I also plotted the high- and low-value breaking strengths, along with the average breaking strength and the yield strength of the strand (Figure 4.3).

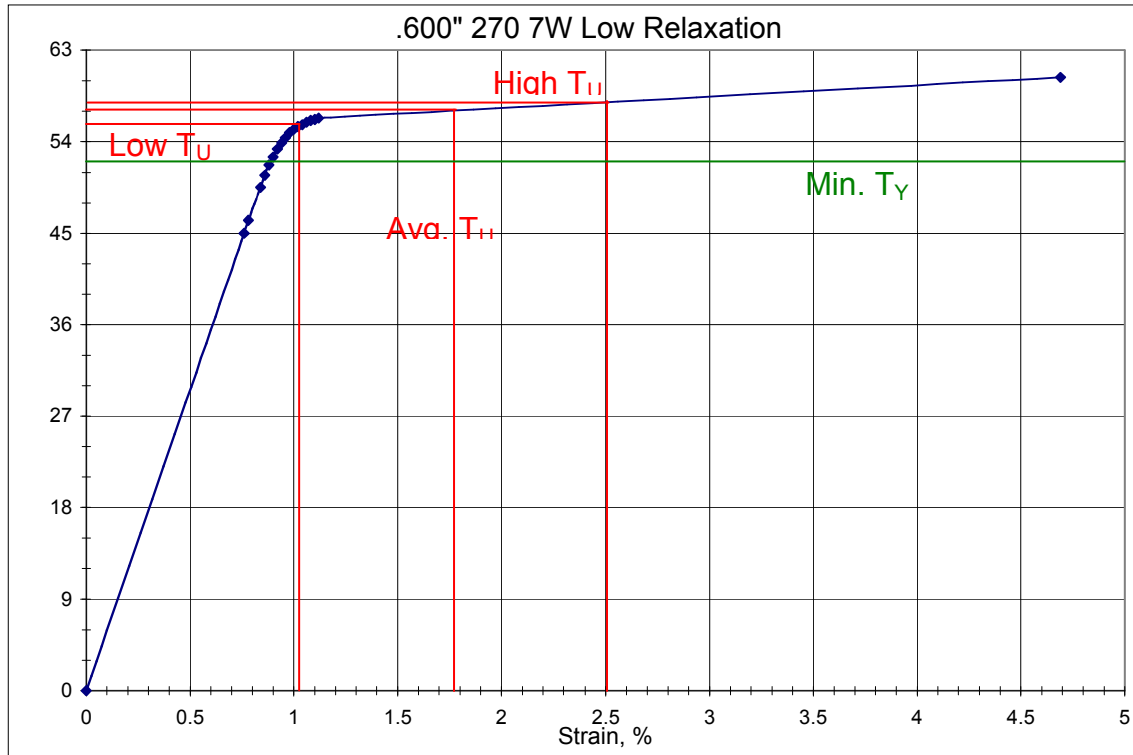


Figure 4.3 PT Strand Stress-Strain curve

5.0 Conclusions

5.1 Anchorage

Although our objectives weren't to find things wrong with the codes and standards, during our testing there was one statistic that stood out. In Table 4.1, it's very evident when you look at the $T_{exp}/T_{u,m}$ value that the anchors don't comply with ACI code 318. Only three of our tests reached 95% breaking strength of the strand, and even those hardly made it past. This finding is important to note because it is part of a building code, and those codes are supposed to be able to be achieved.

Aside from all codes, an important factor we wanted to look at was whether a two-part or a three-part wedge performed better and more reliably. In Figure 4.1, it is shown that a most of the three-wedge tests fall within one standard deviation of the average, making it a strong data set. But the fact that we only performed one two-part wedge test makes it hard to build up any points towards one or the other. We can loosely say that the three-part wedges performed better under loading than the two-part wedges, but more testing should be completed before being able to make a firm statement.

5.2 Strands

In Figure 4.3, we can see the value range of T_{exp} as compared to the yield strength, T_Y . This tells us with confidence that the strands can be taken past their yield point with the conventional anchor system. Even the lowest T_{exp} well exceeded

the yield strength of the strand, making it possible to design something past the yield strength of the strand.

That design knowledge is particularly useful for the Self-Centering Damage-Free Seismic-Resistant Steel Frame Systems projects currently being worked on by Dr. Richard Sause and Dr. James Ricles at Lehigh University. This gives them an upper limit to design to, which could mean higher prestress values, less strands used, and a better designed model from knowing these properties.

6.0 Acknowledgements

Chad Kusko
David Roke
Dr. Richard Sause
Dr. James Ricles
John Hoffner
Gene Matlock
Dr. Eric Kauffman
Lehigh University
ATLSS
NEES
NSF

7.0 References

American Concrete Institute (ACI), “ACI 318-05.” The Structural Concrete Standard (2005).

American Society for Testing and Materials (ASTM), “A416/A416M-06.” Standard Specification for Steel Strand, Uncoated Seven-Wire for Prestressed Concrete 01.04 (2006).

Dywidag-Systems International (DSI), Online (2006). www.dsiamerica.com

Garlock, Dr. Maria “Design, Analysis, and Experimental Behavior of Seismic Resistant Post-Tensioned Steel Moment Resisting Frames.” Lehigh University (2002).

Millfield Group, Online (2006). www.millfield-group.co.uk

Post-Tensioning Institute (PTI), Online (2006). www.post-tensioning.org

Development of Seismic Design Methodology for Precast Diaphragms

Mia Simmons, NEES REU Student

Joe Creek, Graduate Mentor

Dr. Clay Naito, Advisor

Final Paper

August 4, 2006

Table of Contents

1. Abstract
2. Background
3. Experimental Procedure
 - 3.1 *Test Setup*
 - 3.2 *Loading Protocols*
 - 3.3 *Calibration*
4. Results and Discussion
 - 4.1 *Testing Checklist*
5. Summary and Conclusions
6. Acknowledgements
7. References
8. Appendix

1. Abstract

Concrete diaphragms in different seismic regions have been damaged because of various earthquakes. Tests have been developed to test the stability and reliability of the design of these connectors. To examine at a more precise scale, tests have been created to help characterize these connectors' behavior. These tests use certain tension and shear load combinations to get a more in depth look at the connectors embedded in the concrete. The following paper is an overview of the preliminary work required and the process needed to perform such tests.

2. Background

This project is collaboration with three universities: University of Arizona, Lehigh University and University of California at San Diego. The project is a result of the Northridge Earthquake in January 1994. During this earthquake many precast concrete parking structures were damaged. These damaged structures led to a number of questions about the stability of the design in certain seismic regions. This project is multi-phased and currently Lehigh University's part in this project is to test single panel-to-panel connectors to determine the standards and reliability of the designs for seismic regions.



Collapsed Northridge Parking Structure. Photo Courtesy of U.S. Geological Survey.

In Phase 1, Lehigh University tested the performance of common connectors used by the precast industry. Results showed that many of the connectors were unable to meet their expected design strengths. The connectors failed to achieve their capacity and there also was limited ductility.

For Phase 1B of the project, Lehigh University will examine the performance of modified connectors in the hopes that it will improve the strength and ductility of the diaphragm connectors. Within this project, we will analyze the behavior of precast

diaphragms. Under our test setup, we will investigate the behavior under in-plane shear, tension and compression load combinations. A control program needed to be created to look at behavior under these different loading situations. With the program we will be able to send and receive data through three load cells. Different forces and displacements will be recorded and graphed throughout the duration of the test.

3. Experimental Procedure

3.1 Test Setup

There is various types of software available for the required testing, but the program chosen for this phase of the project was Test Point. Test Point is a type of data acquisition software that will acquire and record data from the Analog/Digital and Digital/Analog Boards. For this test setup, three load cells are used. (Figure 3.1) Two actuators (labeled 2 & 3 in Figure 3.1) are used for the tension/compression forces and one actuator (labeled 1 in Figure 3.1) is used for the shear force.

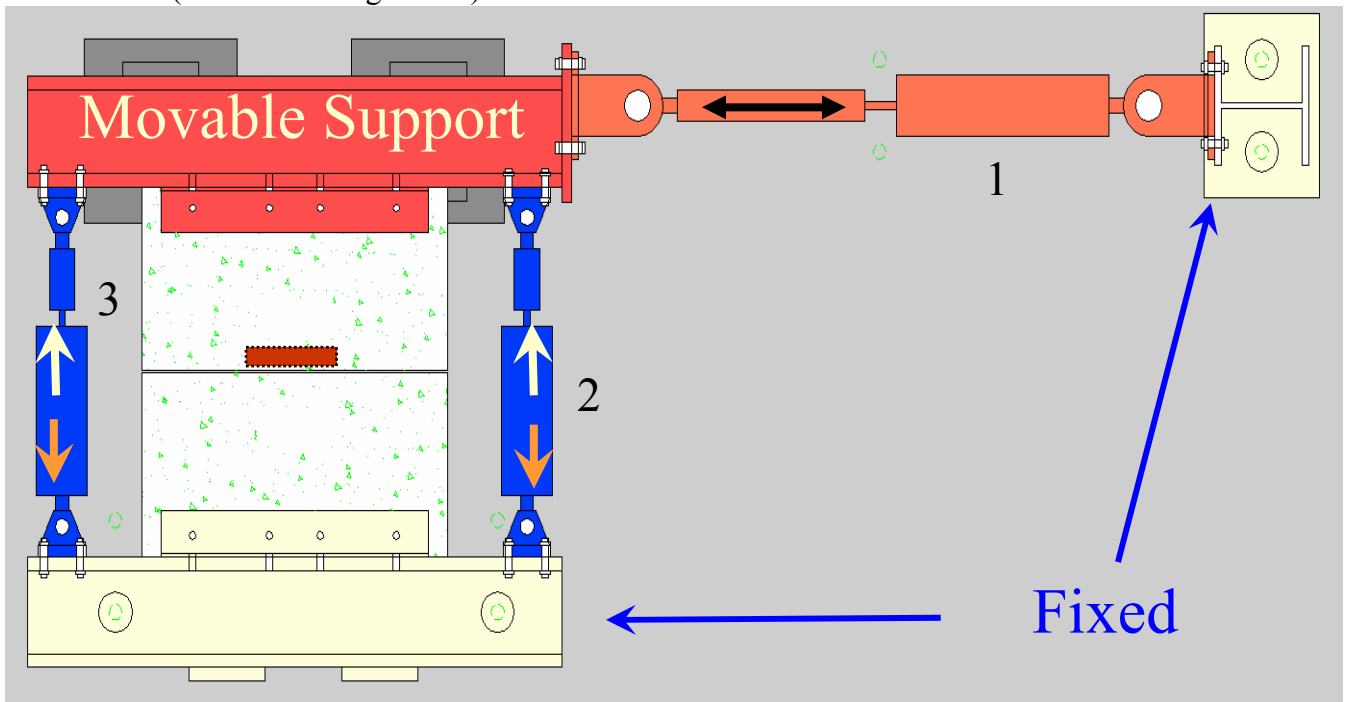


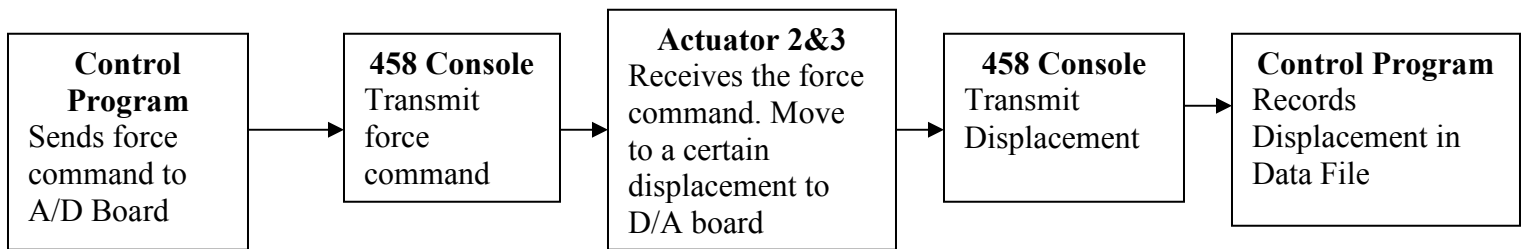
Figure 3.1: Test setup with actuators

Within Test Point there are many objects that can be used to create the right type of control program for data acquisition. The main objective of the test setup is to send data from the A/D board to the 458 machine that will tell the actuators how far to move. Then from the actuators' movement, data will be sent back through 458 console to the control program and record the displacement of the actuator. This will occur continuously throughout the duration of a test.

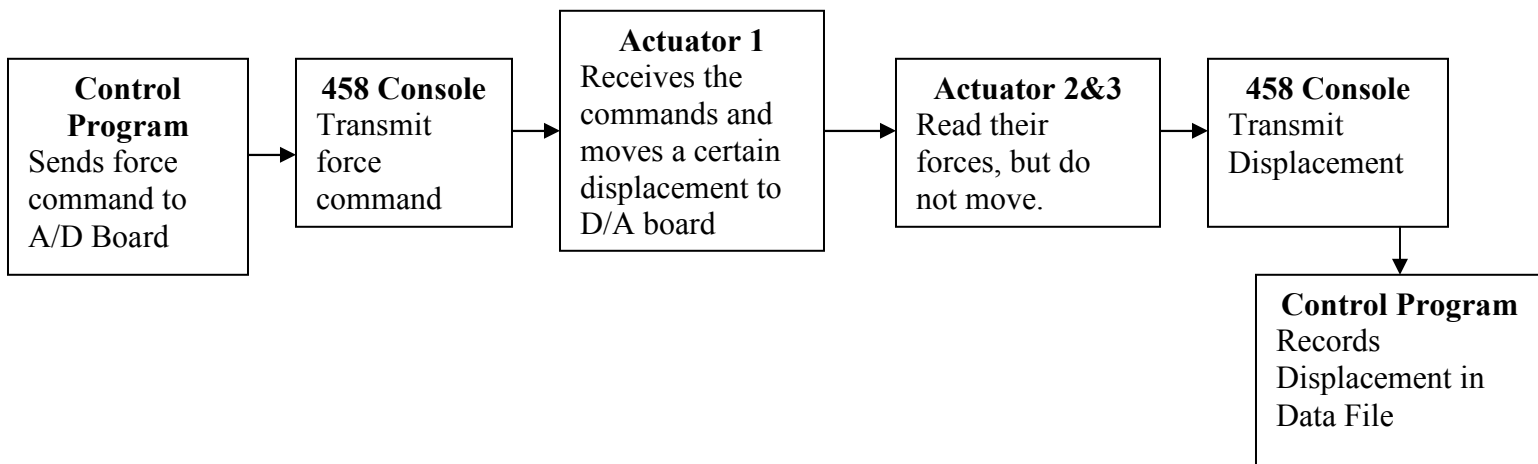
3.2 Loading Protocols

There are certain loading protocols we must also follow to obtain the required results. For our tests, we are using 3 types of monotonic and cyclic protocols (monotonic meaning one way, cyclic meaning back and forth). These 3 protocols are described in detail below:

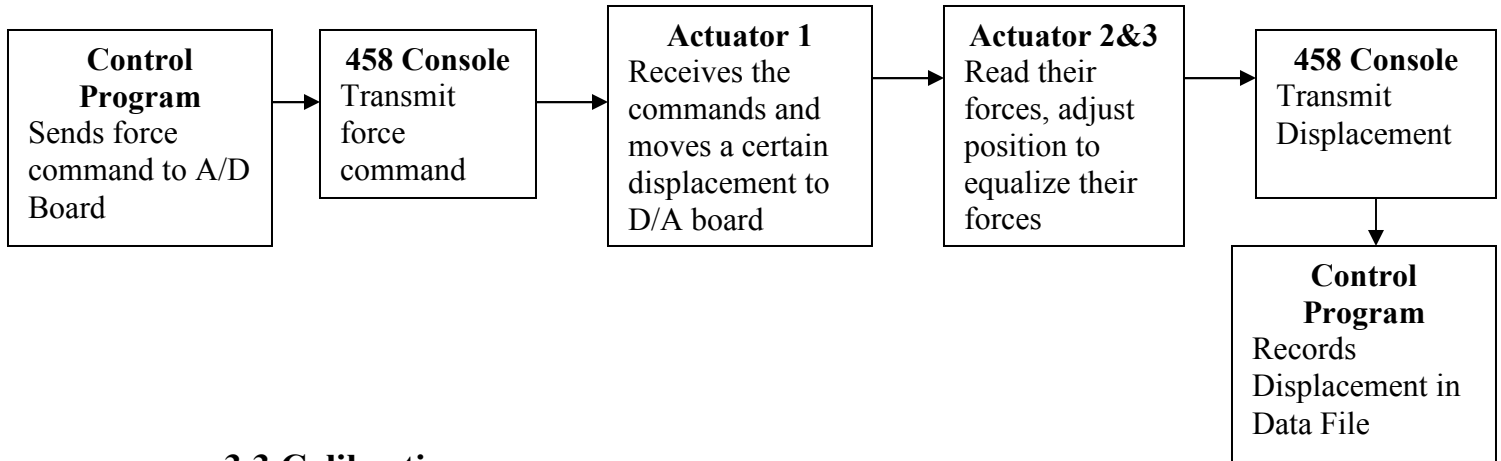
1. **Monotonic/Cyclic Tension with no Shear force** - In this test Actuator 1 (shear force) is not attached and we apply force to Actuators 2 & 3 to record the displacement of both actuators.



2. **Monotonic/Cyclic Shear with no Axial Deformation.** – In this test force and displacement is applied to Actuator 1 while the forces are read from Actuators 2 & 3 without allowing axial displacement.



3. **Monotonic/Cyclic Shear with no Axial Force** – In this test force and displacement are applied to Actuator 1. Then the forces from Actuators 2 & 3 are read, but those forces are equalized in magnitude by adjusting the two actuators the same distance.



3.3 Calibration

After creating the test program, we had to calibrate both the feedback and monitor LVDTs. Without having these calibrations, our math functions in the program would not be effective. We did all the calibrations manually with a simple control program. (Figure 3.2) For the temposonics (feedback LVDTs), we measured over a 5" range at 1/2" increments. In order to get the right voltage for the scaling, we took an average of three voltages reading from the A/D board. The monitor LVDTs were calibrated in a similar fashion by using gauge blocks varying in length up to 5". The results of these calibrations are presented in Figure 3.3. The load cells were calibrated in Phase 1 of this project and these results are presented in Figure 3.4.

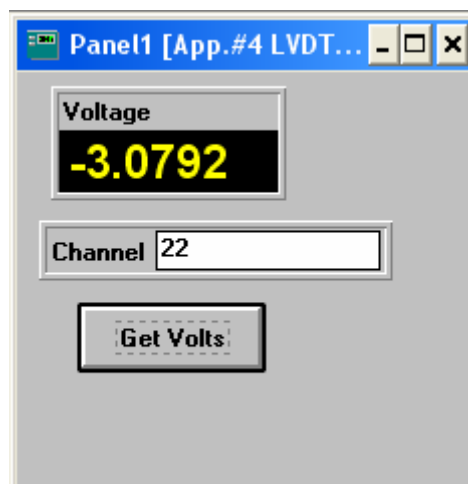


Figure 3.2: Calibration program

				Slope
Channel	Type			V/in
20	Feedback	Jack 1	Shear	3.078474
0	Monitor	Jack 1	Shear	1 (vdc)
21	Feedback	Jack 2	Mid Ax	3.182850
1	Monitor	Jack 2	Mid Ax	1 (vdc)
22	Feedback	Jack 3	End Ax	3.145967
2	Monitor	Jack 3	End Ax	1 (vdc)

Figure 3.3: LVDT and Temposonic calibration data

Load Cell Calibration				
ID	Load Cell	t/c	Slope V/kip	y-int mV
	Shear			
2833	Axial #1	Compression	-0.15684	0.175468
2833	Axial #1	Tension	0.157295	0.1317985
2832	Axial #2	Compression	-0.15754	0.231818
2832	Axial #2	Tension	0.15705	0.232233
687	Shear	Compression	-0.13809	0.123737
687	Shear	Tension	0.139714	0.129725

Figure 3.4: Load cell calibration data

Once the calibration work was finished, the slope was determined so that it could be incorporated into the control program. For the control program, I created a “dummy” version that could be enhanced to create a specific test with the help of our lab technician (Figure 3.5). The dummy version contained three A/D boards that read from each load cell. It also contained three grids, where it could load a file filled with data and display it into the grid. Three graphs were set up that correspond to the three different actuators. With the help of our math functions from our calibrations, we could graph the force versus the displacement.

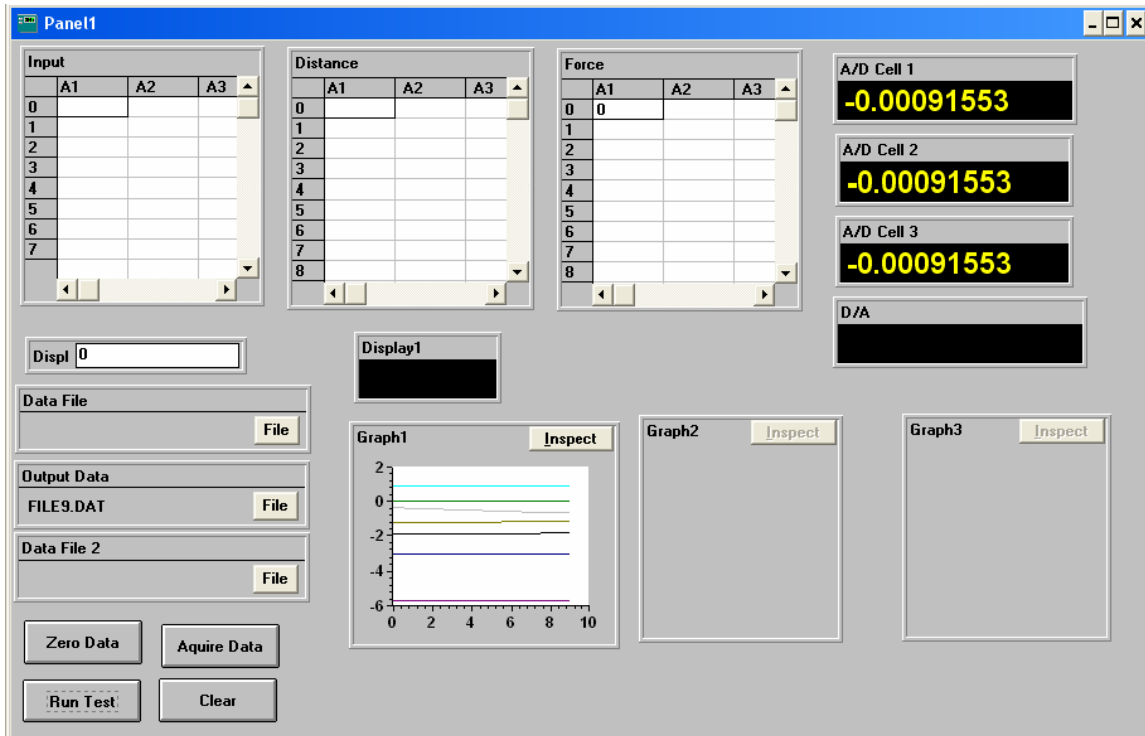


Figure 3.5: “Dummy” version of the control program

Within the control program, a series of loops and functions were incorporated to display the data information into the grid. With this process, two action buttons were included to input all the data at once and then input the data at one line at a time. This process was created so that the actuators moving will not move too much within the testing process.

4. Results and Discussion

To date, we do not have any test results. Currently we are working in the lab to make sure that the final version of the control program works correctly (see Figure 3.6). The final version of the control program will load the data file periodically and record the forces and displacements. Also, the final version will graph force versus the displacement in each actuator as the test is being conducted.

4.1 Testing Checklist

A general start up checklist of the control program has been implemented to show the steps necessary to run the final version. This process is outlined below:

- 1) Create the control and configuration files in which include a text file containing displacement commands. The text file has the hardware configuration parameters used in

the data acquisition program. Files can be created/edited in any text program such as Microsoft Excel.

2) Run the executable program.

3) Program Setup

- a) Run the setup routine (click “Setup” button) – this routine loads channel configuration, load rates and creates the file for acquisition
- b) Run the balance routine (click “Balance” button) – this routine scans analog input channels and apply an offset value for data acquisition. Also used for system checkout.

4) Program Control

- a) Set your system software limits (click “Limit” button) – this routine sets both global and relative displacement limits.
- b) Jack Initialization (click “Initialize” button) – this routine sets your command voltage to your displacement transducer values.

**** At this point this will allow actuator control****

5) Adjust Control Data for current position (click “Adjust Data” button) – this routine scans your current control transducer and applies offset values to all you displacement commands.

*** Ready to run test***

6) Issue displacement commands and run data (click the “Load and Record” button) – this routine issues voltage commands equivalent to displacements and records data.

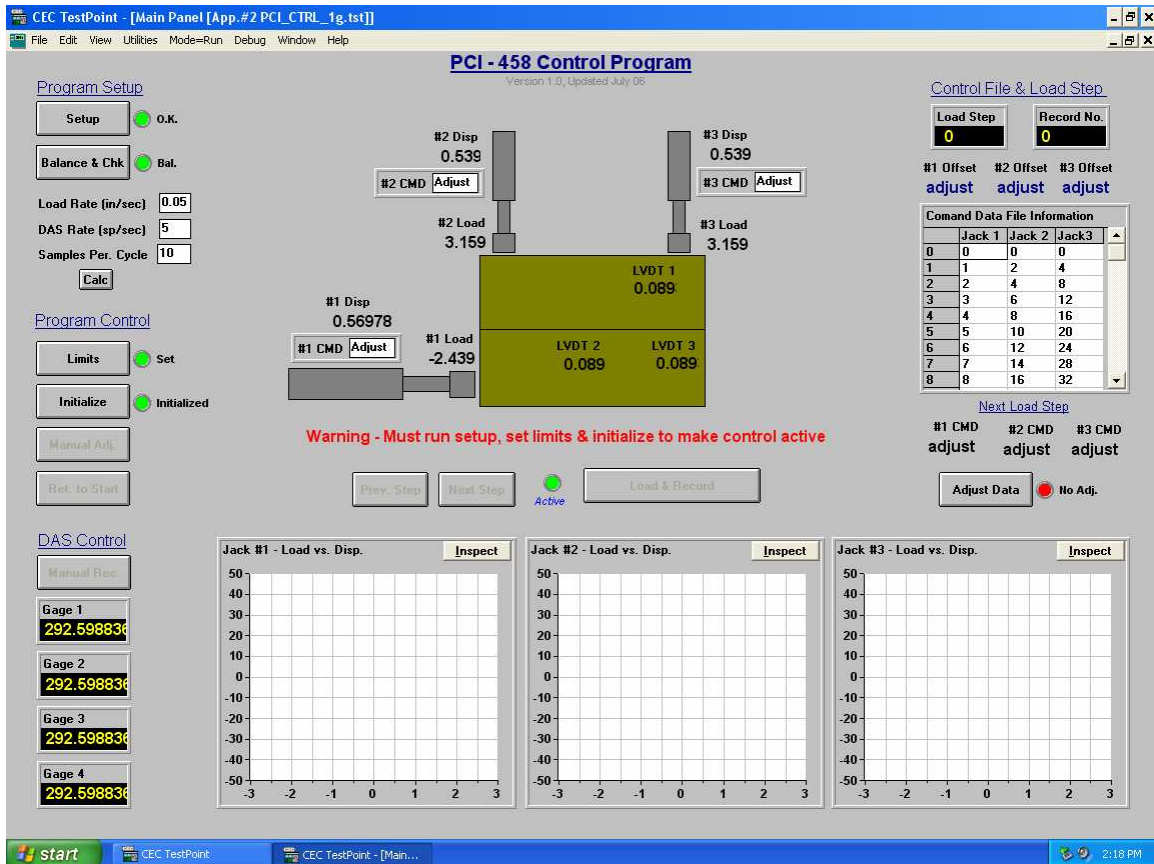


Figure 3.6: “Final Version” of the control program

5. Summary and Conclusions

So far in this project we were able to create an efficient control program that records the data of the tension/compression and shear load combinations. It took a lot of time studying about Test Point and the 458 console. The data input in the program is important in making sure that control program commands were not over loaded in the testing. By importing the array commands into the data files, it gave the program a little more ease so that the program will not shut down with overloading. After a little more “debugging” work is done, we will be able to test our first set of specimens in the near future. The first set of specimens that will be tested are the “Ductile Ladder” connectors that were fabricated at Lehigh University with the actual connector material donated from Ivy Steel.

6. Acknowledgements

-Funding Agencies

- NEES
- NSF/PCI
- Pankow Funded Research

-Dr. Clay Naito, Advisor, Asst. Professor at Lehigh University

-Chad Kusko, Administrator, Lehigh University

-Joe Creek, Mentor, Graduate Student at Lehigh University

-Ed Tomlinson, Lab Technician, Lehigh University

-Jason Thurlow, Applications Engineer, Measurement Computing Corp.

7. References

Journal

- University of Arizona, Lehigh University, University of California San Diego Robert Fleischman, Clay Naito, Jose Restrepo, Richard Sause Dec. 2004. *PCI Research Project: Development of an Inelastic Design Methodology for Precast Floor Diaphragms*
- *Northridge 1994*. Website <http://www.vibrationdata.com/earthquakes/northridge.htm>
- *CEC488*. Test Point. Website www.cec488.com

Books

- CEC Corporation. 1999. Test Point Techniques and Reference. 6th Edition. Billerica, Massachusetts.
- CEC Corporation. 1999. Test Point Quick Start. Billerica, Massachusetts.
- Peter, Wesley and Fahenstock, Larry. Personal Lab Research Notebook. 2004-2005

8. Appendix

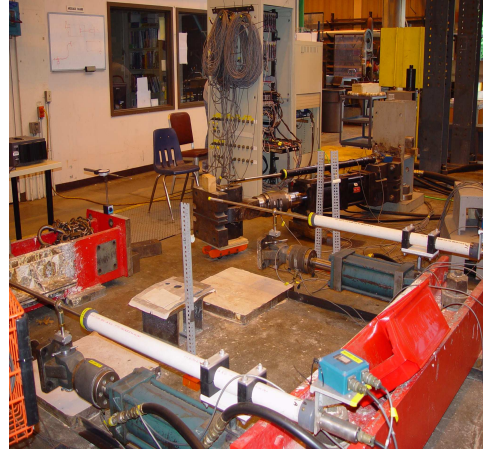
Included below are pictures from the test setup in the ATLSS/NEES Lab.



Control program set up in the lab.



Lab Technician Ed Tomlinson working to help complete the final version of the control program.



Test setup of the 3 actuators in the lab

USER'S GUIDE FOR HYBRID VIZ: A VISUALIZATION TOOL FOR REAL-TIME HYBRID TESTING

Gabriel Valencia

Undergraduate Researcher

San Jose State University

REU Host Institution: Lehigh University – Dr. Chad Kusko, Coordinator

REU Faculty Advisor: Dr. James Ricles

REU Graduate Student Mentor: Oya Mercan

NEES Staff Mentor: Tommy Marullo

NEES Research Experience for Undergraduates

August 4, 2006

Table of contents

1. Abstract.....	79
2. Introduction.....	80
2.1. Structural testing background.....	80
2.2. Objectives and scope of the study.....	83
3. Background	84
3.1. Mathematics	84
3.2. Design and implementation.....	85
3.2.1. The components package	86
3.2.2. The gui package.....	89
4. User's guide	92
4.1. Running the program	92
4.2. The user interface	92
4.3. Grid controls.....	93
4.4. Creating Structures	94
4.4.1. Adding and editing Nodes	95
4.4.2. Adding and editing Elements and Bases.....	96
4.4.3. Adding and editing Actuators.....	97
4.5. Saving and loading a Test Setup.....	98
4.6. Linking with the SCRAMNet	99
4.7. Starting and running a simulation	99
4.8. Reading a displacement record from a file.....	100
5. Summary, conclusions, and future work.....	102
6. Acknowledgments	103
7. References.....	104
Appendix A: Example problem	105
Appendix B: Example problem structural properties.....	109
Appendix C: Example problem integration parameters.....	109

List of figures

Figure 2.1	Structural response in earthquakes.....	80
Figure 2.2	PSD testing with a discretized integration algorithm (ATLSS, 2006).....	81
Figure 2.3	Hybrid PSD testing (ATLSS, 2006)	82
Figure 2.4	Hybrid Viz in the integration process	83
Figure 3.1	Cubic fit from two endpoints.....	85
Figure 3.2	Hybrid Viz taps into the SCRAMNet.....	86
Figure 3.3	An overview of the component package	87
Figure 3.3	A typical Structure	88
Figure 3.4	Steps performed at every cycle in the simulation thread.....	89
Figure 3.5	An overview of the gui package	90
Figure 3.6	Steps performed at every redraw in the display thread.....	91
Figure 4.1	Hybrid Viz startup screen and the main menu.....	93
Figure 4.2	Grid controls.....	94
Figure 4.3	Editing controls for common attributes.....	94
Figure 4.4	Node creation dialog and the Node editing controls.....	96
Figure 4.5	Element creation dialog and the Element editing controls.....	97
Figure 4.6	Actuator creation dialog and the Actuator editing controls	98
Figure 4.7	Simulation controls.....	99
Figure 4.8	Loading a displacement record	101
Figure A.1	Structure setup for the example problem.....	105
Figure A.2	Hybrid Viz runs alongside the RDV and a web cam feed of the damper ..	108
Figure A.3	Structural properties used in example problem.....	109

1. Abstract

Structural testing is critical in the field of structural hazard mitigation. Structural design solutions must be thoroughly tested to determine their ability to mitigate large-scale damage to lives and property. Pseudo-dynamic testing has been in use to evaluate structures since the 1970s (Mercan and Ricles, 2005). The method applies displacements to structures by solving equations of motion using numerical integration algorithms. Usually, this can be done in a quasi-static (non real-time) manner if structural characteristics allow (Mercan and Ricles, 2005). Recently, seismic hazard mitigation devices such as dampers and bearings have appeared with characteristics that necessitate real-time application of forces when tested. Real-time hybrid testing has thus become a highly desirable testing scheme in structural testing. Not only are displacements applied in real-time, but also numerical simulations of structural components not present in the test setup are combined with measured experimental data. This provides large-scale testing of structural systems using small test setups, thereby reducing time and costs while providing more accurate results.

The objective of this study is to create a visualization tool for real-time hybrid testing. The visualization tool is meant to combine the analytical and experimental aspects of hybrid testing so that researchers can see complete structural response regardless of the size of the test setup. The study was a 10-week effort, and the result is Hybrid Viz, a Java-based tool that provides real-time visualization for hybrid testing. This tool is tailored to the capabilities of the NEES Real-Time Multi-Directional (RTMD) seismic testing lab at the Advanced Technology for Large Structural Systems (ATLSS) Research Center at Lehigh University. Hybrid Viz has been successfully integrated into the testing infrastructure in the lab and proven to be a useful first-step in real-time visualization.

2. Introduction

This section presents background information on structural testing. The effects of earthquake forces on structures and the consequent need for structural testing are discussed. This leads into a discussion on the nature and characteristics of the hybrid testing scheme. The objective and scope of the study are then explained in order to see the role of Hybrid Viz in the testing process.

2.1. Structural testing background

Figure 2.1 shows how a typical structure responds in an earthquake. An earthquake produces ground accelerations. Due to the dynamic characteristics of the structure, such as stiffness and mass, the structure sways at a different frequency than the ground movements. This causes a structure to sway as shown. Depending on the size of the earthquake, the resulting motion can be devastating on a structure and its occupants. Structural testing is needed to assess the performance of structures in the laboratory before they are constructed and occupied.

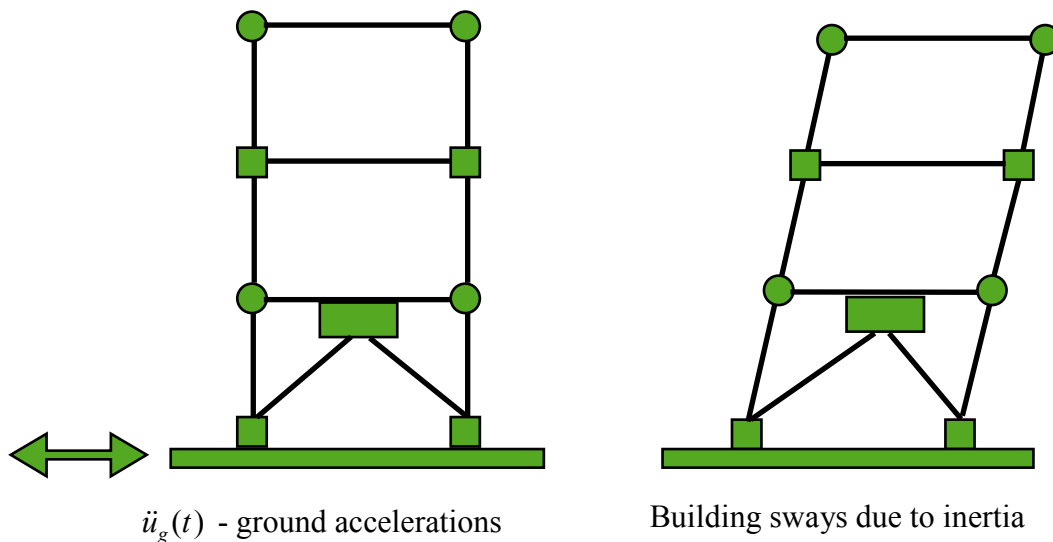


Figure 2.1 Structural response in earthquakes

A common method for simulating this behavior is shake table testing which reproduces the ground accelerations on a moving platform through hydraulic actuators. This testing method imposes limitations in scale and cost. One of the testing methods in use at the RTMD facility at Lehigh University overcomes the limitations of shake tables and is known as pseudo-dynamic (PSD) testing. Pseudo-dynamic testing assumes a fixed ground and applies calculated lateral displacements on the structure itself with hydraulic actuators attached to the facility's reaction wall. The following equation represents the motion of a structure:

$$Ma(t) + Cv(t) + r(t) = P_{eff}(t) \quad (2.1)$$

where M is the mass matrix, C is the viscous damping matrix, K is the stiffness matrix, $a(t)$ is the acceleration vector relative to the support, $v(t)$ is the velocity vector relative to the foundation,

$r(t)$ is the restoring force vector, and $P_{eff}(t)$ is the effective load vector based on the discretized ground acceleration record $\ddot{u}_g(t)$ (ATLSS, 2006). In PSD testing, M , C , and $P_{eff}(t)$ are numerically specified. Load transducers measure the restoring force as displacements are applied to the structure and fed back into an integration algorithm in order to solve Equation 2.1 at each step (see Figure 2.2). PSD testing can be performed in two ways: 1) if the components in the structure are not sensitive to the rate of loading, displacements can be applied over an extended period of time; 2) if components such as visco-elastic (VE) dampers or bearings, which are load-rate sensitive, are being tested, displacements must be applied in real-time to ensure that the response of the structure is accurate. This study focuses on the real-time aspect of PSD testing, though conventional PSD testing is implicitly supported.

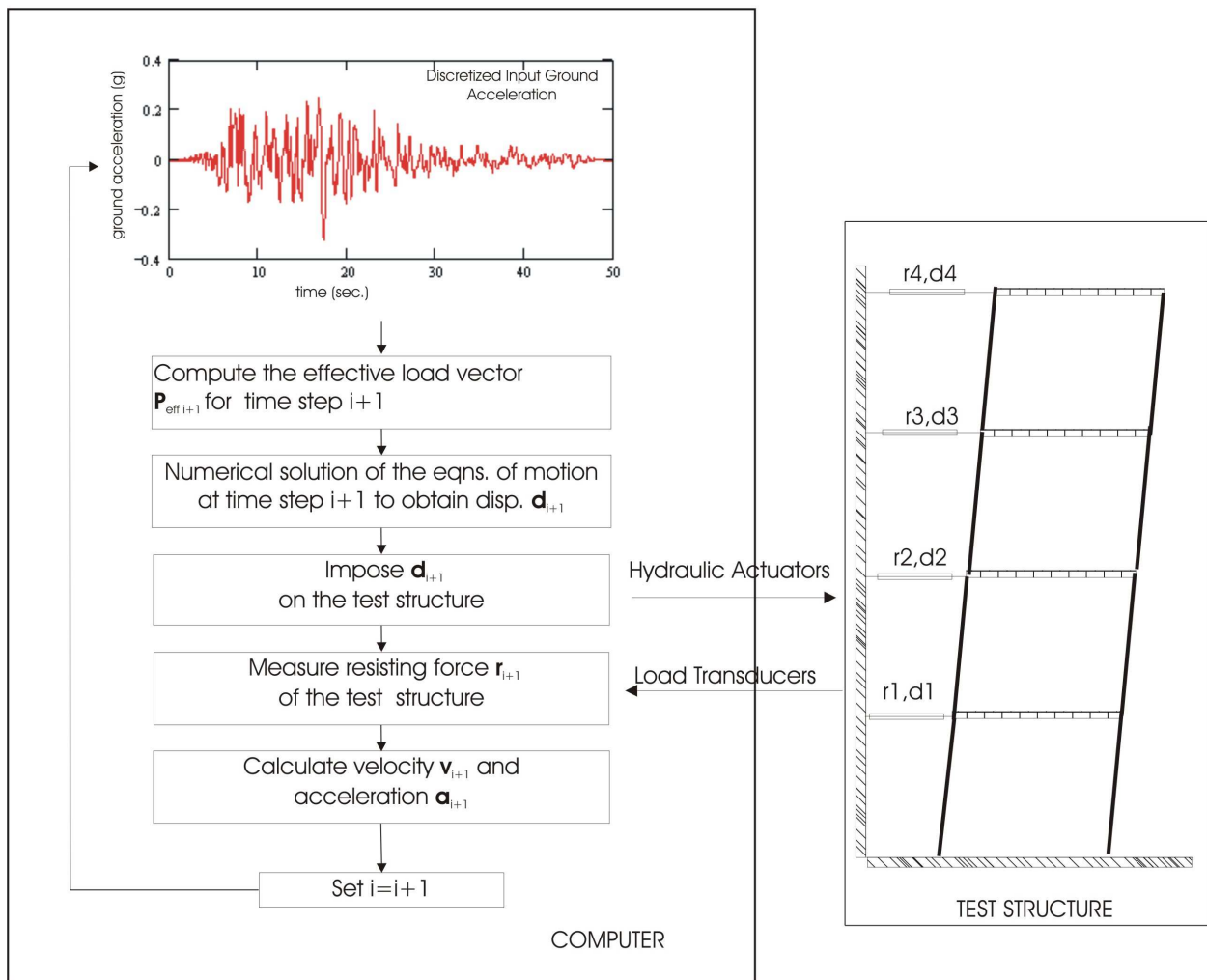


Figure 2.2 PSD testing with a discretized integration algorithm (ATLSS, 2006)

Hybrid testing is a subset of PSD testing that combines a physical substructure (the test setup in the lab) with an analytical substructure (numerical model on a computer) (see Figure 2.3) (ATLSS, 2006). The integration algorithm uses a combined restoring force vector retrieved from both substructures to solve the equation of motion. Hybrid testing offers significant advantages.

Because most of the structure is analytically modeled, large test setups do not have to be constructed, thereby saving time and money. Researchers can consider the effects of structural systems as a whole while testing parts of a structure or even just one component (such as a damper).

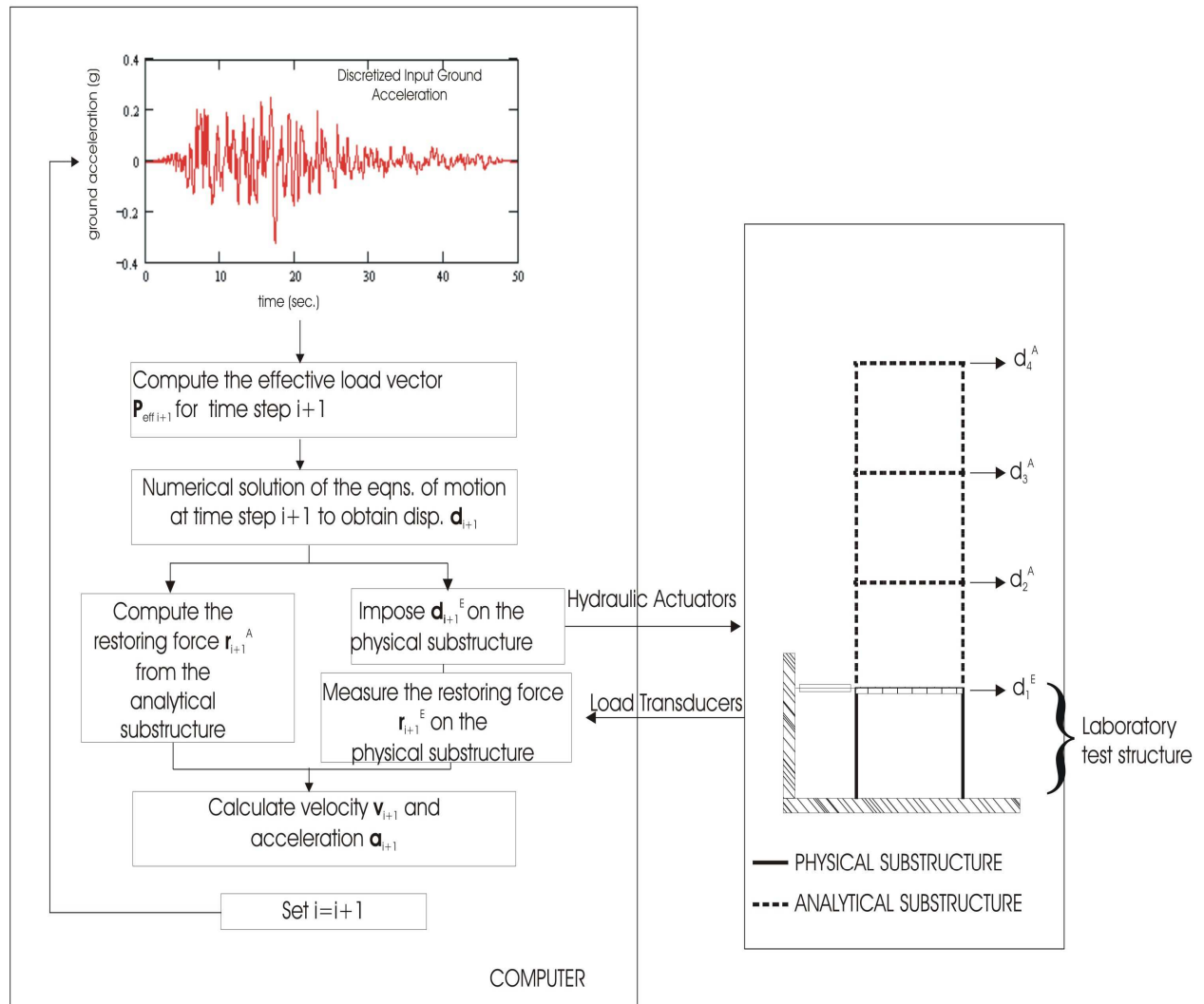


Figure 2.3 Hybrid PSD testing (ATLSS, 2006)

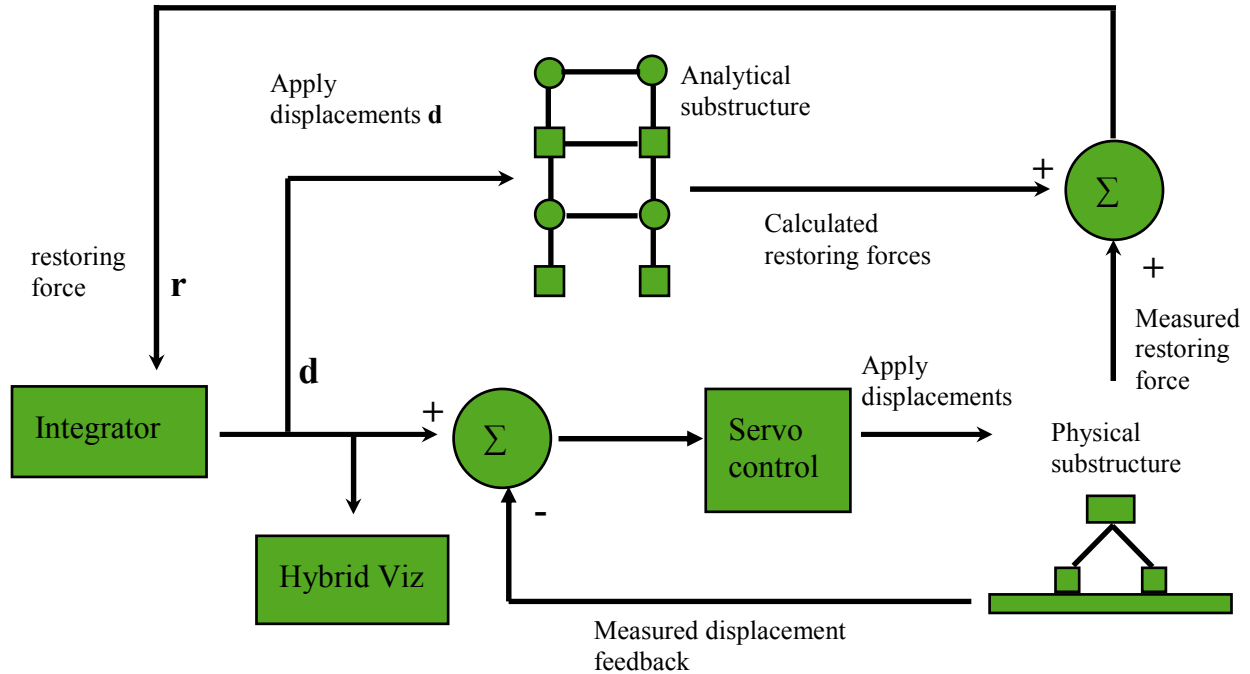


Figure 2.4 Hybrid Viz in the integration process

Figure 2.4 shows where Hybrid Viz lies in the integration algorithm. At each step of the algorithm, displacements are applied to both the analytical and physical substructure, and Hybrid Viz retrieves them at its own update rate via the SCRAMNet. The restoring forces from both substructures are combined and used by the integrator to calculate the displacements for the next step, and the cycle continues.

2.2. Objectives and scope of the study

The purpose of this study is to develop a software tool that can visualize both the experimental and analytical components of hybrid testing simultaneously in real-time. As a test is running in the lab, the tool will provide a look at the response of an entire structure whose configuration is left entirely up to the user. Examining structural response as a test is running assists researchers in assessing the performance of hazard-mitigating devices and structural designs.

A portion of the development time was devoted to software design. One of the main goals of the project is to make an extensible solution, one that lends itself to be modified and expanded in the future, while meeting the desired goal of real-time visualization. For this study, only 2-dimensional animation was planned for basic planar shear structures with a maximum of three degrees of freedom at a node (x, y, and z rotation), though nodes in the program have support for a future transition to six degrees of freedom in three dimensions.

The rest of this document focuses on the design, implementation, and usage of Hybrid Viz. Section 3 presents the mathematics behind structural analysis used in the program as well as a discussion of the design and implementation. Section 4 contains the program's user's guide, and Section 5 has some concluding remarks as well as suggestions and guidelines for future enhancements to Hybrid Viz. The appendices contain an example problem with file listings.

3. Background

This section begins with key mathematical theory behind structural testing that is used in Hybrid Viz. Details about the design and implementation of the program are then presented. The subsections on the packages of Hybrid Viz not only explain the interactions between object classes in the program but also define important terminology that will be used extensively in the user's guide in Section 4.

3.1. Mathematics

The behavior and appearance of beams and columns is based on the interpolations of the displaced shape along the length of the member using Hermitian shape functions. A Hermite shape function is essentially a cubic polynomial. Cubic polynomials have the form:

$$\begin{aligned} y(x) &= ax^3 + bx^2 + cx + d \\ y'(x) &= 3ax^2 + 2bx + c \end{aligned} \tag{3.1}$$

where (x,y) are the coordinates of curve points, y' is the derivative of y with respect to x , and a , b , c , and d are coefficients. Given two endpoints of the member, (x_0,y_0) and (x_1,y_1) , in an x-y 2-D coordinate system (see Figure 3.1), observe that:

$$\begin{aligned} y(x_0) &= y_0 \\ y(x_1) &= y_1 \\ y'(x_0) &= \theta_0 \\ y'(x_1) &= \theta_1 \end{aligned} \tag{3.2}$$

where θ_0 and θ_1 are the angles between the global x-axis and the tangent at each end of the member. In order to find $y(x)$, which is the y-coordinate of the deformed shape at a particular place along the member (referred to herein as a HybridElement, which is the equivalent Java class described in Section 3.2.1), the coefficients must be found by solving a system of four equations with four unknowns. The interpolate() method in HybridElement implements this over a specified number of interpolations. The equations are put into a matrix and solved using the JAMA package (MathWorks and NIST, 2005), where:

$$\begin{bmatrix} x_0^3 & x_0^2 & x_0 & 1 \\ x_1^3 & x_1^2 & x_1 & 1 \\ 3x_0^2 & 2x_0 & 1 & 0 \\ 3x_1^2 & 2x_1 & 1 & 0 \end{bmatrix} \begin{Bmatrix} a \\ b \\ c \\ d \end{Bmatrix} = \begin{bmatrix} y_0 \\ y_1 \\ \theta_0 \\ \theta_1 \end{bmatrix} \tag{3.3}$$

Once the coefficients are calculated, they are simply put back into Equation 3.1 and the corresponding y coordinate is calculated. After a fixed number of interpolations, a set of x and y coordinates for the deformed shape is obtained (see Figure 3.1).

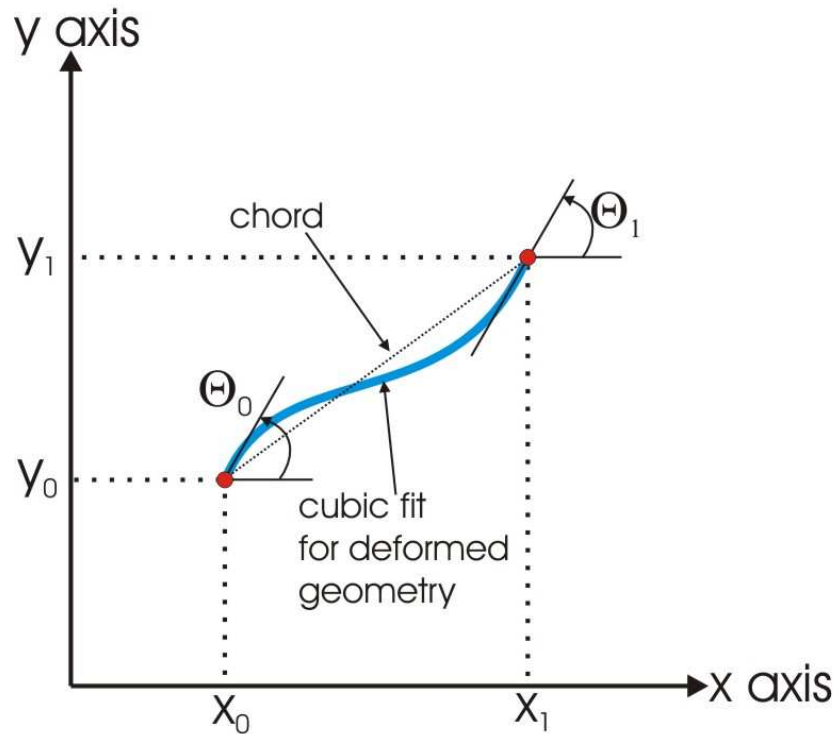


Figure 3.1 Cubic fit from two endpoints

3.2. Design and implementation

Hybrid Viz is written completely in Java. There are two main packages: component and gui. The component package contains fundamental classes and interfaces for creating a Test Setup and linking with the SCRAMNet. The gui package provides the graphical user interface (GUI) as well as interfaces used by component classes to integrate with the GUI. See the Java documentation (available at the NEES@Lehigh RTMD Wiki page at http://www.nees.lehigh.edu/wiki/index.php/Main_Page) for detailed class information.

Hybrid Viz works by integrating into the RTMD architecture through a shared memory network called SCRAMNet (Shared Common RAM Network). The simulation, control, data acquisition and telepresence systems at the RTMD facility use this low-latency data-sharing network to achieve real-time status. The SCRAMNet provides a transparent and seamless interface to the analytical substructure(s) and experimental substructure(s) for telepresence. Hybrid Viz accesses the telepresence data to retrieve displacement and rotation data in order to display a realistic representation of the deformed structure (see Figure 3.2). The next section presents a more detailed discussion of this process.

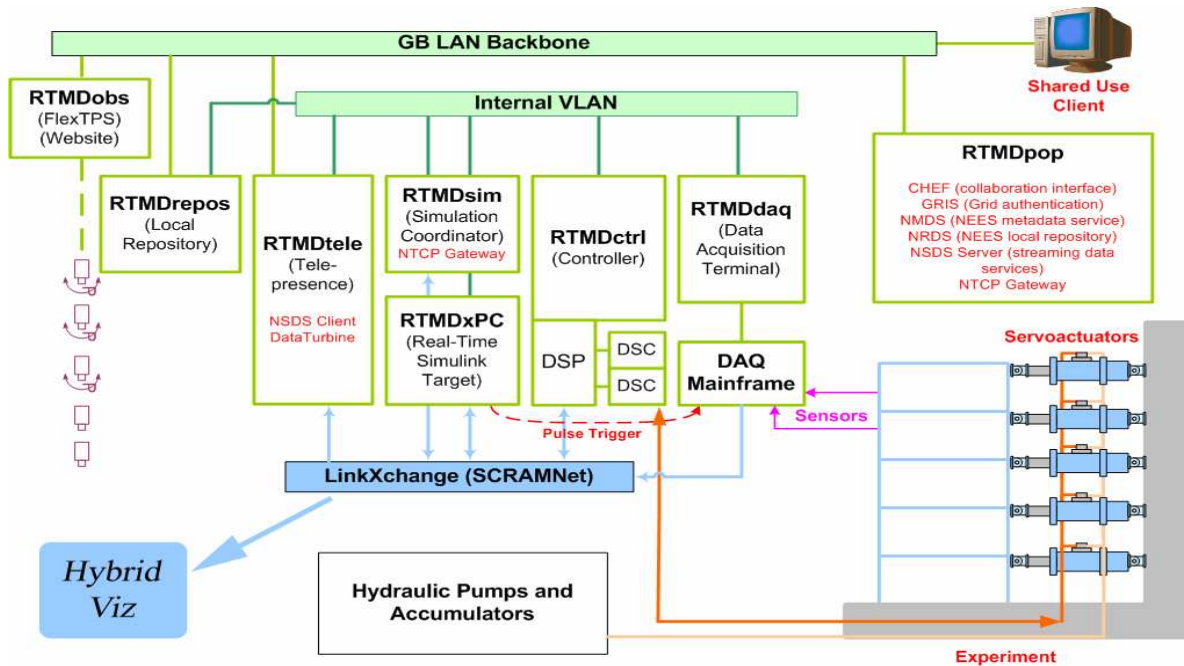


Figure 3.2 Hybrid Viz taps into the SCRAMNet

3.2.1. The components package

Figure 3.3 shows the overall relationships between the main classes in the components package. The Structure class represents the structure in a hybrid test, both analytical and experimental aspects. It should be noted that, as far as Hybrid Viz is concerned, there is no difference between the analytical and experimental substructures. A Structure consists of Nodes (the connection points) and Elements (the connecting edges) (see Figure 3.3). The Actuator class represents the hydraulic actuators used to apply displacements to a structure. The TestSetup class combines a Structure, a set of Actuators, and settings for the Grid (see Section 3.2.2).

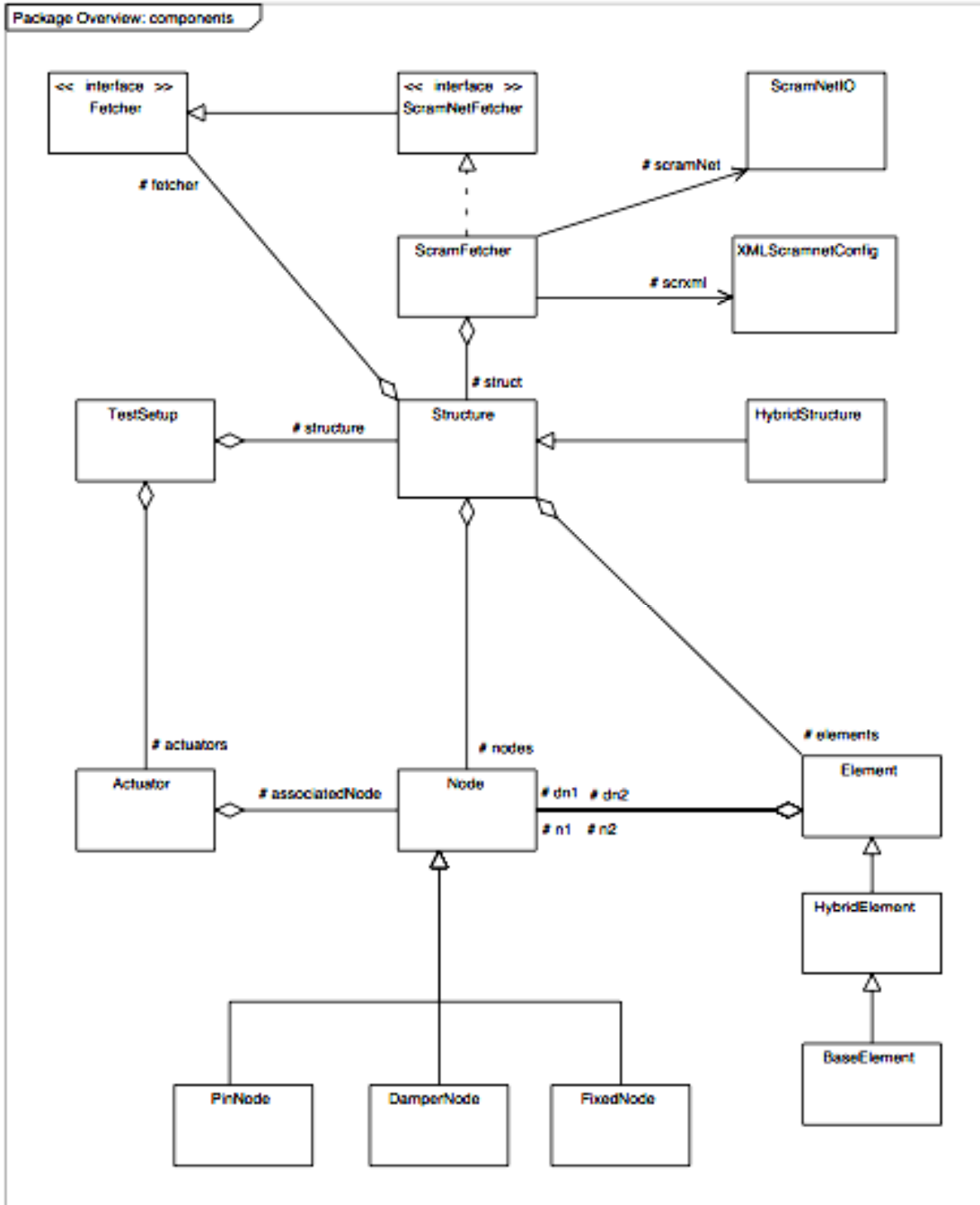
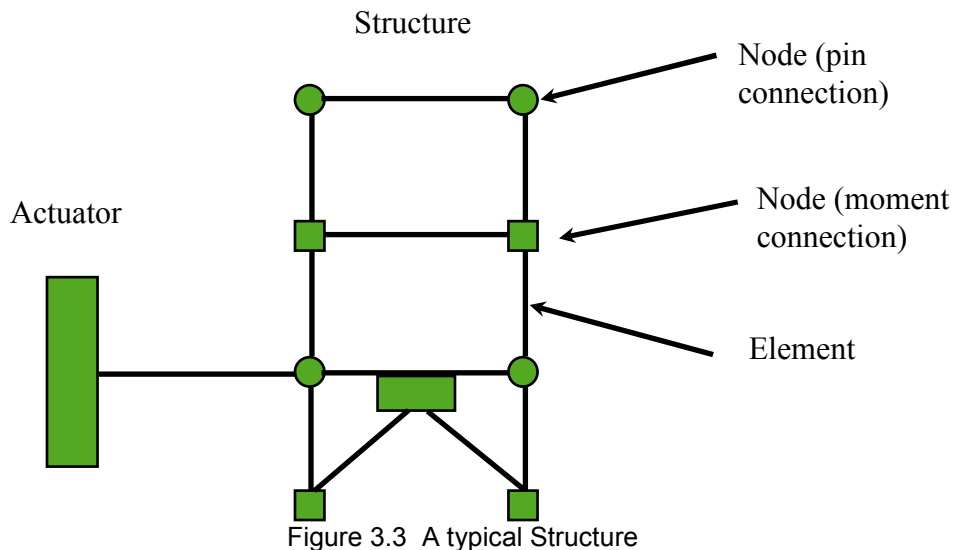


Figure 3.3 An overview of the component package

There are three types of Nodes: pin, fixed (or moment), and damper. Pin nodes are represented by small circles and are pin connections. Fixed nodes are represented by small squares and are rigid connections. Damper nodes represent dampers in a test by small rectangles. A Node has an integer ID and a constraint ID. The constraint ID determines what displacements the Node will get. This allows Nodes on the same floor of a Structure to get the same displacements. A Node

also has up to six degrees of freedom: x, y, z, rotation x, rotation y, and rotation z. Nodes, Elements, and Actuators have an integer identification number. Thus, for example, only one Node with its ID equal to 1 is allowed in any Structure, and the same applies to Elements and Actuators.

A Structure makes use of a class implementing the Fetcher interface to retrieve the displacements for its Nodes. These nodal displacements are used by the Elements to calculate their deformed shapes. The classes shown are at an abstract level of programming which leaves implementation specifics pertaining to behavior and appearance open. HybridStructure, HybridElement, and the nodal classes (PinNode, FixedNode, and DamperNode) provide the implementations currently used by Hybrid Viz. They define the appearance shown in Figure 3.3 as well as the behavior and appearance of the deformed structure. HybridElement implements the abstract (i.e. unimplemented) interpolate() method which solves the Hermitian polynomial discussed in Section 3.1.



At any moment in time, the SCRAMNet contains, among other data, displacement and rotation information for the Nodes in the Structure. A thread of execution called the simulation thread is running at a steady rate of about 35 Hz and is constantly invoking the updateElements() function in HybridStructure. This method causes it to update all of its Elements. HybridStructure retrieves the current displacements for its Nodes through an instance of ScramFetcher. ScramFetcher is able to communicate directly with the SCRAMNet hardware through two classes (ATLSS, 2006): ScramNetIO and XMLScramnetConfig. ScramNetIO provides methods to read and write data from and to the SCRAMNet. XMLScramnetConfig provides a layer of abstraction over the memory map by mapping memory locations to nodal information in a standard XML format. Using these two classes, ScramFetcher retrieves and passes along nodal displacements to HybridStructure, and these are then passed to each HybridElement (see Figure 3.4). The displacements retrieved depend upon the constraint IDs of the Nodes and their respective degrees of freedom. Using these displacements, each HybridElement generates a set of x and y coordinates for its deformed shape by interpolation as discussed in Section 3.1.

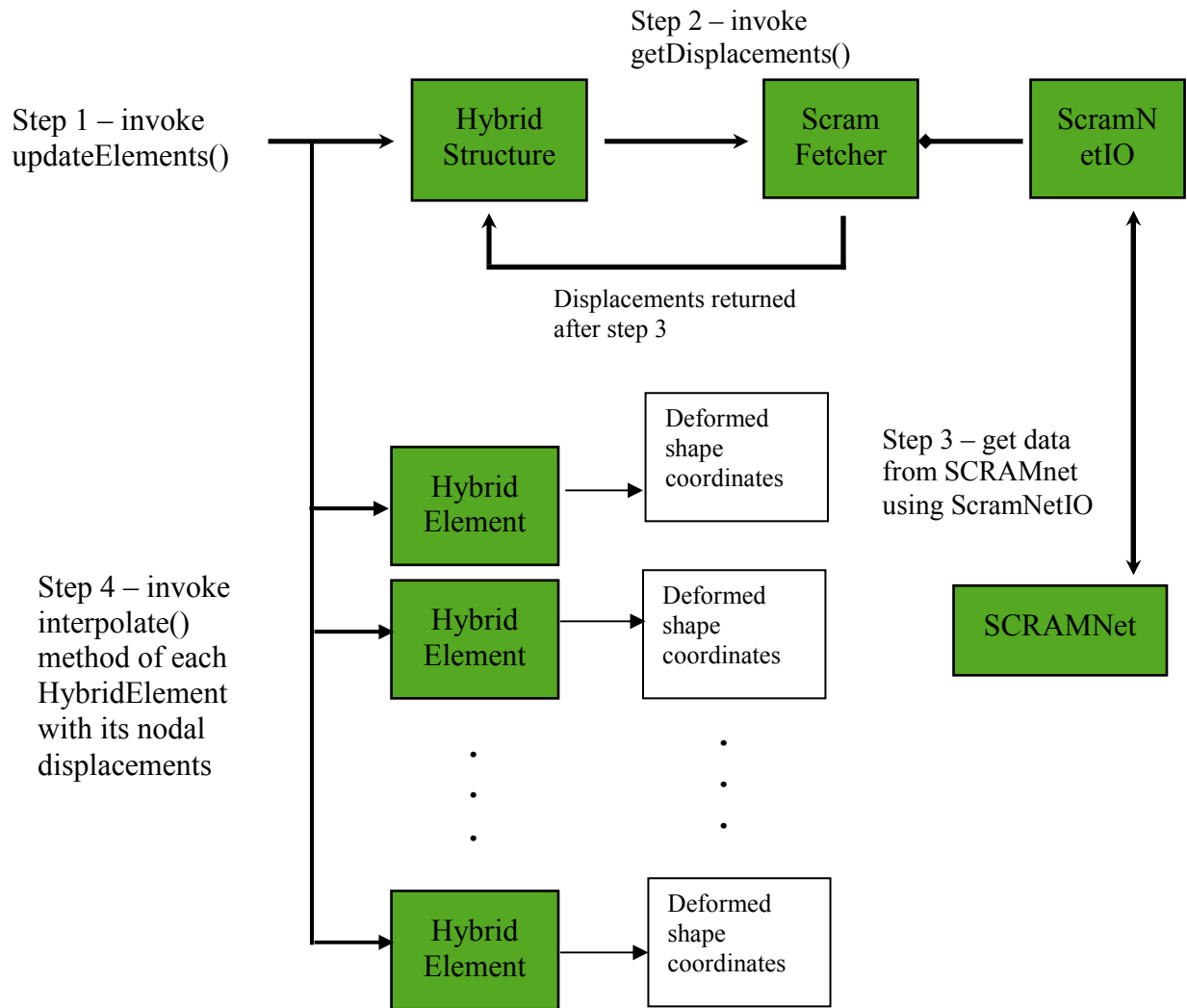


Figure 3.4 Steps performed at every cycle in the simulation thread

3.2.2. The gui package

Figure 3.5 shows the relationships between the main classes in the gui package. The **UserInterface** class consists of the **Display** class which provides on-screen graphics through the **Grid** class. The **Grid** class provides a user-adjustable grid for placing **Nodes**, **Elements**, and **Actuators** in real-world coordinates. Methods are provided which convert from real to pixel coordinate systems based on the **Grid** size and the dimensions of each box (Section 4.3 explains how the **Grid** is adjusted). **Nodes**, **Elements**, and **Actuators** all function in real-world coordinates and use these methods to do conversions before drawing themselves on the screen.

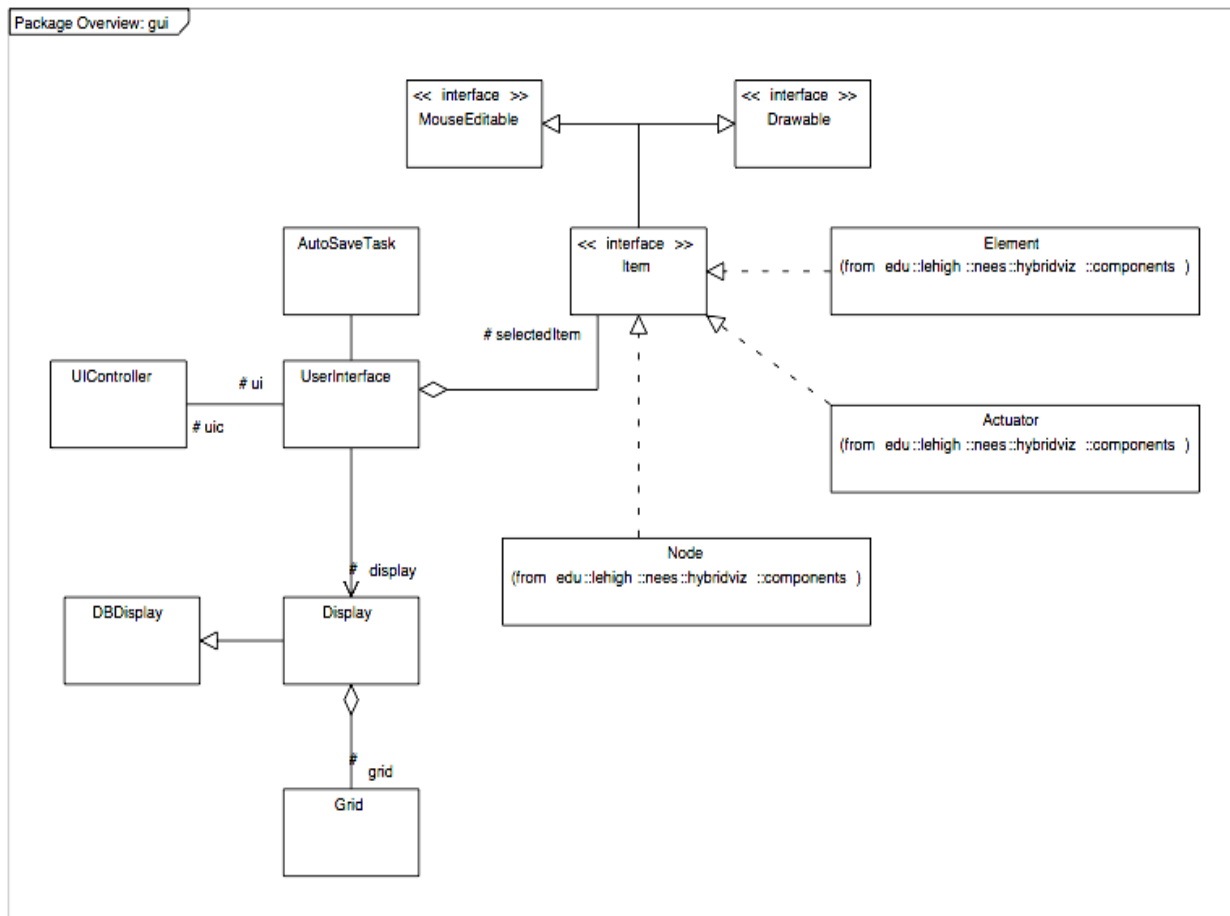


Figure 3.5 An overview of the gui package

A secondary thread called the display thread is responsible for all drawing. Figure 3.6 shows the sequence of steps performed in this thread to get all the graphics onto the screen.

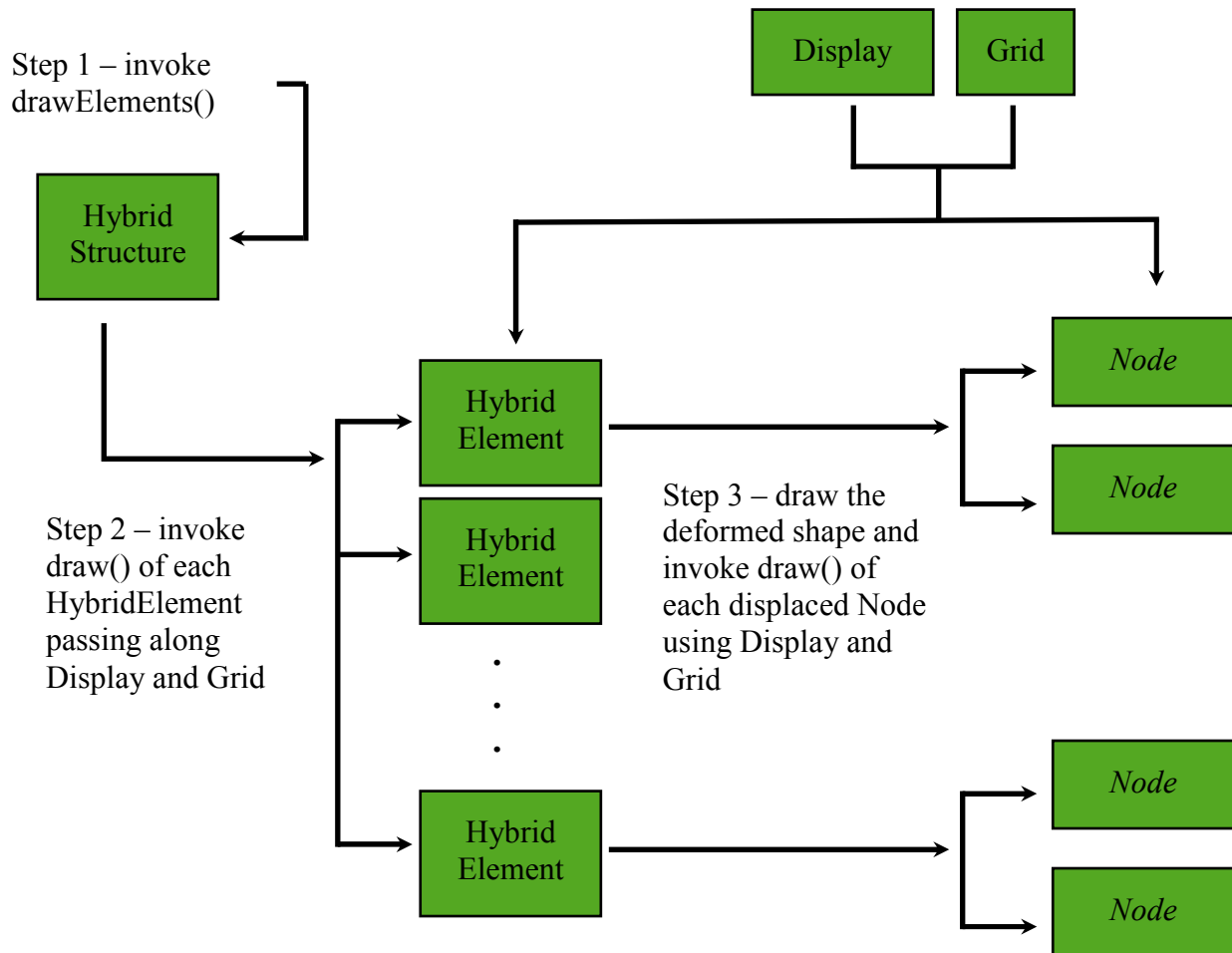


Figure 3.6 Steps performed at every redraw in the display thread

The simulation and display threads are synchronized using object-locking mechanisms in Java. While one thread is working with an object (for example, with a particular instance of HybridElement), that object is locked and the other thread cannot access it. The use of threads provides smoother graphics and the ability to change many settings in real-time (see Section 4.7).

The Item interface facilitates editing of components through the user interface. It defines the methods that modify attributes common to all components (see Section 4.4). It also defines methods useful for mouse and keyboard selection and movement. The abstract component classes Node, Element, and Actuator implement the Item interface, though it should be noted that some methods are left abstract to give subclasses freedom in implementation. Also, for consistency's sake, some Item methods in Element throw an exception indicating that they are not supported.

4. User's guide

This section provides detailed instructions for the Hybrid Viz end-user. Section 4.1 contains instructions for running the program as well as general steps for its use. Section 4.2 gives a general overview of the GUI and is a good starting point to get acquainted with the program's features. Sections 4.3 and 4.4 cover the configuration of the Grid and the creation of Structures. Finally, the last sections discuss saving and loading, coordination with the SCRAMNet, running simulations, and loading displacement records. Refer to sections 3.2.1 and 3.2.2 for an explanation of some of the terminology used.

4.1. Running the program

Hybrid Viz requires Java 1.5 or later. The file HybridViz.jar is the main program executable. The lib folder contains other required resources and must be in the same directory as HybridViz.jar. Double-clicking on the HybridViz.jar file will start the program if Java is properly configured on the system. Otherwise, a standard Windows or Unix command prompt is required. The following command will start the program in non-testing mode:

```
java -classpath "HybridViz.jar;lib/;" edu.lehigh.nees.hybridviz.HybridViz
```

To start the program in testing mode, use the following command:

```
java -classpath "HybridViz.jar;lib/;" edu.lehigh.nees.hybridviz.HybridViz test
```

Note that testing mode can only be accessed via the command shown above. These instructions assume that the system classpath is properly configured for Java. See the Java installation help page at <http://java.com/en/download/help/> for more assistance with Java installation and running Java programs.

Setting up and using Hybrid Viz generally involves the following steps (see the specified sections for details):

1. Set up the real world coordinate system by adjusting the Grid (see Section 4.3).
2. Create the Nodes and Elements of the Structure as well as any desired Actuators (see Section 4.4).
3. Save the setup in a file so that an XML configuration file can be generated (see Section 4.5).
4. Load the generated XML configuration file (see Section 4.6).
5. Start the simulation and adjust settings in real-time if desired (see Section 4.7).

4.2. The user interface

Figure 4.1 shows the window seen at program startup and a close-up of the menu bar. The user interface is divided into three sections. The top of the window contains the menu bar with the File, Edit Mode, Simulation, and Help menu items. On the left side of the window, the control panel contains various controls for modifying the Grid (the Grid controls), running a simulation (the simulation controls), and editing Nodes, Elements, and Actuators (the editing controls). Section 4.4 has information on the use of the Edit Mode menu and these editing controls.

The right side of the window contains the Grid (the box-filled portion) where Structures are created and displayed. The controls that adjust the Grid are described in Section 4.3. Sections 4.5 and 4.6 contain information on the File menu. Sections 4.7 and 4.8 provide information on the Simulation menu and the simulation controls. The Help menu brings up a dialog with basic user instructions.

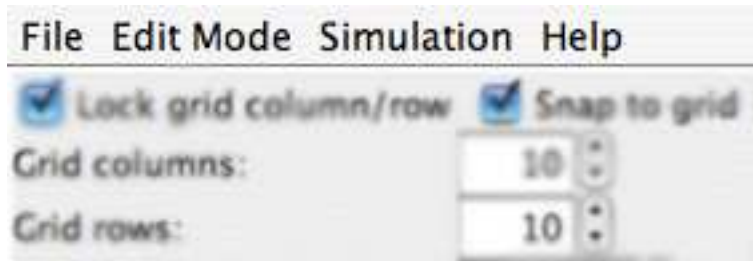
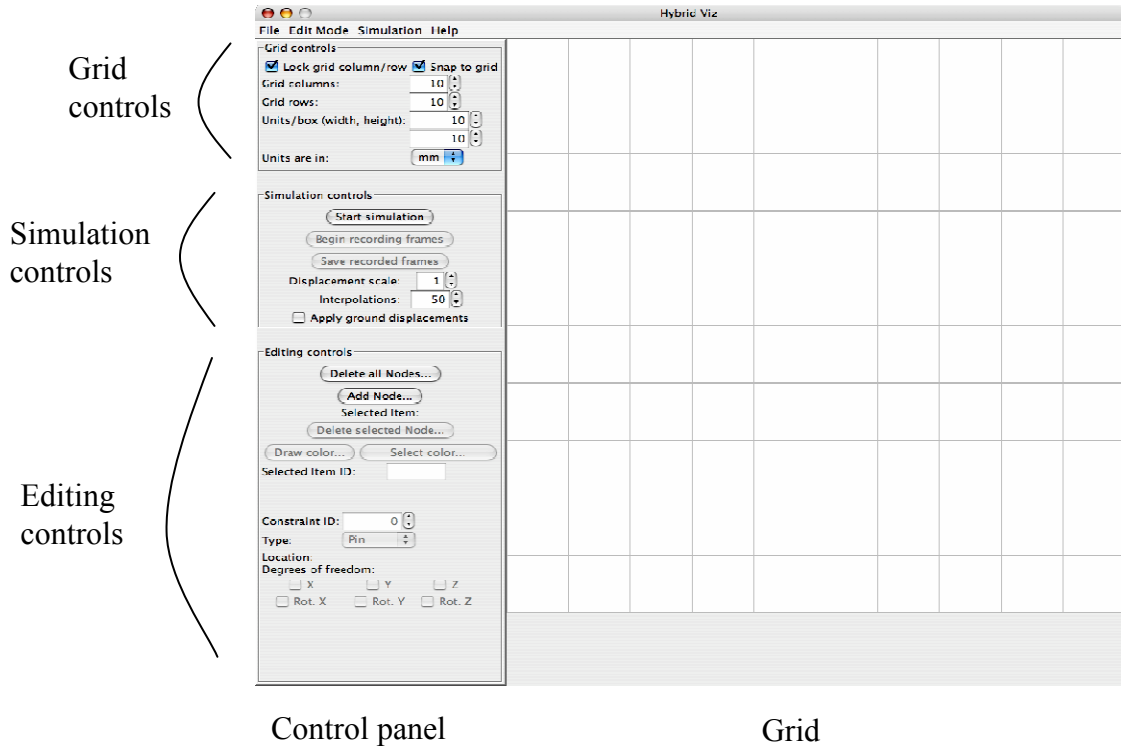


Figure 4.1 Hybrid Viz startup screen and the main menu

4.3. Grid controls

The set of controls at the top of the control panel are used to modify the Grid (see Figure 4.2). Deselecting the “Lock grid columns/rows” checkbox allows the user to have a different value for the columns and rows. When the “Snap to grid” checkbox is selected, Node and Actuator placement is forced to the corners. Clicking the tiny arrow buttons or entering values in the column and row text fields will change the number of columns and rows in the Grid. Below these controls are text fields to control the real size (width and height) of each Grid box. These determine the real world coordinates of the Grid. Below the Grid box controls is a combo box that allows the user to change the units of the Grid. For example, in the figure below, there are 10 column and 10 rows, and each box in the Grid is 10 mm x 10 mm in size. The lower-left corner

of the Grid is always the origin ($x = 0, y = 0$), and so the next corner along the diagonal of the Grid would have coordinates (10, 10), followed by (20, 20), and so on.

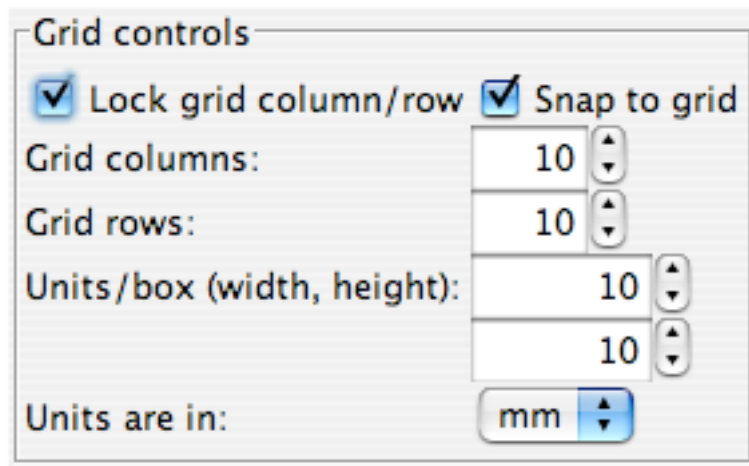


Figure 4.2 Grid controls

4.4. Creating Structures

The Edit Mode menu at the top of the window switches between editing modes to allow the user to add Nodes, Elements, or Actuators. Switching to these modes will alter the editing controls based on the selected option. This menu also has options for adding and deleting items (based on the current editing mode) and options to align a selected Element horizontally or vertically.

In the editing controls, three common attributes of all items in a Test Setup (Nodes, Elements, and Actuators) can be modified (see Figure 4.3):

- Draw color: press the “Draw color...” button to change the color of the item
- Select color: press the “Select color...” button to change the color of the item when selected
- Selected Item ID: enter an integer to change the integer ID number that distinguishes the selected item from all other items of its type. A message will indicate if the value entered is already in use by another item.

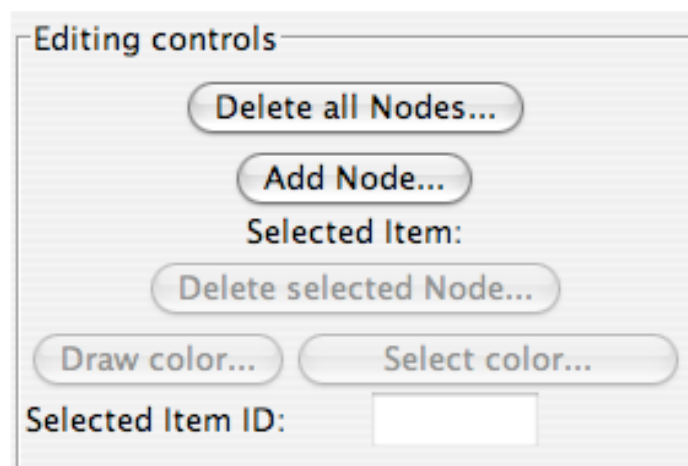


Figure 4.3 Editing controls for common attributes

At any time, selecting an item in the Grid (either a Node, Element, or Actuator) will switch to the corresponding editing mode and show the item's information in the editing controls portion of the control panel.

4.4.1. Adding and editing Nodes

Switching the editing mode to Nodes in the Edit Mode menu allows the user to add and modify Nodes. Right-clicking anywhere in the Grid or pressing the "Add Node..." button will bring up a dialog to create a Node at the Grid corner nearest to the clicked spot (see Figure 4.4). After selecting the ID and type, clicking the "Create" button will create the Node. Note that pin nodes show up as small circles, fixed nodes as small squares, and damper nodes as small rectangles.

Left-clicking on a Node will select it (causing it to change color) and show its information in the Node editing controls. Left-clicking on an empty area in the Grid and dragging will bring up a box to select multiple Nodes. These Nodes can be edited simultaneously for all fields except the ID. Note that a degree of freedom (DOF) checkbox must be pressed in order to apply any changes to the selected Nodes, and the constraint ID field also must be modified with the arrow buttons in order to apply changes to all selected Nodes. Changing the constraint ID value will set that constraint ID to all selected Nodes, and checking a DOF checkbox will apply the currently selected configuration of degrees of freedom to all selected Nodes. The following attributes of a Node can be edited in the Node editing controls (see Figure 4.4):

- Constraint ID: the integer ID that maps the Node to a particular displacement stream from the SCRAMNet. Note that a constraint ID of -1 means that the Node will never move, and constraint ID 0 is reserved for ground displacements.
- Degrees of freedom: the Node will be free to move only in the directions selected. For example, if only X is checked, the Node will move only along the x axis

Pressing the "Delete all Nodes..." button will delete all Nodes (and any associated Elements). Pressing the "Delete selected Node(s)..." button will delete only the selected Node(s).

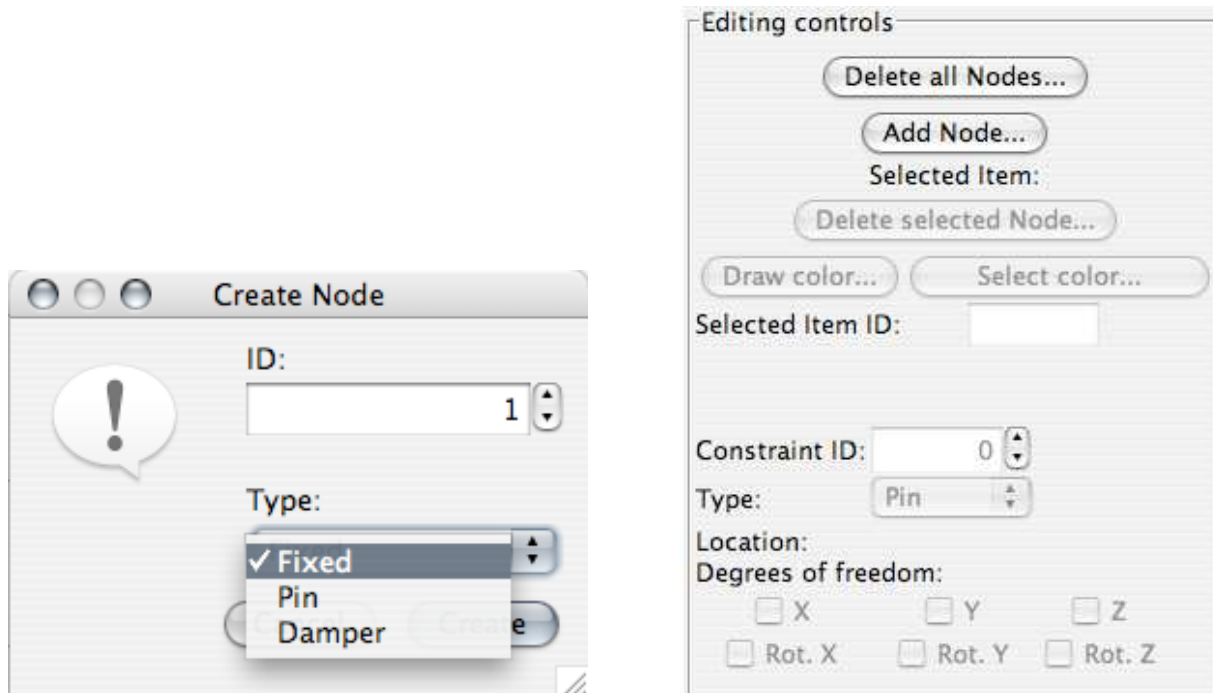


Figure 4.4 Node creation dialog and the Node editing controls

4.4.2. Adding and editing Elements and Bases

Switching the editing mode to Elements in the Edit Mode menu allows the user to add and modify Elements. To add an Element, select the first Node by left-clicking, the second Node by right clicking, and then press the “Add Element...” button or the ‘e’ key to bring up the Element creation dialog (see Figure 4.5). In the Type menu, Element is a standard Structure element while Base represents the foundation of a structure and is used for base motion (represented by a solid-filled rectangle). To select an Element or a set of Elements for editing, left-click on an empty area of the Grid and drag around the Element’s connecting line (or rectangle for bases). The Element will change color based on its select color. The following attributes of an Element can be edited (see Figure 4.5):

- Displaced color: press the “Displaced color...” button to change the color of the Element’s deformed shape
- Fixed base: for base elements, selecting this checkbox will draw the base’s displaced position

Pressing the “Delete all Elements...” button will delete all structural elements and bases. Pressing the “Delete selected Element...” button will delete only the selected Element(s).

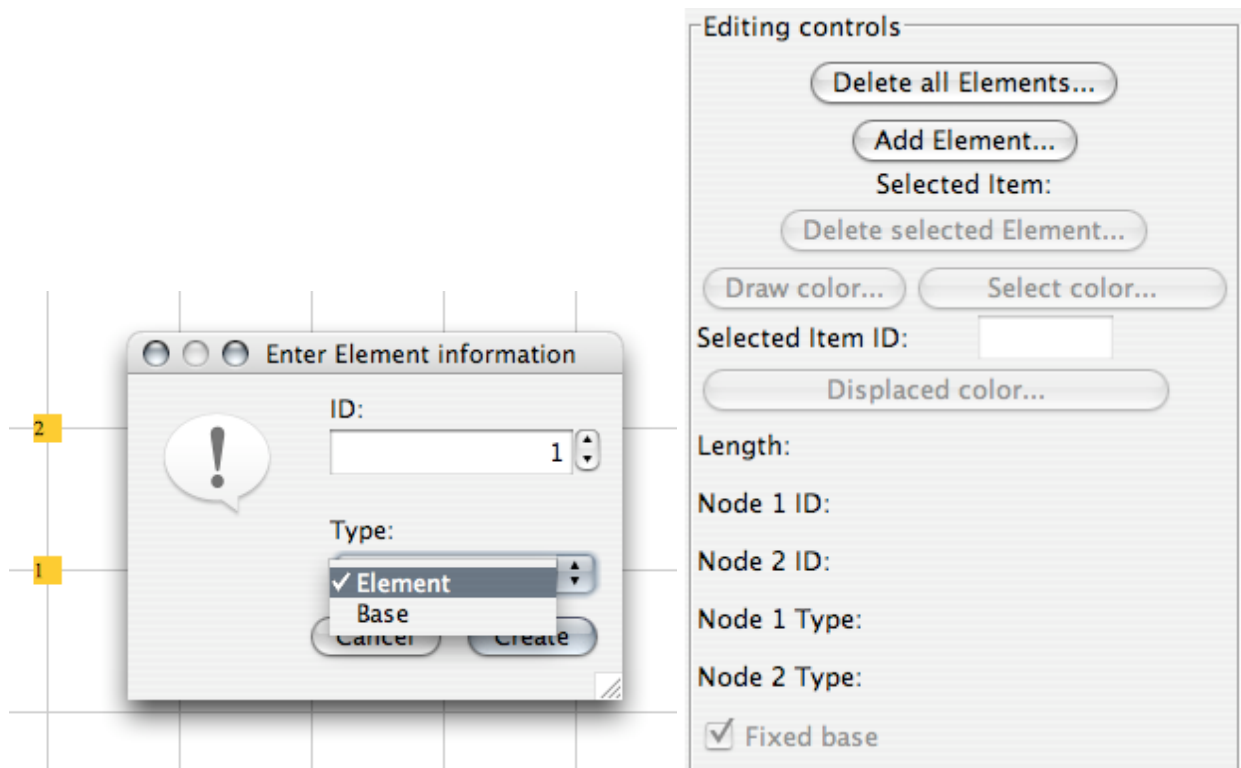


Figure 4.5 Element creation dialog and the Element editing controls

4.4.3. Adding and editing Actuators

Switching the editing mode to Actuators in the Edit Mode menu allows the user to create Actuators. Right-clicking anywhere in the Grid or pressing the “Add Actuator...” button will bring up a dialog to create an Actuator (see Figure 4.6). The dialog has options for selecting the Actuator’s ID and associated Node (based on the IDs of all the current Nodes). The associated Node is the Node used to draw the representation of the actuator as a line extending from a wall section to the Node. Left-clicking on the wall section of an Actuator or dragging over the connecting line will select it for editing in the Actuator editing controls (see Figure 4.6). The associated Node can be changed by selecting its ID in the drop-down menu in the Actuator editing controls. Because an Actuator is actually associated with the displaced Node of an Element, Actuators can be associated only with Nodes that are associated with Elements. Pressing the “Delete all Actuators...” button will delete all Actuators. Pressing the “Delete selected Actuator...” button will delete only the selected Actuator(s).

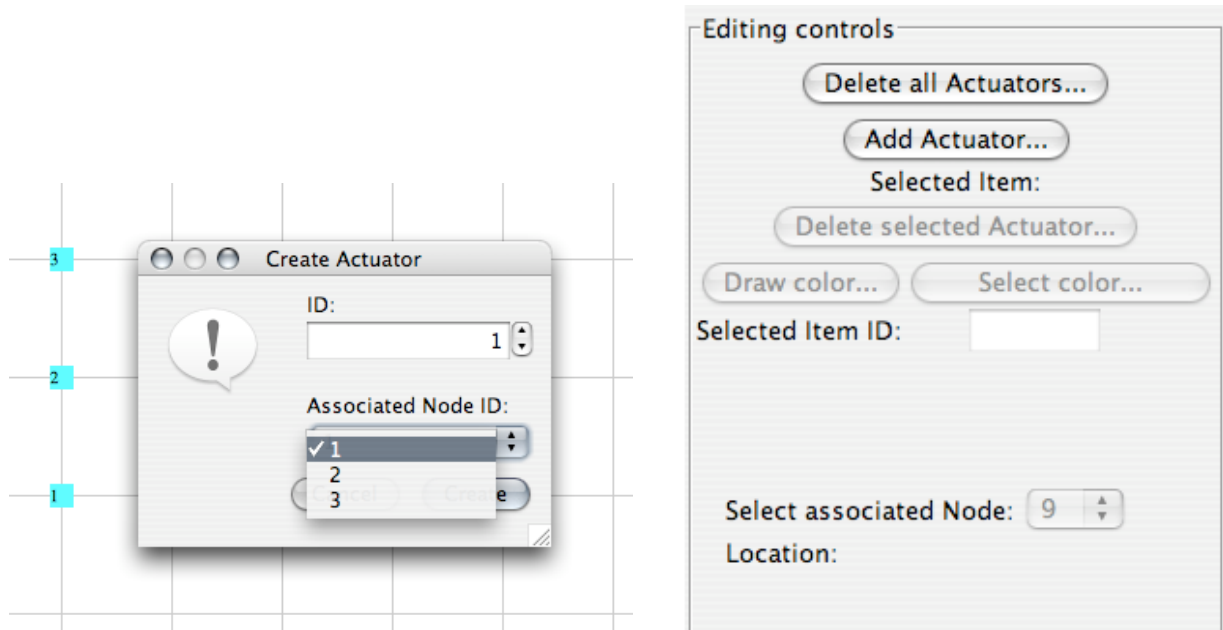


Figure 4.6 Actuator creation dialog and the Actuator editing controls

4.5. Saving and loading a Test Setup

The File menu has the following options:

- Save – Saves the currently loaded file
- Save As... - Saves the current settings and Structure in a new Hybrid Viz Setup file
- Open... - Loads a Hybrid Viz Setup from a .hvs file
- Enable auto-save – Enables or disables the auto-save feature. When enabled, Hybrid Viz will save the currently loaded Test Setup every five minutes to a separate file with the extension “.bk”.
- Load XML configuration... - Loads an XML configuration from a file (see Section 4.6)
- Exit Hybrid Viz – Exits the program

Hybrid Viz saves the information for the current configuration in the class TestSetup. A TestSetup consists of a Structure as well as Actuators and Grid settings. A TestSetup can be written to, and read from, a file for quick setup. This file is known as a Hybrid Viz Setup and has extension “.hvs”. Hybrid Viz uses XML to save these configuration details. The locations and attributes of Nodes and Actuators, Element attributes, and Grid settings are all saved in this file.

The XML file is relatively self-explanatory, with separate XML elements for the Structure (and each of its Nodes and Elements), each Actuator, and one XML element with Grid settings. In order for Hybrid Viz to recognize this XML format, the file must be saved with the extension “.hvs”. Future additions can be more easily supported via XML with simple modifications to the save and load methods in the TestSetup class. Note that Nodes must always be loaded from the file (regardless of format) before Elements in order to ensure that Elements are associated with Nodes that are actually part of the Structure.

4.6. Linking with the SCRAMNet

In order for Hybrid Viz to work with the SCRAMNet, it needs an XML configuration file containing the locations on the SCRAMNet where data will be retrieved. This is achieved through the ReadXMLConfig and XMLScramnetConfig classes (see Section 3.2.1). After the Test Setup is complete, it is saved to a .hvs file (as described in Section 4.5) that will be used by the Integrated Control Configurator (ICC) to generate the necessary XML file (see the RTMD Wiki page at http://www.nees.lehigh.edu/wiki/index.php/Main_Page for more information on the ICC.). Once this XML file is generated, select “Load XML configuration...” from the File menu to load the file. See the example problem in the appendices for a sample of a generated XML file.

4.7. Starting and running a simulation

The Simulation menu has an option to start or stop a simulation and is equivalent to the “Start simulation” button in the simulation controls (see Figure 4.7). The “Displacement scale” field will scale the displacements being applied to the Structure. The value set in “Interpolations” determines the number of interpolations used by each Element to calculate its deformed shape. If the “Apply ground displacements” checkbox is checked, the entire Structure will move side to side according to the ground displacements available on the SCRAMNet. Applying ground displacements offers even more realistic structural behavior.

Once the XML configuration file is loaded, pressing the “Start simulation” button or the equivalent menu item in the Simulation menu will start the simulation loop (the button’s text will change to “Stop simulation”). Hybrid Viz will continuously poll the SCRAMNet for displacements. Note that Hybrid Viz will not begin the simulation loop without a loaded XML configuration file and will indicate if no XML file has been loaded. Furthermore, the user is responsible for switching the XML configuration file if the Test Setup is modified. Deleting Elements or Nodes or modifying the constraint IDs and degrees of freedom of Nodes may result in errors and unpredictable behavior if the XML configuration file is not regenerated and loaded. With a properly generated and loaded XML configuration file, Hybrid Viz will begin reading displacement data from the SCRAMNet and the Structure will respond accordingly.

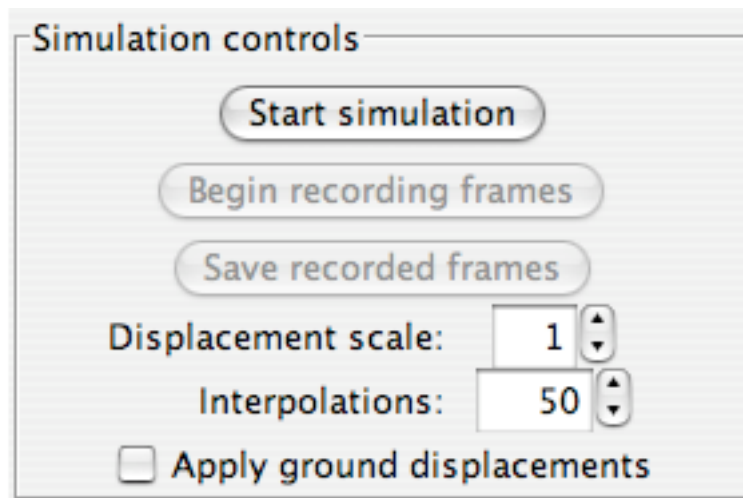


Figure 4.7 Simulation controls

For testing without the SCRAMNet hardware, Hybrid Viz must be started from the command line with the single argument “test” (see Section 4.1). Hybrid Viz will go into testing mode and use simulation SCRAMNet code to produce test displacements for a three-story structure via the TestScramFetcher class. Hard-coded test displacements will be available for constraint IDs 0, 1, 2, and 3 (see Section 4.4.1). See the Java documentation for more details about TestScramFetcher.

While the simulation is running, the following settings can be adjusted in real-time:

- The number of columns and rows in the Grid
- The real-world height and width of each box in the Grid
- The desired units (meters, centimeters, feet, etc.)
- A scale factor on the displacements (maximum of 10)
- The number of interpolations to calculate for each Element
- Whether or not ground displacements are applied to the Structure

No modifications to Nodes, Elements, or Actuators are allowed while the simulation is running. To make changes to one of these components, stop the simulation first by pressing the “Stop simulation” button.

4.8. Reading a displacement record from a file

Hybrid Viz has experimental support for playing back displacements from a file. During a test, displacements applied at each story of the structure (whether physical or analytical) can be recorded and saved. Hybrid Viz is able to read in this data and animate the structure as closely as possible to what was observed in the lab. This feature has not been finalized (see Section 6 for some guidelines for implementing full support) and so the following assumptions are made about the file structure:

- The file is comma-separated (usually generated from a spreadsheet file) with the first column containing the elapsed time at which the displacement was recorded.
- Each subsequent column lists the displacements for each floor, beginning with the first floor.
- The first row of the file is merely a column header and is ignored.
- The displacements were recorded at the data acquisition (DAQ) rate of 1024 Hz used in the ATLSS lab. Thus, displacement files are usually quite large.

To use this feature, users select “Load displacement record” from the Simulation menu to bring up a dialog box. Currently, Hybrid Viz asks for the displacement file as well as three pieces of information: the duration of the playback, the number of lines in the file, and the number of floors recorded (see Figure 4.8). This information is used to collect the displacements from the file that will be used to animate the structure based on the default update rate of 35 Hz. This is necessary because, for example, a 30-second test with a DAQ rate of 1024 Hz (this is the rate used in the RTMD lab) will generate 30,720 displacement values. In order for Hybrid Viz to play back the animation for 30 seconds, it needs to take a sample of the values, or else the animation will always be very slow. However, this implementation has a desirable side effect: it gives the user more control over the animation by simply entering a different playback duration in the dialog shown below. This is possible because of the large number of displacements in the file.

For example, the user could enter one minute or more, and the structure will essentially animate in slow motion, providing a more careful examination of the response.

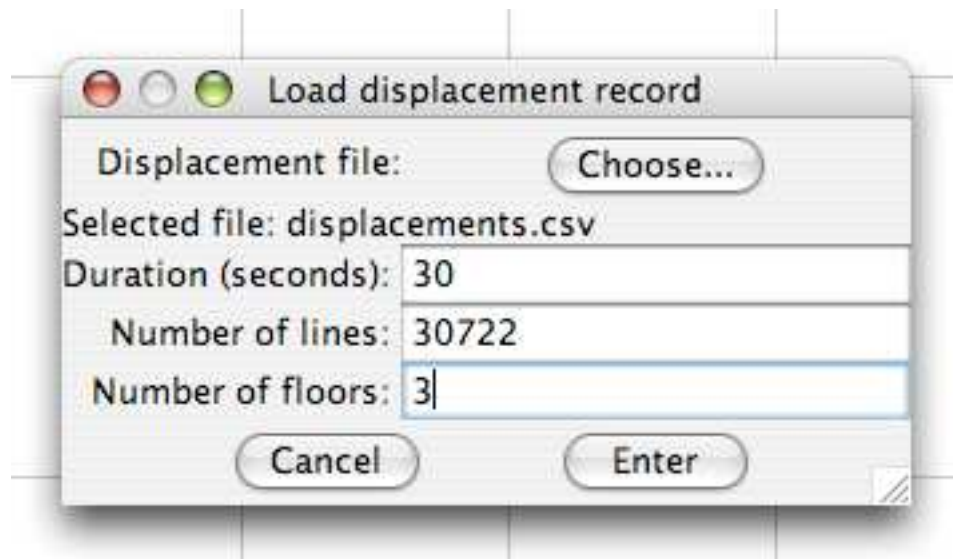


Figure 4.8 Loading a displacement record

Once the displacement file is selected and the information is entered into the dialog, pressing the “Start simulation” button will begin the animation just as if it was running in real-time. After the specified time has elapsed, the animation will stop. To replay the animation, the file must be reloaded as described above. Fortunately, the dialog box will maintain the values previously entered. As an implementation side-note, this feature works by replacing the Structure’s ScramFetcher with an instance of FileFetcher, which is in the components package. This class is responsible for reading in the file and sampling the displacement values. Thus, the Fetcher interface design proves to be flexible by allowing displacement data to come from an arbitrary source. To resume normal, real-time operation, an XML configuration file must be loaded as described in Section 4.6.

5. Summary, conclusions, and future work

The goals that were outlined at the start of the project were successfully completed. Hybrid Viz coordinates smoothly with existing RTMD hardware and software and provides flexible visualization for multi-story, multi-degree of freedom structures. Considering the limited development time and resources, Hybrid Viz is a solid achievement. Extensive testing with the SCRAMNet hardware was carried out to ensure reliability of the visualizations, catch bugs, and generate ideas for improvement.

This first iteration of development resulted in a good foundation for future work. From a design standpoint, the current design can definitely be modified to increase modularity and flexibility. In fact, design modifications might be necessary to support more complex structures. A possible next step in development would be a transition from 2D to 3D. As it stands, however, Hybrid Viz is not equipped to handle 3D visualizations from a performance standpoint, not to mention that the mathematics of structural analysis required are not implemented. Some sort of hardware-accelerated graphics package would be needed, especially for real-time visualizations. The JOGL library, which provides Java bindings for OpenGL (Java.net, 2006), and the Java 3D API (Java.net, 2006), are possible solutions. More complex structures with many more nodes and elements could be supported with hardware graphics acceleration.

Hybrid Viz can also be transformed into an applet so that any outside user can view the visualization as a test is running. This could be implemented in a variety of ways. One way is by writing displacement data to a centralized server location and creating a class that implements the Fetcher interface to retrieve this data. This would probably be the simplest and most efficient method. Alternatively, the objects used in the simulation (Structure, Node, Element, etc.) might be updated through a network interface with standard Java network classes.

Though Hybrid Viz was designed to support real-time visualizations from the ground up, it does not have support for features such as recording and playback control, which would allow researchers to see structure response at particular points in time. Although this could be designed and implemented from scratch, a possible alternative could be integration with the RDV. Such integration would allow researchers to see visualization and other data simultaneously from one application. Performance considerations would have to be made.

Hybrid Viz currently has experimental support for reading and playing back a displacement record (see Section 4.8). For complete support, a standard XML file format could be designed which would easily organize displacements on a per-Node basis. In fact, spreadsheet applications such as Microsoft Excel can save data in XML. The file format for a Hybrid Viz displacement record could be built from this standard.

From a structural engineering standpoint, one recommended development route would be a data-driven materials editor that would allow for user-definable materials, possibly in an XML format for portability. Hybrid Viz could then support complex structures with more than just beams and columns. Integration with the OpenSees framework (PEER, 2006) might facilitate adding support for these complex elements, but performance in real-time visualization would be a major concern.

6. Acknowledgments

The author would like to thank the following people who made the project a success both in results and in experience:

National Science Foundation (NSF) and the George E. Brown, Jr. Network for Earthquake Engineering Simulation (NEES)

Dr. James Ricles

Dr. Richard Sause

Tommy Marullo

Oya Mercan

Dr. Chad Kusko

Peter Bryan

Lehigh University and ATLSS personnel

The Summer 2006 NEES REU students

7. References

“Real-Time Multi-Directional (RTMD) Earthquake Simulation Facility User’s Guide” (2006), Center for Advanced Technology for Large Structural Systems (ATLSS), Lehigh University, Bethlehem, PA

Java.net (2006, July 28). “java3d: Java 3D Parent Project”. Retrieved July 28, 2006 from <https://java3d.dev.java.net/>

Java.net (2006, July 28). “jogl:”. Retrieved July 28, 2006 from <https://jogl.dev.java.net/>

MathWorks, National Institute of Standards and Technology (NIST) (2005, July 13). “JAMA: Java Matrix Package”. Retrieved July 21, 2006 from <http://math.nist.gov/javanumerics/jama/>

Mercan, O., Ricles, J.M., (2005) “Evaluation of real-time pseudo-dynamic testing algorithms for seismic testing of structural assemblages”, ATLSS Report No. 05-06, Center for Advanced Technology for Large Structural Systems, Lehigh University, Bethlehem, PA

NEES@Lehigh. “NEES@Lehigh - Project Summary”. Retrieved July 27, 2006 from <http://www.nees.lehigh.edu/index.php/fuseaction/currentProjects.Damper>

NEESit. “NEESit > Software > RDV (Real-time Data Viewer)”. Retrieved July 28, 2006 from <http://it.nees.org/software/rdv/index.php>

Pacific Earthquake Engineering Research Center (PEER) (2006, June 8). “Open System for Earthquake Engineering Simulation – Home Page”. Retrieved July 28, 2006 from <http://opensees.berkeley.edu/>

Appendix A: Example problem

This run of Hybrid Viz is based on a study conducted at the ATLSS facility called “Experimental Investigation of a Prototype Elastomeric Structural Damper”. The study investigated the performance and behavior of an elastomeric damper known as the Ultra High Damped Elastomer Tube (UHDET), developed by PennState Erie and the Corry Rubber Company. The following Structure setup was used:

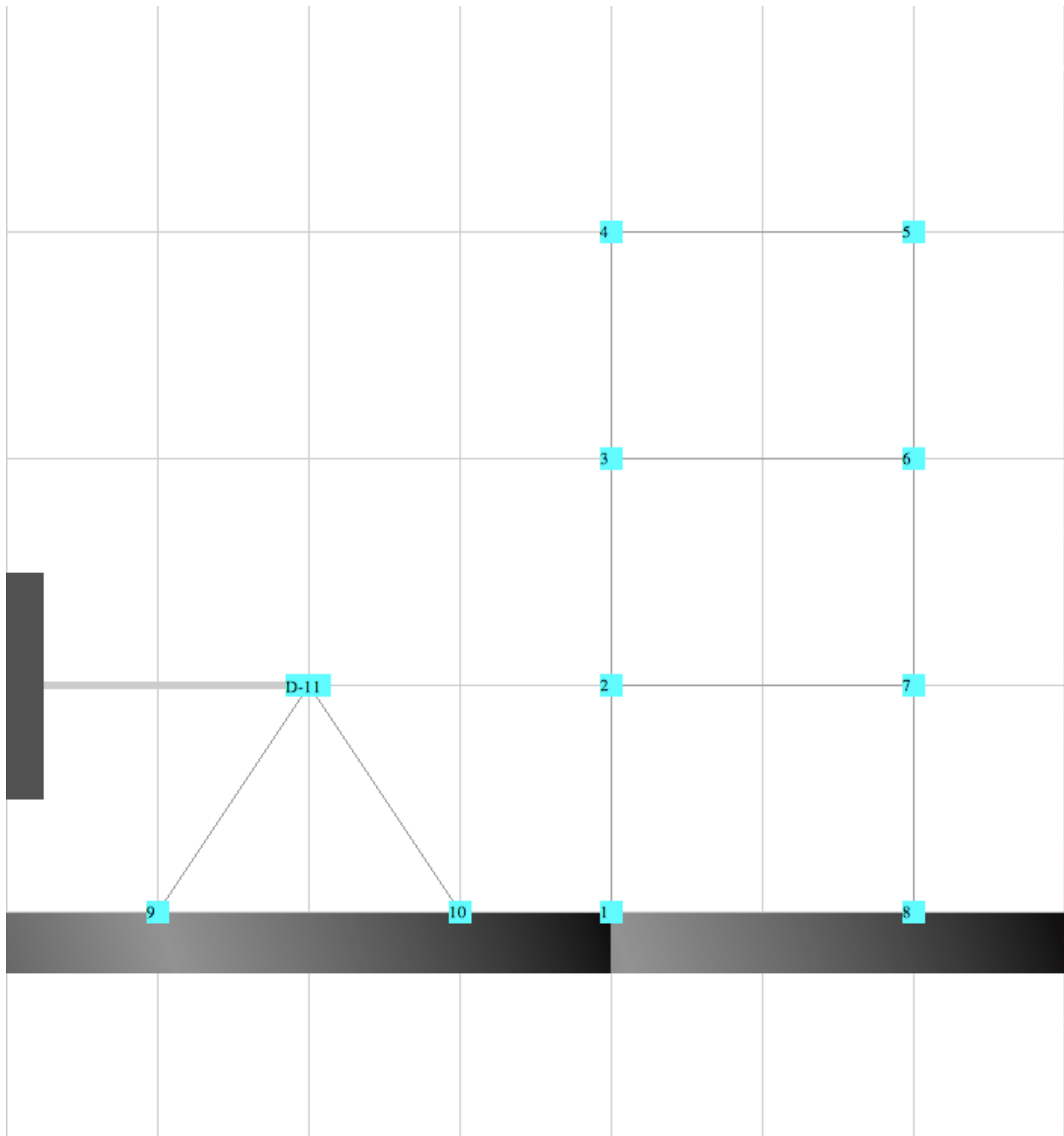


Figure A.1 Structure setup for the example problem

Damper Node 11 on the left represents the UHDET tested in the lab and, just like its physical counterpart, is connected to an Actuator. The three-story structure on the right is the simulated structure. Its deformed shape is calculated in part with the movement of the physical damper (see Section 2.1).

The Grid was set to have seven columns and five rows. Each box in the Grid was 13 ft x13 ft. All the Nodes were restricted to move only in the x direction (only the X checkbox was checked off). Nodes 1, 8, 9, and 10 were given constraint ID 0. Nodes 2 and 7 were given constraint ID 1. Nodes 3 and 6 were given constraint ID 2. Nodes 4 and 5 were given constraint ID 3. Finally, the damper node, Node 11, was given constraint ID 4, which would set it to receive the measured displacement of the damper. The single Actuator was assigned Node 11 (the damper node) for its associated Node.

The contents of the Hybrid Viz Setup file that will generate this Structure are shown below (see Section 4.5 for information on loading files and an explanation of the format):

```
<?xml version="1.0" encoding="UTF-8"?>
<HybridViz>
  <TestSetup>
    <Structure interpolations="50">
      <Node id="1" cid="0" type="fixed" xCoord="52.0" yCoord="13.0" zCoord="0.0"
dofX="true" dofY="false" dofZ="false" dofTx="false" dofTy="false" dofTz="false" />
      <Node id="2" cid="1" type="fixed" xCoord="52.0" yCoord="26.0" zCoord="0.0"
dofX="true" dofY="false" dofZ="false" dofTx="false" dofTy="false" dofTz="false" />
      <Node id="3" cid="2" type="fixed" xCoord="52.0" yCoord="39.0" zCoord="0.0"
dofX="true" dofY="false" dofZ="false" dofTx="false" dofTy="false" dofTz="false" />
      <Node id="4" cid="3" type="fixed" xCoord="52.0" yCoord="52.0" zCoord="0.0"
dofX="true" dofY="false" dofZ="false" dofTx="false" dofTy="false" dofTz="false" />
      <Node id="5" cid="3" type="fixed" xCoord="78.0" yCoord="52.0" zCoord="0.0"
dofX="true" dofY="false" dofZ="false" dofTx="false" dofTy="false" dofTz="false" />
      <Node id="6" cid="2" type="fixed" xCoord="78.0" yCoord="39.0" zCoord="0.0"
dofX="true" dofY="false" dofZ="false" dofTx="false" dofTy="false" dofTz="false" />
      <Node id="7" cid="1" type="fixed" xCoord="78.0" yCoord="26.0" zCoord="0.0"
dofX="true" dofY="false" dofZ="false" dofTx="false" dofTy="false" dofTz="false" />
      <Node id="8" cid="0" type="fixed" xCoord="78.0" yCoord="13.0" zCoord="0.0"
dofX="true" dofY="false" dofZ="false" dofTx="false" dofTy="false" dofTz="false" />
      <Node id="9" cid="0" type="fixed" xCoord="13.0" yCoord="13.0" zCoord="0.0"
dofX="true" dofY="false" dofZ="false" dofTx="false" dofTy="false" dofTz="false" />
      <Node id="10" cid="0" type="fixed" xCoord="39.0" yCoord="13.0" zCoord="0.0"
dofX="true" dofY="false" dofZ="false" dofTx="false" dofTy="false" dofTz="false" />
      <Node id="11" cid="4" type="damper" xCoord="26.0" yCoord="26.0" zCoord="0.0"
dofX="true" dofY="false" dofZ="false" dofTx="false" dofTy="false" dofTz="false" />
      <Element id="1" type="element" node1ID="1" node2ID="2" />
      <Element id="2" type="element" node1ID="3" node2ID="2" />
      <Element id="3" type="element" node1ID="3" node2ID="4" />
      <Element id="4" type="element" node1ID="4" node2ID="5" />
      <Element id="5" type="element" node1ID="5" node2ID="6" />
    </Structure>
  </TestSetup>
</HybridViz>
```

```

<Element id="6" type="element" node1ID="6" node2ID="7" />
<Element id="7" type="element" node1ID="8" node2ID="7" />
<Element id="8" type="element" node1ID="2" node2ID="7" />
<Element id="9" type="element" node1ID="3" node2ID="6" />
<Element id="10" type="base" node1ID="1" node2ID="8" />
<Element id="11" type="element" node1ID="9" node2ID="11" />
<Element id="12" type="element" node1ID="10" node2ID="11" />
<Element id="13" type="base" node1ID="9" node2ID="10" />
</Structure>
<Actuator id="1" xCoord="0.0" yCoord="26.0" zCoord="0.0" associatedNodeID="11" />
<Grid columns="7" rows="5" boxWidth="13.0" boxHeight="13.0" dUnits="ft" tUnits="rad"
/>
</TestSetup>
</HybridViz>

```

The XML configuration file used is listed below. Only the nodal section that Hybrid Viz uses to link with the SCRAMNet is provided for reference. This file is loaded with the ReadXMLConfig class and read via the XMLScramnetConfig class (see Section 3.2.1). The rest of the file deals with SCRAMNet settings used in a test that are beyond the scope of Hybrid Viz. See Section 4.6 for more information on XML configuration files.

```

<NEESsim>
  <Integrator ON="false" />
  <Kinematics ON="false" />
  <RampGenerator ON="false" />
  <Scramnet ON="true">
<!-- SCRAMNet control blocks omitted -->
  <NodeBlock ID="1" ConstraintID="0" DXOffset="1000" DYOffset="" DZOffset=""
TXOffset="" TYOffset="" TZOffset="" DUnits="ft" TUnits="rad" />
  <NodeBlock ID="2" ConstraintID="1" DXOffset="1010" DYOffset="" DZOffset=""
TXOffset="" TYOffset="" TZOffset="" DUnits="ft" TUnits="rad" />
  <NodeBlock ID="3" ConstraintID="2" DXOffset="1020" DYOffset="" DZOffset=""
TXOffset="" TYOffset="" TZOffset="" DUnits="ft" TUnits="rad" />
  <NodeBlock ID="4" ConstraintID="3" DXOffset="1030" DYOffset="" DZOffset=""
TXOffset="" TYOffset="" TZOffset="" DUnits="ft" TUnits="rad" />
  <NodeBlock ID="5" ConstraintID="3" DXOffset="1030" DYOffset="" DZOffset=""
TXOffset="" TYOffset="" TZOffset="" DUnits="ft" TUnits="rad" />
  <NodeBlock ID="6" ConstraintID="2" DXOffset="1020" DYOffset="" DZOffset=""
TXOffset="" TYOffset="" TZOffset="" DUnits="ft" TUnits="rad" />
  <NodeBlock ID="7" ConstraintID="1" DXOffset="1010" DYOffset="" DZOffset=""
TXOffset="" TYOffset="" TZOffset="" DUnits="ft" TUnits="rad" />
  <NodeBlock ID="8" ConstraintID="0" DXOffset="1000" DYOffset="" DZOffset=""
TXOffset="" TYOffset="" TZOffset="" DUnits="ft" TUnits="rad" />
  <NodeBlock ID="9" ConstraintID="0" DXOffset="1000" DYOffset="" DZOffset=""
TXOffset="" TYOffset="" TZOffset="" DUnits="ft" TUnits="rad" />
  <NodeBlock ID="10" ConstraintID="0" DXOffset="1000" DYOffset="" DZOffset=""
TXOffset="" TYOffset="" TZOffset="" DUnits="ft" TUnits="rad" />

```

```

<NodeBlock ID="11" ConstraintID="4" DXOffset="1031" DYOffset="" DZOffset=""
TXOffset="" TYOffset="" TZOffset="" DUnits="ft" TUnits="rad" />
<NodeBlock ID="0" ConstraintID="0" DXOffset="1000" DYOffset="" DZOffset=""
TXOffset="" TYOffset="" TZOffset="" DUnits="mm" TUnits="" />
</Scramnet>
</NEESSim>

```

Hybrid Viz successfully animated structural behavior in this test and was run alongside the Real-time Data Viewer (NEESit, 2006), which displayed ground accelerations in real-time. The RDV's plotter can be seen running below the Hybrid Viz window (see Figure A.2). Coupled with a live web cam feed of the damper in the lab (which is to the left of the Hybrid Viz window), a comprehensive look at structural behavior was obtained.

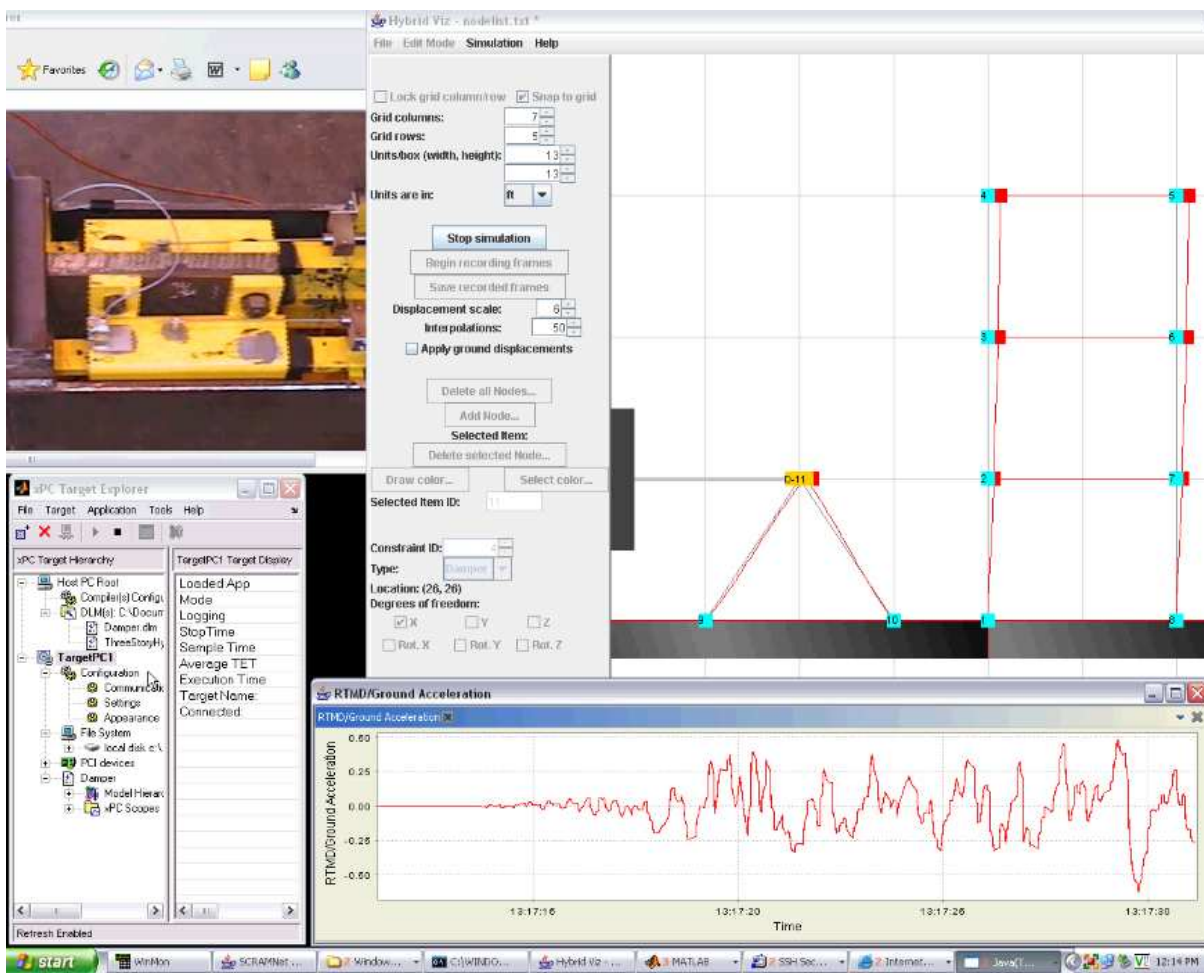


Figure A.2 Hybrid Viz runs alongside the RDV and a web cam feed of the damper

Appendix B: Example problem structural properties

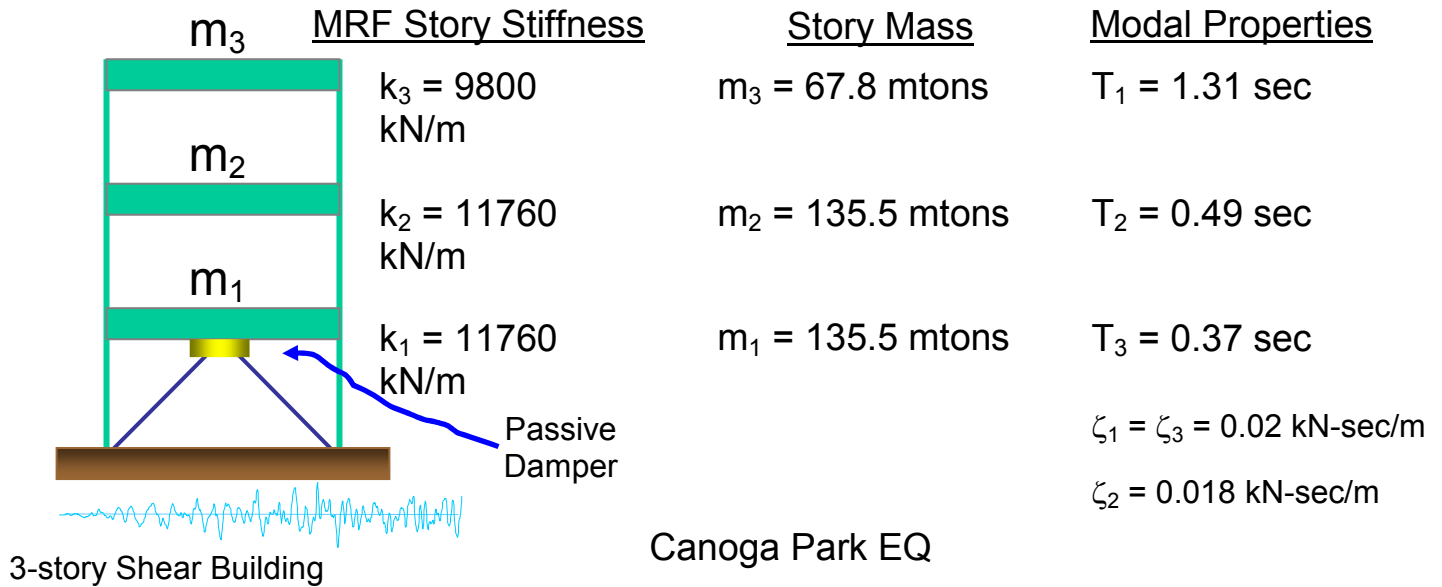


Figure A.3 Structural properties used in example problem

Appendix C: Example problem integration parameters

- α - method
 - $\alpha = -1/12$
 - $\Delta t = 20/1024$ sec
 - 20 substeps within Δt
- Canoga Park earthquake (1994)
 - Scaled to peak ground acceleration = 0.04922 g, min. ground acceleration = -0.0644 g

ATLSS REPORT

Forensic Evaluation of Beams from Lake View Drive Bridge Over I-70

Lehigh University

ATLSS Research Center

Research Team: Clay Naito, Ian Hodgson, Stephen Pessiki, and Richard Sause, Chintan Desai

Goal:

The goals of the research program are to:

- Develop inspection training guidelines, aides, and techniques that can be used to assess the condition of strands in non-composite prestressed concrete bridge box beams that are in service.
- Ensure, verify and substantiate the load rating procedures developed by University of Pittsburgh and presented in the Full Scale Load Testing Report are applicable, useable, and will be defensible in the academic and professional bridge engineering discipline by executing a Comprehensive Peer Review.

Destructive Evaluation Program:

Three beams are dissected using a combination of cross-section cutting, core hole boring and/or mechanical chipping of concrete to allow inspection of the prestressing strands can be performed. The inspection of the prestressing strands will consist of examination by both visual and microscopic methods. Assess the chemical composition of the existing beam concrete for chloride content, chloride profile and carbonation (Note: fabrication practices at that period may have used calcium chloride). Determine mechanical properties of the prestressing strand. Determine failure mechanism of prestressing strands, i.e. corrosion, stress corrosion, hydrogen embrittlement, etc.

Dissect the box beam and document the geometry of the box beam, thicknesses of web, top slab, bottom slab, the size and spacing of mild reinforcing steel, and the size and spacing of prestressing steel. Compare the measured dimensions to design drawings, standards, shop drawings, specifications and construction tolerances.

Comprehensive Peer Review

The following comprehensive reviews will be required of the research work performed by University of Pittsburgh:

Review of full scale load test program.

Review of interim report documenting full scale load test results.

Review FEA model and parametric studies.

Review draft report and final report.

In addition to the reviews, following the load rating recommendations proposed by the University of Pittsburgh, utilize PennDOT's PS3 and PSLRFD Program to analyze two representative adjacent box beams; specifically, one interior and one exterior beam as directed by the Department. Verify applicability of proposed load rating recommendations to be used by practicing engineers.

Deliverables:

Draft Destructive Evaluation Report documenting the destructive evaluation methods and findings, geometry and properties of the beams, inspection procedures, and visual aides for inspection training. Comprehensive Peer Review Report summarizing the Comprehensive Peer Review and providing guidance on analysis approach proposed by the University of Pittsburgh.

Report Outline

Abstract

On the evening of December 27th, 2005 the fascia beam supporting the east parapet wall of the third span of the Lakeview Drive Bridge failed under the action of dead load. The span is an 89' 10'' long pre-stressed adjacent box girder structure comprised of eight 48'' wide girders. Given that other similar bridges exist in the surface transportation system of the Commonwealth, there is an interest in understanding the failure and improving the assessment of reserve capacities of this type of bridge; particularly those with 40 or more years of service.

Introduction

On December 27, 2007 the east-side fascia beam of Lakeview Drive Bridge, failed under dead load. The Lake View Drive Bridge is a two lane, four span pre-stressed concrete adjacent box beam structure that spans over Interstate 70 in Washington, Pennsylvania. Fig1.1 provides the location of the bridge.

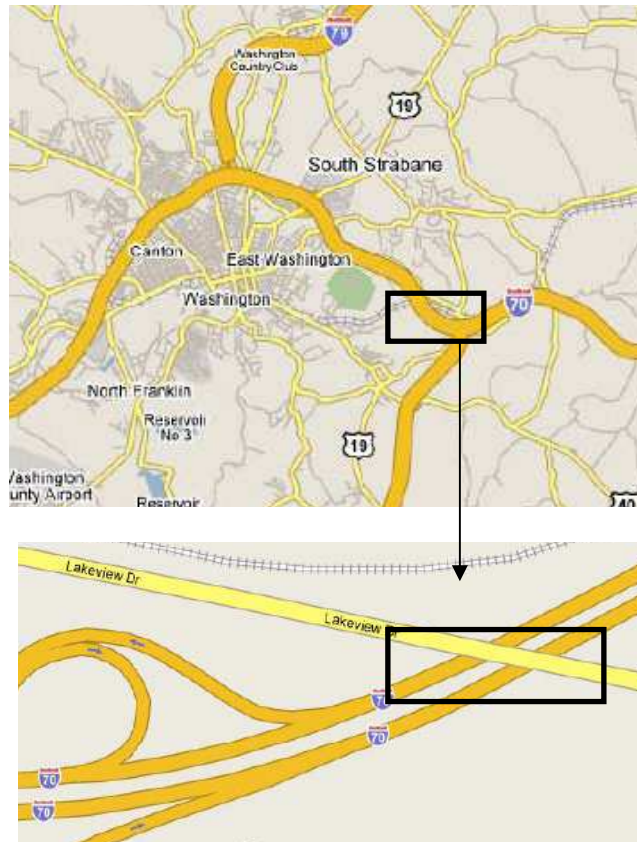


Figure 1.1 Location of Lakeview Drive Bridge (Google Maps).

The bridge is 28 feet curb to curb. Spans 2 and 3 cross I-70 and are comprised of eight pre-stressed box beams 42'' deep x 48'' wide. The riding surface consisted of a minimum 2-1/4" thick bituminous wearing course with no waterproofing membrane. The structure was constructed in 1960 on a longitudinal tangent with a skew of 39 degrees.

Objectives

The objective of this project is to develop inspection training guidance, aides and techniques for such pre-stressed box beams by destructively evaluating the box beam that have been removed from service from Lake View Drive Bridge over I-70 and similar beams identified by PennDOT.

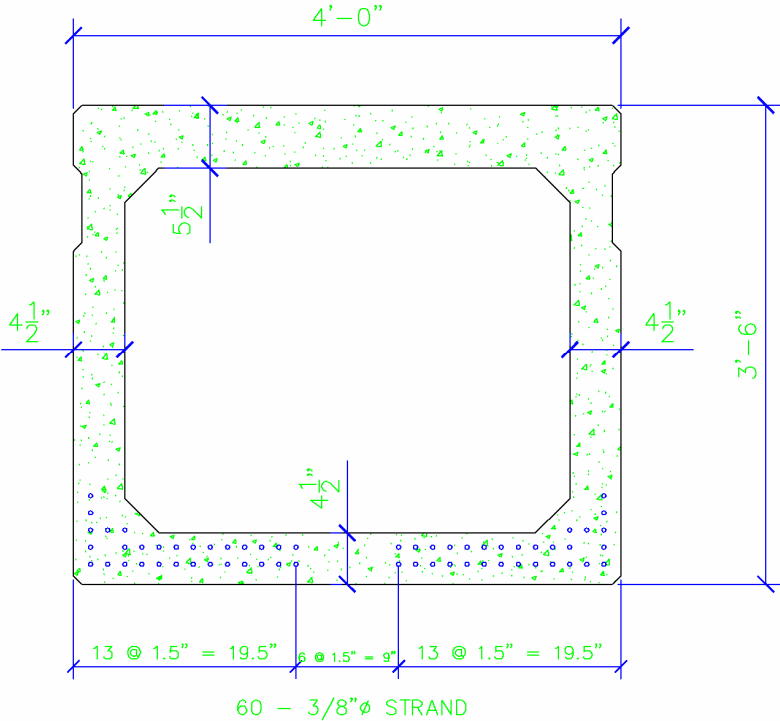
Forensic Evaluation

The beams used for destructive evaluation are beam no. 8, 9, 16, 19, 31 32. The positions of the beams are shown in Appendix A, which shows the plan view of the Lakeview Drive Bridge. Although all the above mentioned beams were inspected most of the work was done on beams 9, 16, 19.

The field inspection was carried on from 19th June to 22nd June. The field inspection included destructively evaluating the beams using a combination of cross-section cutting, core hole boring and/or mechanical chipping of concrete so that inspection of the pre-stressing strands can be performed. The locations of the chip sections and cores, for beams 9, 16, 19, are as shown in the Appendix 2.

End Section Detail

The typical cross-section of the box girder along with the strand locations is as shown in the fig 1.2.



Wall Thickness Along Span

Beam	Section	Thickness (in)		
		North Web	South Web	Bottom Flange
9	9B-1	4.875	4.000	4.625
	9B-2	5.125	3.875	4.125
	9B-3	6.500	3.250	5.125
	9B-4	5.875	3.000	4.250
	9B-5	5.125	4.875	4.500
16	16B-1 Near Pier 1	4.625	4.375	4.375
	16B-2 Near Pier 2	4.750	5.000	4.875
	16B1	5.000	4.500	4.750
19	19B-1	4.250	4.750	4.375
	19B-2	4.000	4.875	4.250
	19B-3	4.125	4.250	3.875
	19B-4	4.375	4.875	4.250
	19B-5	4.125	4.750	4.125
Design Dimensions		4.500	4.500	4.500

The thickness of the webs and the flange are very inconsistent. The thickness values range from 6.5 to 3 in.

Correlation of Surface Conditions with Internal Corrosion

Various degrees of damage were observed on the bottom flange of the box beam members. To provide guidance for inspectors the surface conditions observed were correlated with internal strand condition. This was achieved by photographing representative sections along the beams, chipping the concrete cover away, and removing the wire for further evaluation. The number of wires lost, the number of wires with surface corrosion, the number of wires with light pitting, and the number of wires with heavy pitting was visually assessed. Light pitting is defined as a section loss of less than 20% of the cross section. Heavy pitting is defined as a section loss of greater than 20%. Typical representations of these conditions are presented in

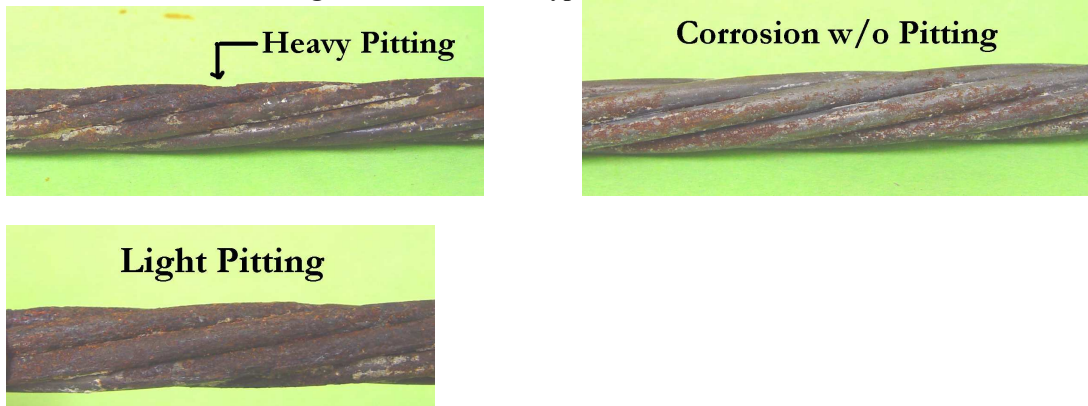


Figure 1. The strand assessment was conducted for only the six exterior strands. The strands examined are 3/8-in. diameter 250 ksi seven wire prestressing strand. The measured pitch of the strand is 5.2-in. and the diameter of the individual wires is approximately 0.12-in. resulting in an area of 0.079-sq.in. (0.085-sq.in. PCI).

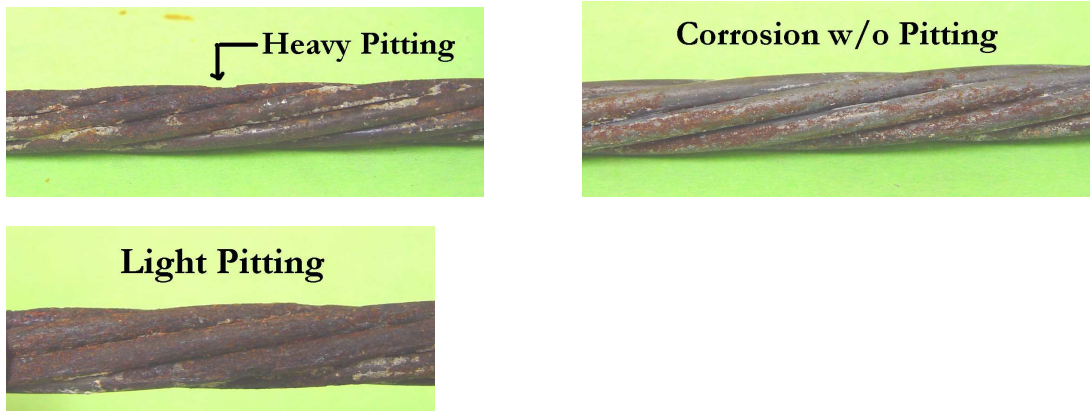


Figure 1.3: Corrosion and pitting identification

The following table identifies various degrees of surface damage originating from a crack location. The conditions are broadly characterized as: exposed strand, heavy efflorescence with rust stain, heavy efflorescence, moderate efflorescence, light efflorescence, partial efflorescence, heavy corrosion stain, moderate corrosion stain, light corrosion stain, and two levels of crack size (0.02 and 0.01-in.). The table also identifies the condition of the strand shown in the photo over one pitch. To provide a representative assessment of the impact of the surface condition on the strand other locations are also examined and averaged. The average condition of the strand and the adjacent strands are presented.

- Crack Width for various chip sections along the segments is as follows

Chip Section	Location	Crack Width (mm)
CH3A	1	0.4
	2	0.3
	3	0.2
	4	0.4
	5	0.5
	6	0.4
CH3B	1	-
	2	-
	3	1
	4	-
	5	-
	6	1
CH3C	1	0.2
	2	-
	3	-
	4	0.75
	5	0.5
	6	0.2
CH2A	1	1.1
	2	0.7

	3	0.8
CH2B	1	0.6
	2	0.5
	3	0.5
	4	0.7
	5	0.9
CH2C	1	0.5
	2	0.4
	3	0.5
	4	0.7
	5	0.4
	6	0.3
CH1	1	0.5
	2	1.1
	3	1.3
	4	0.6
	5	0.3
	6	0.5
	7	0.2

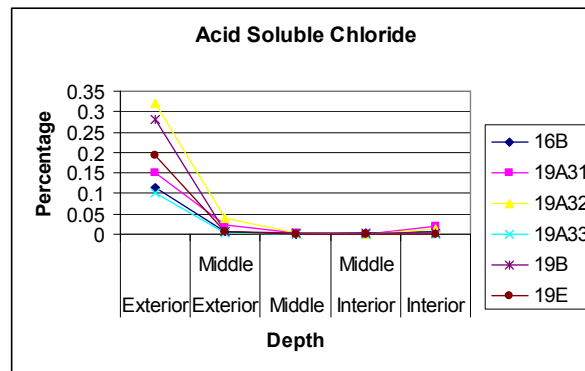
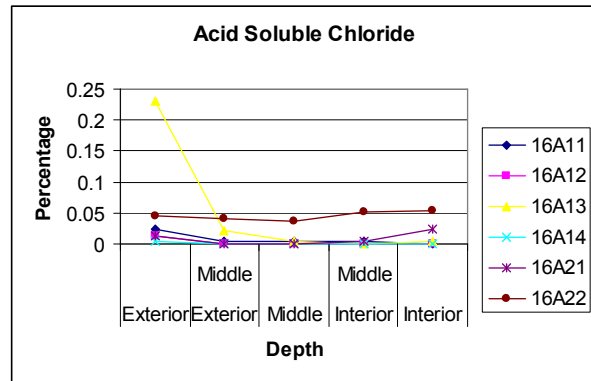
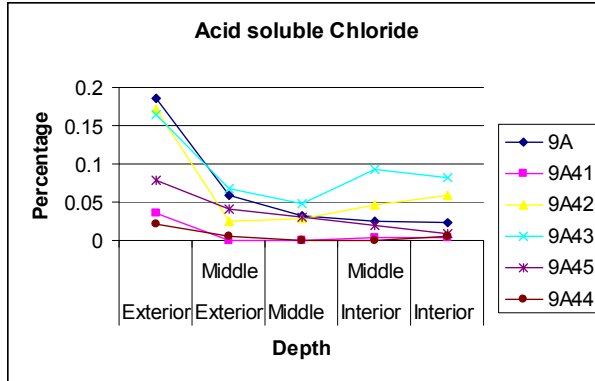
- = Crack size to big to be measured

- Net Section of Steel Remaining Along Patch
- Chloride and Carbonation Relative to Each Patch
 - CH2 – Cylinder 19E
 - CH1 – 19B
 - CH3 – 9A
 - CH5 – 16B

Chloride and Carbonation Relative to Beam Location

Core samples were taken from the beams to figure out the chloride content along the depth. The core locations used for Chloride test are given in Appendix 2. The plots of Chloride Content vs. through Depth are as follows

The chloride content was found to be more at the bottom surface of the beam compared to the top and also it was greater in the interior beams compared to the exterior. The highest chloride content was for beam no. 19, which is an interior beam.



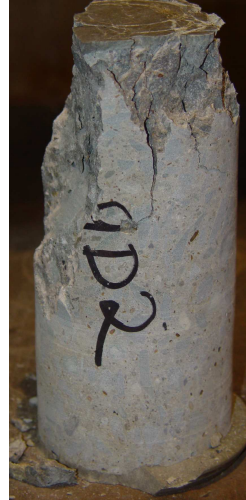
Entrapped Water Quality

- Include Discussion of Top Flange Holes and why they are there.
- Show photos of holes.
- Discuss location of trapped water in beam 8
- Beam condition and water sample from voided section
- Report levels of chloride in water, etc
- Show breakdown and non-breakdown of cardboard on either side of beam 9

Compressive Strength

Locations of the cylinders used for compressive testing are shown in Appendix 2. the data from the test is given below

Specimen Name	Stress at peak (ksi)	Load at peak (kips)
16D(2)	5.29	66.52
19D1	6.91	86.87
9D2	7.18	90.17
16D1	4.62	50.04
19D2	5.00	62.78
9D1	5.40	67.82
16D2	5.25	65.91



Photos from the compressive test

Conclusion

Using all the above data we need to come up with new inspection aides and techniques for pre-stressed box beam bridges. To pursue this we must develop a relationship between the external surface and the internal strand condition.

Appendix A

Plan view of the Lakeview Drive Bridge

Appendix B

Locations of Chip Sections and Cores

REU Final Report - National Cooperative Highway Research Program (NCHRP) Project 10-70: Cost-Effective Connection Details for Highway Sign, Luminaire, and Traffic Signal Structures

By Andrew R. Adams, ATLSS Undergraduate Researcher

Research Advisor: Dr. Sougata Roy, Graduate Student Mentor: Charlie LaBarbera

1. Abstract

Due to their lack of redundancies, failure of connections in sign, luminaire and traffic signal structures is almost always catastrophic. Recent failures have caused specifications to be developed to design against fatigue, their main mode of failure. The specifications however do not always correctly assess the fatigue behavior of the structures. Also, the specifications lead to structures whose cost effectiveness is debatable. The first task of NCHRP Project 10-70 was to verify the validity of the existing specifications that evaluate the fatigue strength of details, and develop new protocols which will more accurately describe the real life behavior of these structures.

Various “hot-spot” stress methods were looked into, all coming from codes written for offshore structures. DNV and ABS protocols were examined, but the ABS method does not involve using solid elements for the finite element analysis so mostly different protocols suggested by DNV for tubular and nontubular joints were looked into.

Using models of poles tested at the University of Texas at Austin and their fatigue test data, S-N curves were developed using the offshore structures methods and finite element analysis, to see if the data would follow the design curves given in the codes.

The DNV approach for nontubular joints was found to produce an S-N curve which closely followed the design curve for that method, significantly better than other methods looked into.

2. Introduction

Increased occurrences of cracking and failure in the connections of cantilevered sign, luminaire and traffic signal structures in the past twenty years has led to the creation of research projects to establish the cause of the failures and to develop design specifications which would prevent said failures. Many of the findings from these recent projects were incorporated into AASHTO (American Association of State Highway and Transportation Officials) *Standard Specifications for Structural Supports for Highway Signs, Luminaries, and Traffic Signals, 4th edition* (2001), and revisions in 2002 and 2003. In spite of the recent research, it has been found that the specifications do not always accurately predict the fatigue behavior of various connection details. Many existing structures (built before the specifications were enforced) were found to handle fatigue well, even though they do not meet specification requirements. Clearly the fatigue performance of these structures is not fully understood. In addition, as the present specifications tend to cause new structures to be more costly, and due to the extremely large number of these types of structures in service, it would be preferred that the specifications not only produce structures that will resist fatigue, but ones which will be cost effective as well.

To tackle the problems stated above, one of the goals of this project is to develop a protocol that will reliably and consistently predict the fatigue performance of the connections in these structures. Then the validated protocols will be used to develop a specification that will provide cost effective fatigue resistant design.

2.1 Geometry of Highway Sign, Luminaire, and Traffic Signal Structures

Cantilevered sign, luminaire and traffic signal structures are built using either an upright pole (luminaires) or an upright pole with a cantilevered mast arm or cantilevered truss (sign and traffic signal structures). The most common type of connection involves a fillet weld connecting the socketed pole to a base-plate, which is then bolted to either a foundation in the ground or to a connection on a pole, forming a cantilevered member. Other common connections involve the use of stiffeners to strengthen the pole to baseplate connection.

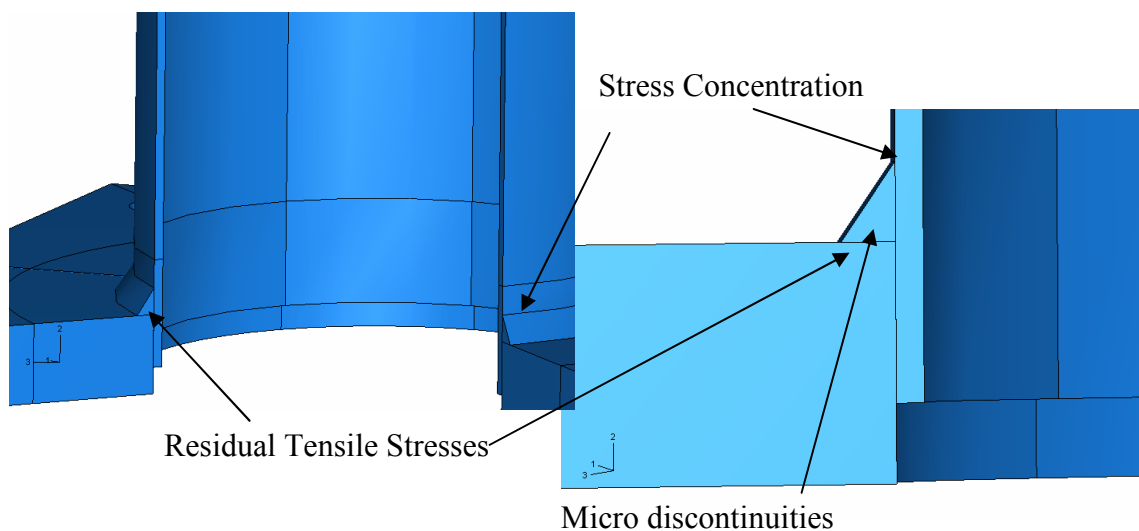
The poles and mast arms of these structures have very thin walls, making them very light in order to minimize their dead load. As a result of the thin walls and normally large length to diameter ratios, these structures tend to have a natural frequency of about 1 Hz, high flexibility, and low damping capabilities. This causes many cycles of loading to occur in a relatively short period of time, which can have a large effect on the fatigue life of the structure.

2.2 Failure

The failure of these structures is almost exclusively due to fatigue cracking. Fatigue cracking occurs when the structure is subjected to cyclic loading that is below the yield strength of the material. The cyclic loading is due to wind and aeroelastic phenomena between wind and the structures. These aeroelastic phenomena include vortex shedding, in which the structure bends in-plane perpendicular to the wind loading, and galloping, in which the structure bends out-of-plane perpendicular to the wind loading. The cracking failure occurs at the fatigue prone area of these structures; the weld toe connecting the pole to the baseplate, or, if there are stiffeners present, at the termination of the stiffener on the pole wall.

2.3 Fatigue Prone Area

Three factors help to exacerbate the fatigue cracking process in these structures; stress concentrations, residual tensile stress from welding, and micro-discontinuities. The locations that these three phenomena take place can be seen below in Figure 2.3.1. Those three factors work together and can cause cracks to grow rapidly during loading conditions like those mentioned above.



2.3.1. The Fatigue Prone Area of Socket Pole to Base-Plate Connections

Figure

2.3.1. Stress Concentration

In areas of a structure where the stresses are influenced by local geometry there is typically a stress concentration. In these areas, the nominal stress calculated from basic structural analysis is not accurate. Sometimes a stress concentration factor is known or can be calculated for the type of geometry in question to relate the nominal stress to the actual stress the structure is experiencing. In the case of a simple socket connection, the geometry of the weld toe causes there to be a theoretically infinite stress concentration at that point (see Figure 2.3.1.). For poles with stiffeners, a stress concentration develops at the termination of the stiffener on the pole wall as well as at the weld toe.

2.3.2. Residual Stress from Welding

In the welding process, the two metals to be joined are melted at their connection with each other and then allowed to cool with some filler metal being placed in the connection area. The result of locally melting a metal and then allowing it to cool is the formation of areas of residual stress. In the area of the weld toe, the residual stress is tensile. If the residual tensile stress is larger than the compressive part of the cyclic loading it could cause a state in which the area of the weld toe is in tension at all times.

2.3.3. Micro-discontinuities

The existence of defects in any structure is an unavoidable condition, and in these structures the defects can have drastic fatigue life effects due to the other factors that also contribute to fatigue. The micro-discontinuities in the weld toe and the surrounding base-plate and pole wall can be thought of as microscopic cracks. The geometric shape of a crack is very sharp, and therefore, like the weld toe geometry, there is a stress concentration at the tip of the crack. The stress concentration that develops at the tip during the cyclic loading causes the crack to propagate under failure occurs.

3. Analysis Methods

3.1 Background Information

Reliable protocols have been developed to determine the fatigue life of offshore structures using finite element analysis, however the geometries of offshore structures and pole to baseplate connected structures are different. As a result, it is not well known whether or not offshore structure methods can be applied for use with sign, luminaire and traffic signal structures. Approaches put forth by DNV (Det Norske Veritas) for tubular and nontubular joints were both examined.

3.2 Hot Spot Stress

To develop S-N curves for structures in which local geometry affects the stress, a reference stress, or hot spot stress, is normally found and then used to find a stress concentration factor (SCF). The SCF is related to the nominal stress by Equation 1 shown below.

$$\sigma_{\text{hot spot}} = \text{SCF} * \sigma_{\text{nom.}} \quad (\text{Eqn. 1})$$

By this method, once the SCF is known, simple structural analysis can be used to find the hot spot stress and then design curves can be used to find the fatigue life. Since the goal is to validate whether or not the offshore protocols will work for pole to baseplate connections, SCFs will be found for various models that have already been fatigue tested. Then the resulting S-N curve will be plotted to see if it does indeed follow the design curve given in the specification.

3.3 DNV Approach for Tubular Joints

Using this method, maximum principle stress values at two specified distances away from the weld toe on the pole wall are found and then extrapolation is used to find a value at the weld toe. The two distances used are $t/2$ and $3t/2$, where t is the thickness of the pole wall. The hot-spot stress is then calculated by Equation 2 as shown in Figure 3.1.1.

$$S_{H.S.} = (3S_{t/2} - S_{3t/2})/2 \quad (\text{Eqn. 2})$$

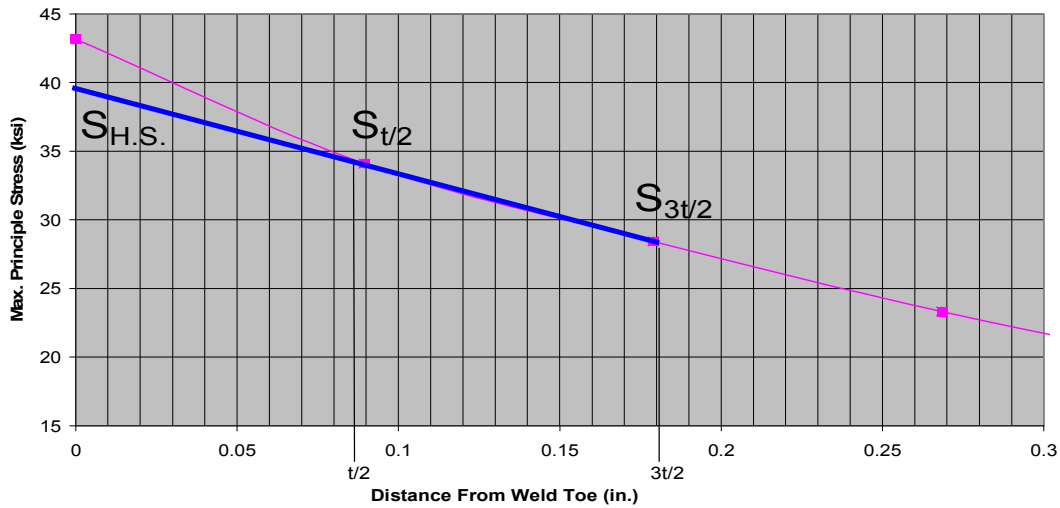


Figure 3.3.1.

Also, there has been very similar method proposed by other organizations in which the stress components at locations $t/2$ and $3t/2$ away from the weld toe are extrapolated to the weld toe and then the hot spot principle stress is calculated. A computer program was written and run in ABAQUS to accomplish this efficiently.

3.4 DNV Approach for Nontubular Joints

For nontubular joints, DNV recommends simply taking a principle stress value at a distance away from the weld toe and using that to calculate the SCF. The distance suggested is $0.1 \cdot \sqrt{r \cdot t}$, where r is the radius of the pole and t is the pole thickness. The nominal stress used to calculate the SCF is still the value at the weld toe, not the nominal stress value at $0.1 \cdot \sqrt{r \cdot t}$ away from the weld toe.

4. Procedure

4.1. Modeling

Models were drawn up as solids in a finite element analysis software package called ABAQUS. The models were created using the specifications and descriptions for poles from the University of Texas report. Five different models from the University of Texas report were looked into; a Valmont Industries pole, a TxDOT pole, each of those models with six inch

stiffener attachments, and then the Valmont Industries pole with six inch stiffeners offset 45 degrees. A brief description of the dimensions of the models can be seen in Table 4.1.1.

	Valmont Pole	TxDOT Pole
Pole Length	89.35 in.	89.35 in.
Pole Thickness	0.179 in.	.239 in.
Baseplate Thickness	1.5 in.	1.5 in.
Baseplate Length	9.5 in.	9.5 in.
Baseplate Width	9.5 in.	9.5 in.
Bolt Diameter	1.5625 in.	1.5625 in.
Bolt Offset from Baseplate Edge	2 in.	2 in.
Socket Depth	1 in.	1 in.
Weld Long Leg	0.5 in.	0.5 in.
Weld Short Leg	0.35 in.	0.35 in.

Table 4.1.1

The long leg is the height of the weld on the pole wall, while the short leg is the height on the baseplate. The stiffeners used are triangular in shape, with a triangular piece cut out at the right angle section of stiffener so that the fillet weld connecting the baseplate to the pole can run through it. The piece cut out of the stiffener had a height of 0.7 inches and a width of 0.55 inches. Dimensions for the stiffeners can be seen below in Table 4.2.

Stiffener Dimensions (in.)	
Height	6
Thickness	0.375
Width	2
Weld legs	0.25

Table 4.1.2

Both of the legs of the weld on the stiffeners had the same dimension. Also, to ensure that the load placed on the structure would be uniformly distributed throughout, an essentially rigid 5 inch solid loading plate was placed on top of the pole. A load of 1.65 kips was then placed at the center node of the top of the loading plate.

4.2. Mesh Convergence

Normally finite element model solutions converge to the real life solutions with a relatively fine mesh. However the singularity at the weld toe causes the solutions to be mesh dependent; the smaller the mesh size, the closer the output at the weld toe come to the infinite theoretical result. Because the hot-spot stress approach uses values at locations away from the weld toe, the results at those specified locations must converge to produce accurate results. Therefore, the first task that had to be accomplished was to determine what mesh size requirements were needed to obtain converged solutions at a distance of $t/2$ away from the weld toe. Six different mesh sizes were tested, each having a different combination of length and width, while the depth of the elements remained t in size (0.179 inches, because the Valmont model was used). Since the sizing of the mesh was only focused on the pole wall and not on the weld, to keep the data consistent between the different meshes, a change had to be made to the way ABAQUS reports data. Normally it averages values it gets from different directions at a node to report one value. Instead, the program can be told to only average values if they are

within a certain range of each other. Giving the program a 15% averaging value resulted in the program generating smooth plots with no effects from the size of the meshing on the weld. The table below, Table 4.2.1 explains the six sizes of meshes tested, and Figure 4.2.1 shows the length and width directions of the elements on the pole.

	Length of Element	Width of Element
Mesh 1	t	$4t$
Mesh 2	$t/2$	$2t$
Mesh 3	t	t
Mesh 4	$t/2$	$t/2$
Mesh 5	$t/2$	t
Mesh 6	t	$2t$

Table 4.2.1.

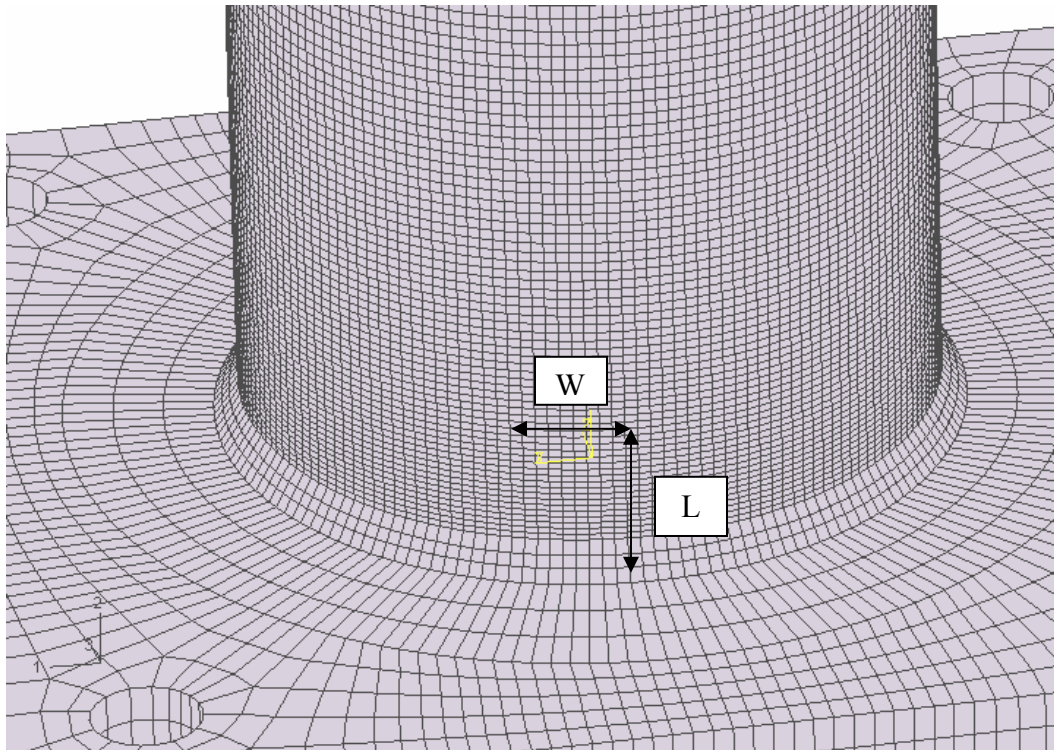


Figure 4.2.1.

5. Results

5.1. Mesh Sizing

The results can be seen in the appendix at the end of the report under Graph 1 and Graph 2. The local effects of the socket connection are extremely visible in Graph 1. The singularity occurs at the weld toe and as the distance from the weld toe increases the stress value actually dips down below the Mc/I value before converging with it later. This results in an out of plane bending like shown in Figure 2 below.

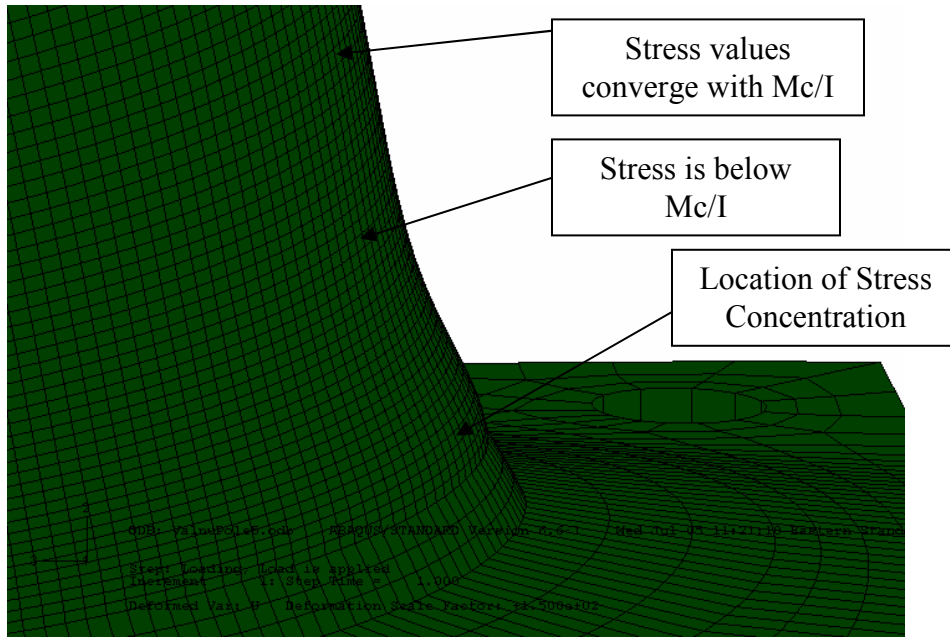


Figure 5.1.1: Local Geometry Effects on Bending

As can be seen in Graph 2, all of the mesh sizes chosen for testing converge up to the $t/2$ location, which means all are sufficient to be used for the hot spot stress analysis.

Hot-spot stresses and stress concentration factors (S.C.F) were calculated for all six mesh sizes tested, to see how the size of the mesh influences the results. The values obtained can be seen in Table 3.

S.C.F. by Extrapolating the Max. Principle Stress to the Weld Toe

$\sigma_{nom} = 11.50$ ksi

Mesh Size	$\sigma_{t/2}$	$\sigma_{3t/2}$	$\sigma_{H.S.}$	S.C.F. = $\sigma_{H.S.}/\sigma_{nom}$
Mesh 1: $t \times 4t$	35.1426	23.7386	40.8446	3.5517
Mesh 2: $.5t \times 2t$	34.0955	23.3204	39.4831	3.4333
Mesh 3: $t \times t$	34.9158	23.5811	40.5832	3.5290
Mesh 4: $.5t \times .5t$	34.2387	23.4172	39.6495	3.4478
Mesh 5: $.5t \times t$	34.1565	23.3579	39.5558	3.4396
Mesh 6: $t \times 2t$	34.8098	23.5418	40.4438	3.5169

Table 5.1.1

The nominal stress ($\sigma_{nom.}$) is the value of stress obtained at the weld toe using simple structural analysis ($\sigma = Mc/I$) based on the loading and geometry of the pole. The calculations for the nominal stresses and moments of inertia for the different models can be seen in the calculations section of the appendix. The results show a slight dependence on the size of the meshes around the weld toe. It should be noted how the larger mesh sizes actually result in a higher hot-spot stress and stress concentration factor. This is contrary to what is expected, but can be explained by noting the tendency of the results in Graph 2. The larger mesh sizes result in a higher $t/2$ stress but a lower ABAQUS calculated weld toe stress than the smaller mesh sizes. When the values are extrapolated, that result ends up causing the larger mesh sizes to have a larger slope between the $3t/2$ and $t/2$ stress values than the smaller mesh sizes. Since the slope is larger and

the values for the hot-spot stress are being calculation by linear extrapolation, the larger mesh sizes result in higher hot-spot stresses and stress concentration factors.

Based on the results of the initial mesh size tests, it was determined that a t by t mesh size (Mesh 3) at the weld toe is sufficient to get good results. It was decided on because of its efficiency to run the program at this mesh size, the good results it provides, and because previous suggestions for hot-spot stress analysis suggest a t by t mesh size when using models with shell elements.

5.2. DNV Approach for Tubular Joints Results

The results of extrapolating the principle stresses at distances t/2 and 3t/2 away from the weld toe for all five models can be seen below in Table 5.2.1.

Model	$\sigma_{t/2}$	$\sigma_{3t/2}$	$\sigma_{H.S.}$	S.C.F.
Valmont Pole	34.9158	23.5811	40.5832	3.5290
Valmont Pole- 4 Stiffeners@90°	37.8814	29.6958	41.9742	3.8793
Valmont Pole- 4 Stiffeners@45°	29.7312	23.3139	32.9399	3.0443
TxDOT Pole	26.6580	15.6271	32.1735	3.6686
TxDOT Pole- 4 Stiffeners@90°	26.1346	18.6661	29.8689	3.6200

Table 5.2.1.

According to the DNV recommendations, these SCFs should be combined with the D curve. The calculations of points for the D curve based off of the parameters given by DNV can be seen in the Calculations section of the appendix. The fatigue test data from the University of Texas, a graph of the fatigue data using these SCFs, and the D curve can be seen plotted together in Graph 3 in the appendix.

Using the computer program to extrapolate the stress components instead of the principle stresses to the weld toe resulted in the data shown below in Table 5.2.2.

Model	$\sigma_{H.S.}$	S.C.F.
Valmont Pole	39.9326	3.4724
Valmont Pole- 4 Stiffeners@90°	42.0435	3.8857
Valmont Pole- 4 Stiffeners@45°	32.9940	3.0494
TxDOT Pole	32.2181	3.6737
TxDOT Pole- 4 Stiffeners@90°	29.9635	3.6315

Table 5.2.2.

Again, these SCFs are combined with the University of Texas' fatigue test data and the D curve to produce Graph 4 in the appendix.

5.3. DNV Approach for Nontubular Joints Results

By simply taking a reference stress at a distance of $0.1 \cdot \sqrt{r \cdot t}$ away from the weld toe and using that to calculate an SCF produced the results shown below in Table 5.3.1.

Model	$\sigma_{.1\sqrt{rt}}$	S.C.F.
Valmont Pole	34.9158	3.0362
Valmont Pole- 4 Stiffeners@90°	37.8814	3.5011
Valmont Pole- 4 Stiffeners@45°	29.7312	2.7478
TxDOT Pole	26.6580	3.0397
TxDOT Pole- 4 Stiffeners@90°	26.1346	3.1674

Table 5.3.1.

For the nontubular approach recommended by DNV, the SCFs found should be combined with the T curve. The T curve and D curve have the same parameters, so they are actually the same curve. The plotted results of using this method can be seen in Graph 5 of the appendix.

5.4. Comparing Results

Shown below in Table 5.4.1. is a comparison of the three methods for all five models.

Model	Tubular Joints Method 1 SCF	Tubular Joints Method 2 SCF	Nontubular Joints Method SCF
Valmont Pole	3.5290	3.4724	3.0362
Vamont Pole w/stiffeners @ 90°	3.8793	3.8857	3.5011
Valmont Pole w/stiffeners @ 45°	3.0443	3.0494	2.7478
TxDOT Pole	3.6686	3.6737	3.0397
TxDOT Pole w/stiffeners @ 90°	3.6200	3.6315	3.1674

Table 5.4.1.

Note that “Tubular Joints Method 1” refers to extrapolating the principle stresses to the weld toe, while “Tubular Joints Method 2” refers to extrapolating the stress components. A graphical representation of this table can be seen in Graph 6 in the appendix.

6. Discussion

The results for all three methods are very similar. Even the tendencies of how the SCFs change between models using the different methods are similar, as seen in Graph 7. One variance in the similarities that should be noted is the change in SCF between the TxDOT pole and the stiffened TxDOT pole. For the tubular methods the stiffened TxDOT pole has a lower SCF than the unstiffened pole, while for the nontubular method the stiffened pole has a higher SCF. Looking at Graph 7, this appears to be due to the nontubular method producing a relatively lower SCF for the TxDOT model than the other models.

The overall results for the nontubular method are lower than that for the tubular methods, causing all the data points to shift downward on the S-N curve. Because the two tubular methods result in data points on the S-N curve that are well above the design line (D curve), the effect of having lower SCFs for the nontubular method results in S-N data points that more closely follow the design curve.

7. Conclusions

1. A t by t mesh size at the weld toe is sufficiently small enough to get convergence at the necessary locations, while being large enough to be efficiently run by a desktop computer.
2. Extrapolating the maximum principle stresses from the $t/2$ and $3t/2$ locations away from the weld toe results in almost the same values as when the stress components are extrapolated. The difference is not significant enough to suggest that either method is better than the other at representing the behavior of the structure.
3. The DNV recommended approach for nontubular members produces an S-N curve which closely follows the design curve for that method. However, more models need to be analyzed to ensure that this method can consistently produce accurate results for any type of modeled pole to baseplate connections.

References

Koenigs, Mark T., Botros, Tamer A., Freytag, Dylan, and Frank, Karl H. "Fatigue Strength of Signal Mast Arm Connections" The University of Texas at Austin, August 2003.

NCHRP Project 10-70 Research Plan

Ocel, Justin M., Dexter, Robert J., Hajjar, Jerome F "Fatigue-Resistant Design for Overhead Signs, Mast-Arm Signal Poles, and Lighting Standards" University of Minnesota, Department of Civil Engineering, March 2006.

Acknowledgements

I would like to thank Lehigh University and Dr. Chad Kusko for providing this program and selecting me, Dr. Sougata Roy and Charlie LeBarbara for all their help and expertise, and the other REU students for always keeping office life interesting.

Appendix

Calculations

Valmont Pole

$$\sigma_{nom.} = Mc/I = PLc/I$$

$$P = 1.65 \text{ kips}$$

L = 89.35 in. + 5 in. loading plate - 1 in. socket depth - 0.5 in. weld height

$$L = 92.85 \text{ in.}$$

$$c = 5 \text{ in.}$$

$$I = \pi/64(d_{out}^4 - d_{in}^4)$$

$$I = \pi/64(10^4 - 9.642^4)$$

$$I = 66.61 \text{ in.}^4$$

$$\sigma_{nom.} = 1.65 \cdot 92.85 \cdot 5 / 66.61$$

$$\sigma_{nom.} = 11.50 \text{ ksi}$$

Valmont Pole Stiffened

(note: both stiffened models have the same $\sigma_{nom.}$ values)

$$\sigma_{nom.} = Mc/I = PLc/I$$

$$P = 1.65 \text{ kips}$$

L = 89.35 in. + 5 in. loading plate - 1 in. socket depth - 6 in. stiffener height

$$L = 87.35 \text{ in.}$$

$$c = 5 \text{ in.}$$

$$I = \pi/64(d_{out}^4 - d_{in}^4)$$

$$I = \pi/64(10^4 - 9.642^4)$$

$$I = 66.61 \text{ in.}^4$$

$$\sigma_{nom.} = 1.65 \cdot 87.35 \cdot 5 / 66.61$$

$$\sigma_{nom.} = 10.82 \text{ ksi}$$

TxDOT Pole

$$\sigma_{nom.} = Mc/I = PLc/I$$

$$P = 1.65 \text{ kips}$$

L = 89.35 in. + 5 in. loading plate - 1 in. socket depth - 0.5 in. weld height

$$L = 92.85 \text{ in.}$$

c= 5 in.

$$I = \pi/64(d_{out}^4 - d_{in}^4)$$
$$I = \pi/64(10^4 - 9.522^4)$$
$$I = 87.34 \text{ in.}^4$$

$$\sigma_{nom.} = 1.65 \cdot 92.85 \cdot 5 / 87.34$$

$$\sigma_{nom.} = 8.77 \text{ ksi}$$

TxDOT Pole Stiffened

$$\sigma_{nom.} = Mc/I = PLc/I$$

$$P = 1.65 \text{ kips}$$

L = 89.35 in. + 5 in. loading plate - 1 in. socket depth - 6 in. stiffener height

$$L = 87.35 \text{ in.}$$

c= 5 in.

$$I = \pi/64(d_{out}^4 - d_{in}^4)$$
$$I = \pi/64(10^4 - 9.522^4)$$
$$I = 87.34 \text{ in.}^4$$

$$\sigma_{nom.} = 1.65 \cdot 87.35 \cdot 5 / 87.34$$

$$\sigma_{nom.} = 8.25 \text{ ksi}$$

T/D Curve Data

$$N = AS_r^{-m} \text{ -----} \rightarrow S_r = (A/N)^{1/m}$$

$$\text{for } N \leq 10^6: \log A = 12.164 \text{ -----} \rightarrow A = 1.4588E12$$
$$m = 3$$

$$S_r = (1.4588E12/N)^{1/3}$$

N	S _r (Mpa)	S _r (ksi)
1.00E+07	52.642	7.6351
1.00E+06	113.41	16.4492
1.00E+05	244.34	35.4388

$$\text{for } N \geq 10^6: A = 4.0365E15$$
$$m = 5$$

$$S_r = (4.0365E15/N)^{1/5}$$

N	S _r (Mpa)	S _r (ksi)
1.00E+07	52.626	7.6328
1.00E+08	33.205	4.8159

1.00E+09	20.951	3.0387
1.00E+10	13.219	1.9172

S-N Curve Data

Valmont Pole

Specimen Name	Stress Range (ksi)	Stress Range * SCF (extrap. principle stress)	Stress Range * SCF (extrap. stress components)	Stress Range * SCF (.1*√[rt] method)	Cycles to Failure
Phase 1					
Valnu A	11.9	41.9951	41.3216	36.1308	249446
Valnu B	11.9	41.9951	41.3216	36.1308	453948
Valnu C	6.29	22.1974	21.8414	19.0977	2072592
Valnu D*	6.2	21.8798	21.5289	18.8244	6856881
Valnu EP	11.4	40.2306	39.5854	34.6127	393767
Valnu FP	11.5	40.5835	39.9326	34.9163	353103
Phase 2					
Valnu A	11.9	41.9951	41.3216	36.1308	389428
Valnu B	11.8	41.6422	40.9743	35.8272	265540
Valnu G A	11.6	40.9364	40.2798	35.2199	183132
Valnu G B	11.5	40.5835	39.9326	34.9163	151679

* Run-Out - No Cracking

Valmont Pole - 4 Stiffeners @ 90°

Specimen Name	Stress Range (ksi)	Stress Range * SCF (extrap. principle stress)	Stress Range * SCF (extrap. stress components)	Stress Range * SCF (.1*√[rt] method)	Cycles to Failure
Phase 1					
VAL 6x3/8 A	11.2	43.4482	43.5198	39.2123	242728
VAL 6x3/8 B	11.3	43.8361	43.9084	39.5624	653292
VAL 6x3/8 C	5.9	22.8879	22.9256	20.6565	3592372

Valmont Pole - 4 Stiffeners @ 45°

Specimen Name	Stress Range (ksi)	Stress Range * SCF (extrap. principle stress)	Stress Range * SCF (extrap. stress components)	Stress Range * SCF (.1*√[rt] method)	Cycles to Failure
Phase 2					
VAL 6x3/8@45 A	11.96	36.4098	36.4708	32.8637	238515
VAL 6x3/8@45 B	11.98	36.4707	36.5318	32.9186	161843
VAL 6x3/8@45 C	4.3	13.0905	13.1124	11.8155	6066817
VAL 6x3/8@45 D	4.3	13.0905	13.1124	11.8155	6066817

TxDOT Pole

Specimen Name	Stress Range (ksi)	Stress Range * SCF (extrap. principle stress)	Stress Range * SCF (extrap. stress components)	Stress Range * SCF (.1*√[rt] method)	Cycles to Failure
Phase 1					
TXu A	6	22.0116	22.0422	18.2382	2199343
TXu B	6.1	22.3785	22.40957	18.54217	2816706
TXu C	11.8	43.2895	43.34966	35.86846	177596
TXu D	12	44.0232	44.0844	36.4764	194694
TXu EP	11.8	43.2895	43.34966	35.86846	320915
TXu FP	11.7	42.9226	42.98229	35.56449	141155

TxDOT Pole- 4 Stiffeners @ 90°

Specimen Name	Stress Range (ksi)	Stress Range * SCF (extrap. principle stress)	Stress Range * SCF (extrap. stress components)	Stress Range * SCF (.1*√[rt] method)	Cycles to Failure
Phase 1					
TX 6x3/8 A	11.2	40.5440	40.6728	35.4749	783857
TX 6x3/8 B	11.3	40.9060	41.0360	35.7916	783857
TX 6x3/8 C	5.76	20.8512	20.9174	18.2442	7503037